NTNU – Trondheim
Norwegian University of
Science and Technology

Identification of Hydrodynamic Parameters for Remotely Operated Vehicles

Ole Alexander Eidsvik

Marine Technology
Submission date: June 2015
Supervisor: Ingrid Schjølberg, IMT

Norwegian University of Science and Technology
Department of Marine Technology

NTNU
Norges teknisk-naturvitenskapelige universitet
Institutt for marin teknikk

MASTER THESIS 2015

for

Stud. Techn. **Ole Alexander Eidsvik**

Identification of Hydrodynamic parameters for ROVs

Identifisering av hydrodynamiske parametere for ROVer

UUVs are today common in deep water industries such as oil and gas exploration, telecommunications, geotechnical investigations and mineral exploration.
One type of UUVs are the Remotely Operated Vehicles. (ROVs) ROVs are the workhorses in subsea engineering and the tasks performed by ROVs become increasingly more challenging. Good knowledge of the ROV behavior and characteristics are hence of great importance.

The hydrodynamic forces can often be referred to as the forces acting on the ROVs when submerged in water. Added mass, damping and restoring forces are all important factors in the dynamic equation of motion for ROVs. The hydrodynamic coefficients are the constants that describe these forces in the equation of motion. Acquiring good knowledge of the characteristics of the ROVs hence becomes synonym with the ability to estimate these constants accurately.

The set of constants that are related to the hydrodynamic forces are often referred to as the hydrodynamic coefficients. Different methods exist today for estimating these coefficients. The different conventional methods all have advantages and disadvantages compared to each other. Usually the procedures for obtaining accurate parameters require great effort. The hydrodynamic coefficients are important not only in the design and operational stages of ROVs. The implementation of model based controllers also requires accurate estimates of these coefficients to give the desired results. The Results of this work will therefore be important for development of future simulations and mathematical models for control.

The purpose of this work is to evaluate and quantify the hydrodynamic properties of a general ROV.

The work is proposed carried out in the following steps:

1) Determine the hydrodynamic forces and moments that are relevant for a typical ROV

2) Evaluate the hydrodynamic parameters related to the forces and moments.

3) Investigate different methods for obtaining knowledge of these parameters.

4) Based on the previous steps to develop a complete procedure for obtaining the parameters. Experimental tests on either full scale or models are suggested as an important part of this step.

5) Test the procedure on different ROVs and evaluate the obtained results.

6) A complete evaluation the procedure should be performed.

7) Conclusion and suggestions for further work

Literature studies of specific topics relevant to the thesis work may be included.

The work scope may prove to be larger than initially anticipated. Subject to approval from the supervisors, topics may be deleted from the list above or reduced in extent.

In the thesis the candidate shall present his personal contribution to the resolution of problems within the scope of the thesis work.

Theories and conclusions should be based on mathematical derivations and/or logic reasoning identifying the various steps in the deduction.

The candidate should utilise the existing possibilities for obtaining relevant literature.

Thesis format
The thesis should be organised in a rational manner to give a clear exposition of results, assessments, and conclusions. The text should be brief and to the point, with a clear language. Telegraphic language should be avoided.

The thesis shall contain the following elements: A text defining the scope, preface, list of contents, summary, main body of thesis, conclusions with recommendations for further work, list of symbols and acronyms, references and (optional) appendices. All figures, tables and equations shall be numerated.

The supervisors may require that the candidate, in an early stage of the work, presents a written plan for the completion of the work. The plan should include a budget for the use of computer and laboratory resources which will be charged to the department. Overruns shall be reported to the supervisors.

The original contribution of the candidate and material taken from other sources shall be clearly defined. Work from other sources shall be properly referenced using an acknowledged referencing system.

The report shall be submitted in two copies:
- Signed by the candidate
- The text defining the scope included
- In bound volume(s)
- Drawings and/or computer prints which cannot be bound should be organised in a separate folder.

- The report shall also be submitted in pdf format along with essential input files for computer analysis, spreadsheets, MATLAB files etc in digital format.

Thesis supervisor

Prof. Ingrid Schjølberg

Deadline: June 10, 2015

Trondheim, January 14, 2015

PREFACE

This report is the result of the Master's Thesis in Marine Technology at the Norwegian University of Science and Technology carried out during the spring of 2015. The main motivation of the thesis was to acquire knowledge of the hydrodynamic properties of ROVs. Which again can be utilized when designing ROVs or developing model based control systems.
The idea was presented by Tor B Gjersvik during the summer of 2014. Some preparation work was hence carried out during the fall of 2014. The assumed background for the reader is an education in ocean engineering or equivalent, or just a general interest in the hydrodynamics of ROVs.

Trondheim, ***2015-06-10***

Ole Alexander Nørve Eidsvik

ACKNOWLEDGMENT

I want to thank my advisor Professor Ingrid Schjølberg at the Department of Marine Technology. Professor Schjølberg has provided great support both technical and theoretical in addition to interesting conversations. This thesis would not have been made possible without the help of professor Schjølberg.

I would like to thank Professor Tor B. Gjersvik at the department of Petroleum Engineering and Applied Geophysics for interesting inputs and conversations.

I would like to thank Senior Engineer Torgeir Wahl at Department of Marine Technology for the help received regarding the experiments performed in MC-lab. I would also like to thank Fredrik Sandved for the assistance during the experiments. The assistance received from these two made the experiments possible.

Last but not least, I would like to thank my family and friends for supporting me through these five years. A special thanks to the guys at the office C.1077

O.E.

SUMMARY

The hydrodynamic parameters that characterize the behaviour of a general work class Remotely Operated Vehice(ROV) are evaluated. This is done by deriving the equation of motion for an ocean vessel moving in 6 degrees of freedom. The equation of motion is then applied to a general work class ROV. The resulting hydrodynamic parameters are then evaluated and the two main hydrodynamic quantities of interest is shown to be the added mass and hydrodynamic damping. These two quantities are in combination with the rigid body mass and restoring forces the main contributors that dictates the motion of a ROV in water.
Different methods for obtaining the hydrodynamic parameters are discussed. Already established, but also new methods are evaluated. These include experimental, numerical, analytical and empirical methods.

A complete procedure for obtaining the hydrodynamic parameters is suggested. The procedure includes an empirical method which uses basic empirical coefficients and already established theory. Additional new theory is introduced where lack of existing literature made it necessary. The empirical method is tested on 5 ROVs with completely different geometries. The procedure also consists of an experimental method. The experimental method is based on towing/rotation tank trials, where the ROV is towed or rotated to record the hydrodynamic forces acting on the ROV at different speeds. The experimental setup is designed to be low cost and easy to perform even with limited means. The experimental procedure is tested on ROV Neptunus and VideoRay Pro-4 which are two small ROVs with very different characteristics.

Computational Fluid Dynamics(CFD) and potential flow theory is used to verify the two methods. This is done by comparing the numerical results to the obtained experimental and empirical estimates.

The added mass estimates are compared to results produced by WADAM(Wave

Analysis by Diffraction and Morison Theory) which is a program in the Sesam software package that utilizes the panel method to estimate hydrodynamic coefficients using potential flow theory. The results from the empirical added mass estimates shows good correspondence with the reference results. The relative difference is for the translational degrees of freedom in the range of 10 to 20% and for the rotational degrees of freedom in the range of 30-100%. These results show that there are room for improvements, but based on the basic nature of the method and complex shapes of the ROVs it still provides results that can be deemed satisfactory.

The damping forces are verified by using SolidWorks Flow Simulation which is a CFD program incorporated in the SolidWorks program package. The empirical and experimental estimates shows promising results with the exception of the experimental values obtained for VideoRay Pro-4 where the experimental damping is substantially larger than both CFD and empirical estimates. The empirical method generally overestimates the damping, but usually lies in the correct range. The experimental method shows for ROV Neptunus very good correspondence with regards to the CFD results.

The procedure described presents a robust way of determining the hydrodynamic coefficients of a ROV with a relative uncertainty of less than approximately 100% for a number of different ROVs with completely different characteristics. The method has great room for improvement, especially the experimental procedure can be improved drastically as some results are very accurate while other results shows great deviation with regards to the referenced values.

SAMMENDRAG

De hydrodynamiske parameterne som karakteriserer oppførselen til en typisk fjernstyrt undervannsfarkost(ROV) er evaluert. Dette blir gjort ved å først utlede en generell bevegelsesligning for et typisk overflatefartøy som kan forflytte seg i 6 frihetsgrader. Bevegelsesligningen er deretter overført til en ROV som opererer langt under havoverflaten og som dermed ikke blir påvirket av de samme kreftene som et overflatefartøy. De to mest interessante hydrodynamiske parameterne som kommer ut av denne analysen er hydrodynamisk masse (added mass) og hydrodynamisk demping. Disse to parameterne er i kombinasjon med fjærkreftene og treghetskreftene de viktigste faktorene som bestemmer oppførselen til en ROV langt under havoverflaten.

Forskjellige metoder eksisterer i dag for å anslå disse parameterne og en del av disse metodene blir diskutert. Gamle veletablerte metoder så vel som nye relativt uprøvde metoder blir evaluert. Disse inkluderer eksperimentelle, numeriske og empiriske metoder.

En komplett prosedyre for å anslå de hydrodynamiske parameterne blir foreslått. Prosedyren består av en empirisk metode som bruker enkle empiriske og analytiske koeffisienter og allerede veletablert teori. I tillegg er ny teori introdusert der manglende litteratur gjorde det nødvendig. Den empiriske kalkulasjonsmetoden er testet på fem forskjellige ROVer med veldig forskjellige karakteristikker. Prosedyren består også av en eksperimentell metode. Den eksperimentelle metoden er basert på en slepe/rotasjons-test utført i en slepetank. Her blir ROVen festet til en slepevogn som også har muligheten for å rotere. ROVen blir deretter slept eller rotert under vann og de kreftene som virker på ROVen blir registrert. Disse testene gjøres for ulike hastigheter og dempingskreftene kan deretter bestemmes ved å interpolere resultatene. Dette eksperimentet er designet for å være billig og for å kunne gjennomføres i løpet av relativt kort tid. Den eksperimentelle metoden blir testet på ROV Neptunus og VideoRay Pro-4 som er to relativt små

ROVer med ganske forskjellige karakteristikker. De forskjellige karakteristikkene gjør at robustheten til prosedyren blir evaluert for geometrier som avviker ganske mye.

Computational Fluid Dynamics(CFD) og potensialteori blir brukt for å verifisere de to metodene ved sammenligning av de oppnådde resultatene. Den hydrodynamiske massen blir sammenlignet med resultater produsert i WADAM (Wave Analysis by Diffraction and Morison Thoery) som er et panelprogram i DNVs Sesam programpakke. De empiriske resultatene for hydrodynamisk masse korresponderer bra med de resultatene oppnådd i WADAM. Den relative forskjellen er for translasjonsfrihetsgradene i området 10 til 20% og for rotasjonsfrihetsgradene i området 30-100%. Disse resultatene viser at den empiriske metoden har rom for forbedring, men tatt i betraktning metodens enkle natur og den relativt komplekse geometrien på referanse ROVene er resultatene ganske nøyaktig.

Dempingskreftene blir sammenlignet med Flow Simulation som er et CFD-program i SolidWorks programpakken. De empiriske og eksperimentelle resultatene viser lovende resultater med unntak av de eksperimentelle resultatene oppnådd for VideoRay Pro-4. For VideoRay Pro-4 er den eksperimentelle dempingen mye større enn det som er oppnådd i de empiriske og numeriske analysene. De avvikende resultatene fra dette eksperimentet tyder på feil at feil resultat ble registrert i eksperimentet, men det er vanskelig å anslå hvor feilen ligger. Den empiriske metoden overestimerer generelt dempingen, men ligger hovedsakelig i korrekt område. Den eksperimentelle dempingen for ROV Neptunus stemmer godt overens med CFD-resultatene.

Prosedyren som er utarbeidet presenterer en robust måte å bestemme de hydrodynamiske koeffisientene for en ROV med relativ usikkerhet på mindre enn 100%. Metoden har stort rom for forbedring, spesielt den eksperimentelle prosedyren kan bli forbedret en god del. Dette på bakgrunn av de sprikende resultatene oppnådd for de to ROVene som ble testet eksperimentelt.

CONTENTS

LIST OF FIGURES

Page

LIST OF TABLES

Page

LIST OF SYMBOLS

β	Phase angle
η	Earth fixed position vector
ω	Frequency
Ω	Non dimensional frequency
ω_n	Natural frequency
$\vec{\omega}$	Rotation Vector
ω_{bn}^b	Body-fixed angular velocity
ρ	Fluid density
λ	Scaling factor
λ	Wave length
ν	Velocity vector (BODY)
$\dot{\nu}$	Acceleration vector (BODY)
ν_c	Velocity vector of waves/current
ν_{rel}	Relative Velocity vector
$\dot{\nu_c}$	Acceleration vector of waves/current
σ	Standard deviation
τ	Body fixed forces
τ_{rad}	Radiation induced forces
τ_{Diff}	Diffraction induced forces
Θ	Attitude(Euler angles)
ϕ	Velocity potential
ϕ_2	2nd order Velocity potential

Φ	Non dimensional Velocity potential
ζ	Surface elevation
ζ_a	Wave amplitude
$1D$	1 dimensional
$2D$	2 dimensional
$3D$	3 dimensional
A_D	Amplitude of oscillating drag force
A_{jk}	Added Mass Force in $\boldsymbol{j}$ DOF due to acceleration in $\boldsymbol{k}$ DOF
A_R	Reference Area in strip theory calculations
B	Buoyancy Force
B_{jk}	Damping in $\boldsymbol{j}$ DOF due to velocity in $\boldsymbol{k}$ DOF
B_{jk}^{LIN}	Linear damping in $\boldsymbol{j}$ DOF due to velocity in $\boldsymbol{k}$ DOF
B_{jk}^{NL}	Quadratic damping in $\boldsymbol{j}$ DOF due to velocity in $\boldsymbol{k}$ DOF
C_a	Coefficient for finding added mass in DNV-table[29]
C_A	Added mass Coriolis and centripetal matrix
C_D	Drag Coefficient
C_{jk}	Restoring Force in $\boldsymbol{j}$ degree of freedom due to position in $\boldsymbol{k}$ degree of freedom
C_L	Lift Coefficient
C_M	Mass Coefficient
C_p	Projected Area Coefficient of ROV
C_{RB}	Rigid body Coriolis and centripetal matrix
D_M	Damping due to vortex shedding(Morrison's damping)
D_P	Potential(wave) damping
D_{RAD}	Radiation damping
D_S	Skin friction damping
D_W	Wave drift damping(2nd order)
f_b^b	body-fixed force
f_b^n	Buoyancy force vector (NED)
f_g^n	gravity force vector (NED)
F_D	Drag Force
F_L	Lift Force
$F_{quadrant}^j$	Drag force acting on quadrant in j-DOF
$g(\eta)$	Restoring matrix
I_j	Moment of inertia in $\boldsymbol{j}$ DOF
I_{jk}	Product of inertia in $\boldsymbol{j}$ DOF due to rotation in $\boldsymbol{k}$ DOF
k	Wave Number
m	Mass

m_a	Added mass force in single DOF system
M_A	Added mass matrix
m_b^b	Body-fixed moment
M_{FK}	Froude-Kriloff force matrix
M_{RB}	Rigid body mass matrix
$M^j_{quadrant}$	Drag Moment acting on quadrant in j-DOF
n	Normal Vector
N_V	Viscous damping due to current/waves
p	Pressure
$p^n_{b/n}$	NED position
R_N	Reynold's Number
$R^n_b(\Theta_{nb})$	Translational transformation matrix
r^b_g	Vector from o_b to COG expressed in BODY-coordinate system
St	Strouhal Number
$T_\Theta(\Theta_{nb})$	Rotational transformation matrix
T	Wave period(can in some cases denote kinetic energy
V	Fluid velocity vector
W	Gravity Force
v^b_{bn}	Body-fixed linear velocity
$\overline{X}$	Position in 1 DOF system
z_g	Vertical distance between center of origin and center of gravity

LIST OF ABBREVIATIONS

DOF	Degree of freedom
AUV	Autonomous Underwater Vehicles
BBC	Bottom Boundary Condition
$\overline{BG}$	Distance between center of gravity and center of buoyancy
$\overline{OB}$	Distance between center of coordinate system and center of buoyancy
BODY	Body fixed reference frame (body fixed coordinate system)
CAD	Computer Aided Design
CFD	Computational Fluid Dynamics
CO	Center of Origon of body fixed coordinate system
COB	Center of Buoyancy
COG	Center of Gravity
DFSBC	Dynamic Free Surface Boundary Condition
DNV	Det Norske Veritas
GZ	Vertical distance from Center of Gravity to origin of coordinate system
IMU	Inertial Measuring Unit
KFSBC	Kinematic Free Surface Boundary Condition
LBC	Lateral Boundary Condition
NACA	National Advisory Committee for Aeronautics
NED	North-East-Down reference frame (earth-fixed)
NURB	Non-Uniform Rational B-Spline
OpenFOAM	Open source Field Operation And Manipulation
PMM	Planar Motion Mechanism
RANS	Reynold averaged Navier Stokes
RMS	Root Mean Square
ROV	Remotely Operated Vehicle
SNAME	Society of Naval Architects and Marine Engineers
UUV	Unmanned Underwater Vehicle
WADAM	Wave Analysis by Diffraction and Morison Theory
WAMIT	Wave Analysis at M.I.T

CHAPTER 1

INTRODUCTION

1.1 Background

Unmanned underwater vehicles(UUVs) are today common in deep water industries such as oil and gas exploration, telecommunications, geotechnical investigations and mineral exploration[22]. Most underwater vehicles are either box shaped or slender and cylindrically shaped. The design depends on which operations the UUV is designed for. One type of UUVs are the Remotely Operated Vehicles.(ROVs) ROVs are the workhorses in subsea engineering and the tasks performed by ROVs become increasingly more challenging. For ROV's the operating velocities are usually fairly small and they are therefore most often designed as a box. This design enables the ROV to carry different equipment and tools rather than having good hydrodynamic properties(i.e. low drag). For AUVs high cruising velocities and range are important hence they are usually designed as slender cylinders to achieve small drag forces.

The hydrodynamic properties of UUVs describes the behaviour of the UUVs when operating in water. Required thrust, operational range, maximum speed and manoeuvrability are just some of the characteristics dictated by the hydrodynamic properties. It therefore follows that hydrodynamic properties plays a crucial role for the performance of UUVs. Hence knowledge of these properties are important not only for controller purposes or in the operational phase, but also in the design phase as good knowledge about the hydrodynamic properties can optimize the design and improve performance. In most cases theoretical derivation of these values is practically impossible, and experimental measurements are generally complicated and expensive[21].

In the design stage of a UUV empirical calculations can often estimate the hydrodynamic parameters with sufficient accuracy if only brief estimates are needed. However if accurate parameter estimation is required real experiments are often needed.

Different experimental procedures exist, but the most conventional procedures involve towing tank trials of the vehicle itself or of a scaled model of the vehicle, expecting, in this case an error in the estimate of some parameters up to 50%[17]

Literature suggests some experimental methods concerning particular procedures where on-board sensor data is used without requiring any towing tank tests[17]and [20]. In [21] an on-board sensor experiment is described using a Inertial Measuring Unit. Here the "known" thrust force is applied and the resulting acceleration is measured. This method shows great potential, but the numerical results are not satisfactory. One big weakness in these types of experiments comes from the fact that the thrust force must be known. As variation of the ROV configuration and velocity affects the thrust forces supplied by the thrusters accurate knowledge of the thrust can be hard to obtain. In Caccia 2000[17] a procedure of modelling the propeller-hull interactions is introduced. However also here it is experienced relative large error in estimates, especially the inertia forces are inaccurate.

Another experimental method using pendulum motion is described in Eng et. al 2009.[15]. In this experiment the accuracy towards the reference CFD estimates are very good with a relative difference of a few %. However this method is time consuming and cannot be adapted to account for varying ROV configuration

Little literature is presented on empirically or analytically estimating the hydrodynamic coefficients. Empirically or analytically estimates are usually only used for reference values due to the generally poor accuracy of the estimates. As the empirical estimates presented in literature is usually based on basic formulas such as DNV-standards[29] and Blevins 2003[4] big improvements can be done on these estimates to increase accuracy.

One of the greatest problems encountered i designing model based controllers for the vehicles is the difficulty in knowing the values of the hydrodynamic coefficients. As the tasks performed by UUVs become increasingly more challenging the performance requirements for the automatic controllers also become higher. Designing model based control systems can therefore be challenging since these controllers require accurate parameters.

1.2 ROVs

Multiple ROVs are used as reference in this thesis. The method developed will be applied to a total of 5 different ROVs. The characteristics of these ROVs are completely different. The mass of the ROVs vary from 3 kg to almost 2000 kg and the shapes vary from NACA-foil shaped to prismatic shaped. The ROVs chosen for this thesis are all ROVs that can potentially be tested experimentally as they are owned and operated by NTNU. The different ROV characteristics will help to verify the versatility of the method developed. In this section these ROVs will be presented. Note that detailed information regarding the ROVs can be found in appendix E.

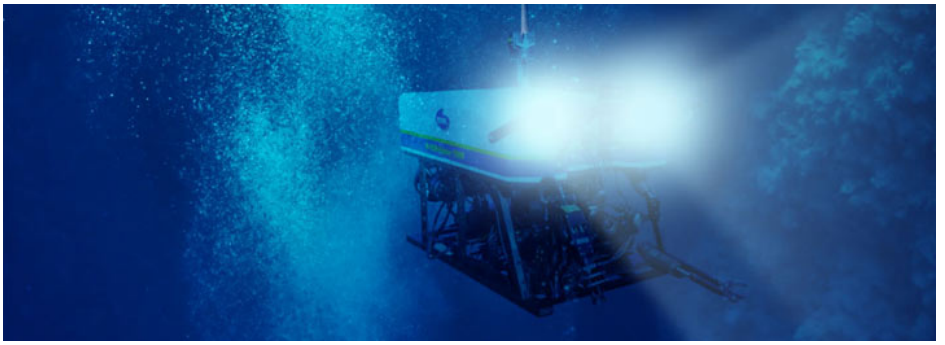

Figure 1.1: Illustration photo of submerged ROV (taken from http://sperre-as.com/produkter/rov/systemer/)

1.2.1 Sf-30k

The SF-30k is a standard ROV model produced by Sperre ROV technology. The standard design makes makes CAD-models and other data easy to obtain. For custom made ROV's like NTNU's Minerva [33] this data could be difficult to obtain.

(a) Standard SF-30k ROV (taken from www.Sperre-as.com)

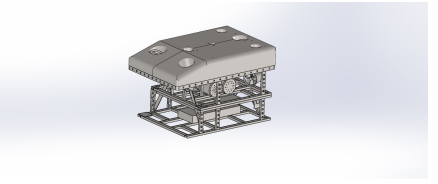

(b) CAD model of SF-30k ROV(Taken from [25])

Figure 1.2: SF-30k ROV

Specifications

The main dimensions for the SF-30k are shown in the table below. Note that center of gravity and center of buoyancy are given as distance relative to the topside. (In addition it is worth mentioning that the center of buoyancy and projected areas are taken from a simplified CAD-model created by V. Berg 2012[25])

Sf-30k	*Parameter*	*Value*
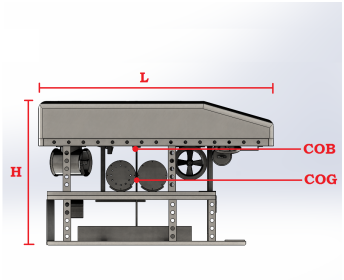	Mass	1862.87 kg
	Length	2500 mm
	Height	1500 mm
	Width	1600 mm
	COG(Z)	856.1 mm
	COB(Z)	468.6 mm
	Projected Area front	1678091 mm^2
	Projected Area side	1956253 mm^2
	Projected Area top	4 000 000 mm^2

Table 1.1: Dimensions of SF-30k

Design

The Sf-30k has a very standard ROV hull design. It has an open frame powered by 6 thrusters supplying 3kW of power each.[32] The top speed is achieved at 2.1 knots(1.1 m/s) in surge. The open frame has much space for installing tools and equipment and the total payload carried can be up to 60kg. The ROV has a topside buoyancy element giving an almost neutrally buoyant vessel.

1.2.2 ROV Netpunus

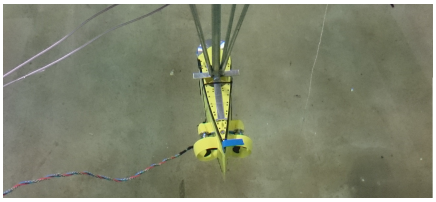

(a) Picture of ROV Neptunus

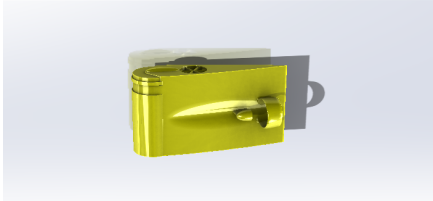

(b) CAD-model of ROV Neptunus

Figure 1.3: ROV Neptunus

ROV Neptunus is a small foil shaped ROV developed by students at NTNU.[1] ROV Neptunus is based of a NACA foil to give low resistance in surge. The electric components and thrusters are taken from the openROV which is an open source, low cost exploration ROV.[36].

Specifications

The mass of the ROV is 3.46 kg hence the weight in air is 33.94 N. The ROV is neutrally buoyant which means a buoyancy force of 33.94 N. The top speed is 1 m/s and maximum forward thrust delivered by the two horizontal thrusters is 12 N. The center of gravity (COG) is located at $(145mm, 0, 100mm)$ from the front bottom center line. The center of Buoyancy (COB) is located 30 mm directly above the COG. The ROV is therefore passive stable in pitch and roll. The ROV has a total of 3 thrusters, 2 which produces thrust in surge and 1 that produces thrust in heave. The ROV is under actuated since sway cannot be controlled.

ROV Neptunus	*Parameter*	*Value*
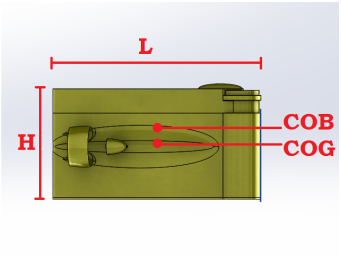	Mass	3.46 kg
	Length	404 mm
	Height	214 mm
	Width	108 mm
	COG(Z)	100 mm
	COB(Z)	130 mm
	Projected Area front	23112 mm^2
	Projected Area side	1956253mm^2
	Projected Area top	86456 mm^2

Table 1.2: Dimensions of ROV Neptunus

Design

The body of the ROV is based on the NACA foil series with minimization of forward drag as the highest priority(surge). The hull consists of a multiple plastic sections glued together and a transparent plastic cylinder located in the front which contains the electric equipment such as camera and sensors. The battery package is located inside the foil to create a passive stable vehicle.

[1] The ROV was designed by Jostein Follestad at NTNU during the autumn of 2014.

1.2.3 Seabotix LBV600-6

LBV600-6 is a small workclass ROV produced by Seabotix. CAD-data is for this ROV hard to obtain and therefore have to be created.

(a) Standard LBV600-6 ROV (taken from http://www.seabotix.com/)

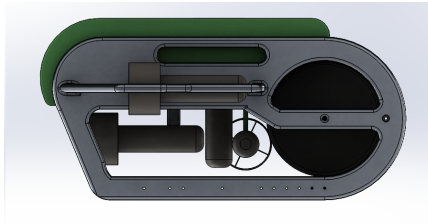

(b) CAD model of LBV600-6

Figure 1.4: Seabotix LBV600-6

Specifications

The ROV is neutrally buoyant with a weight in air of 15.3 kg. It has a top speed in surge of 1.8 m/s. The ROV is powered by 6 brushless thrusters each supplying approximately 30 N of thrust. There are 4 thrusters in surge direction, 1 vertical and 1 thruster in sway direction. The center of gravity(COG) is located at (278mm,0, 135mm) from the front bottom center line. Center of Buoyancy (COB) is located 30 mm vertically above COG.

Seabotix LBV600-6	*Parameter*	*Value*
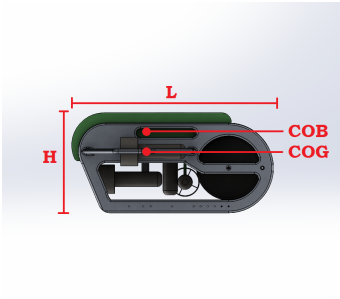	Mass	15.3 kg
	Length	540 mm
	Height	270 mm
	Width	484(300) mm
	COG(Z)	135 mm
	COB(Z)	165 mm
	Projected Area front	69063 mm^2
	Projected Area side	103104mm^2
	Projected Area top	142275 mm^2

Table 1.3: Dimensions of Seabotix LBV600-6

Design

The body of the ROV is based of a prismatic shape with smooth edges. The front is cylindrically shaped to reduce forward drag. A bumper frame covers the sides

of the body to reduce damage on vital components in case of a collision. Below the camera housing in the front there is a mounting bracket to install a grabber. The buoyancy element is placed on the top which gives a passively stable vehicle.

1.2.4 AC-ROV 100

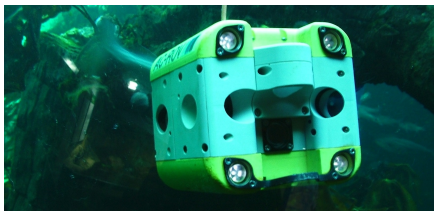

(a) Standard AC-ROV 100 (taken from http://www.ac-cess.com/gallery)

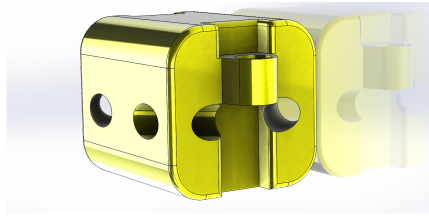

(b) CAD model of AC-ROV 100

Figure 1.5: AC-ROV 100

AC-ROV 100 is a small observation class ROV produced by AC-Cess. Its special design enables the ROV to have great manoeuvrability in surge, sway, heave and yaw . Its small size makes it practical for inspection, however the ROV can only carry a payload of 200 grams

Specifications

The ROV is neutrally buoyant with a weight in air of 3 kg which makes it approximately the same size as ROV Neptunus. The ROV is powered by 6 thrusters. There are 4 vectored thrusters in the horizontal plane and 2 vertical thrusters. The center of gravity(COG) is located at (112mm,0, 74mm) from the front bottom center line. Center of Buoyancy (COB) is set to be located 20 mm vertically above COG.

AC-ROV 100	*Parameter*	*Value*
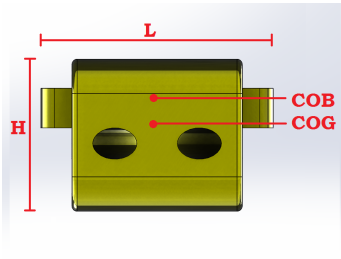	Mass	3 kg
	Length	203 mm
	Height	152 mm
	Width	146 mm
	COG(Z)	74 mm
	COB(Z)	94 mm
	Projected Area front	21554 mm^2
	Projected Area side	30450mm^2
	Projected Area top	32212 mm^2

Table 1.4: Dimensions of AC-ROV 100

Design

The ROV is based of a prismatic shape with rounded off edges. Contrary to many other ROVs this frame is not open. The 4 horizontal thrusters are positioned inside the body and all are vectored. The vectored thrusters gives the ROV equal thrust in surge, sway and yaw. This again gives the ROV good manoeuvrability. However the closed frame, relative large projected areas and vectored thrusters gives bad hydrodynamic properties especially in surge. This because the drag forces will be quite large and the thrusters will give a large thrust in unwanted DOFs.(when moving purely in surge direction thrust will still be applied in the sway DOF)

1.2.5 VideoRay Pro 4

(a) Standard VideoRay Pro 4 (taken from http://www.atlantasmarine.com/product/videoray-pro-4)

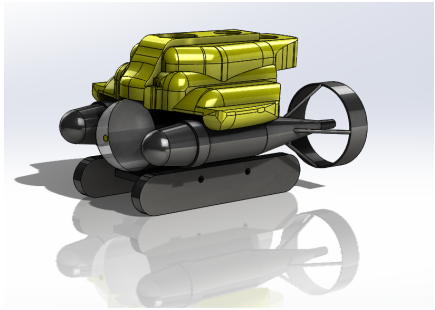

(b) CAD model of VideoRay Pro 4

Figure 1.6: VideoRay Pro 4

VideoRay Pro 4 is a small observation class ROV equipped with 3 thrusters. It has a mass of 6.1 kg. The ROV can be modified with extra equipment to fulfil a number of different tasks such as grabbing and lifting.

Specifications

The ROV is equipped with 3 thrusters, 2 in surge direction and 1 vertical. The sway DOF can hence not be controlled which makes the ROV under actuated.

VideoRay Pro-4	*Parameter*	*Value*
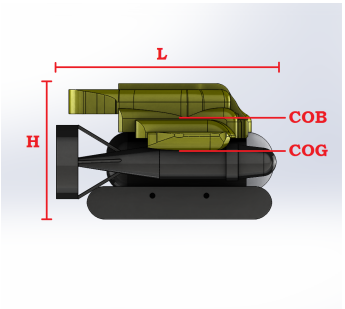	Mass	6.1 kg
	Length	375 mm
	Height	289 mm
	Width	223 mm
	COG(Z)	110 mm
	COB(Z)	140 mm
	Projected Area front	40000 mm^2
	Projected Area side	63753mm^2
	Projected Area top	70518 mm^2

Table 1.5: Dimensions of VideoRay Pro-4

Design

VideoRay PRO-4 has a smooth bluff hull made up by cylindrical elements. In the center a cylinder containing electrical equipment such as camera and motherboard etc. is located. The horizontal thrusters are mounted behind the ROV while the vertical thruster is mounted in the center vertical axis of the ROV(about right above the center of gravity). The buoyancy element is quite complex and therefore hard to create accurately using a CAD-tool. Some error in the CAD-file is therefore expected.

1.3 Methods for Determining Hydrodynamic Parameters

There are a number of different ways to determine the hydrodynamic coefficients for UUVs ranging from simple empirical estimates to advanced experimental procedures. In this section a variety of different methods is discussed. It should be noted that only a handful of methods are mentioned of the many different methods available.

1.3.1 Empirical Estimates

Strip Theory

In order to calculate the coefficients for a ROV strip theory can be used. Strip theory is based on the assumption that a 3-D body can be evaluated as a sum of 2-D strips along the body. Strip theory assumes that the variation of the flow in the cross-sectional plane is much larger than the variation of the flow in longitudinal direction. For a ROV this will not be correct at the ends of the body and will thus

give an error in the calculations.

Today strip theory is used widely due to the fact that other methods are often very complex and may not give better results.
The basic assumption in strip theory is that the length of the body is much greater than the width. Physically this assumption means that the contributions from the edges would be insignificant. However for a ROV the length is of the same order as the width. It therefore follows that for a ROV strip theory would not give very good results. However if the error of strip theory can be estimated and then be accounted for it can still provide good results.

Figure 1.7 shows how the strips can be divided. (here a 2D-rectangle is used as reference geometry)

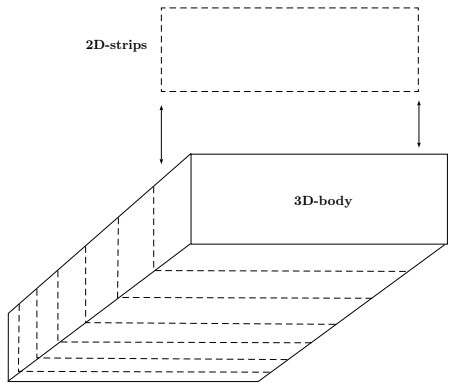

Figure 1.7: 2D-strips

Empirical 3D data

Another way to calculate the hydrodynamic coefficients for the ROV is by assuming a shape where experimental results or empirical and analytical solutions exists. As many ROVs are very similar to a prism one can often assume this shape. The main difference between a prism and a ROV is that a ROV is not a solid block, but more carved out. In other words water has the ability to flow through the ROV. This difference needs to be taken into account. A possible way of adjusting the results for a prism is to use the projected area of the ROV and scale the prism-result after this.
A rectangular prism is a very common object which is easy to analyse. It therefore exists very accurate results and empirical /analytical data for this shape. The main challenge will be to convert these data to a ROV. Here engineering intuition and experience comes into play.
The DNV standard is a fairly good reference for these data[29] in addition to Blevins 2003[4].

1.3.2 Potential Flow Theory

Panel methods(WAMIT/WADAM)

A good way to find the hydrodynamic coefficients for a ROV is to use the panel method. The principle behind the panel method builds on the solution of the Green integral equation:

$$\frac{1}{2}\phi_i + \sum_{j=1}^{N} \phi_j \int_{S_j} \mathrm{d}S_X \frac{\mathrm{d}G(\vec{X};\vec{\varepsilon_i})}{\mathrm{d}n_j} = \sum_{j=1}^{N} V_j \int_{S_j} \mathrm{d}S_X G(\vec{X};\vec{\varepsilon_i}) \qquad i = 1:N \tag{1.1}$$

Where i is the facet number, ϕ_i is the unknown velocity potential value and S_j is the surface of each panel

The structure is divided into small 2D or 3D panels. By solving the green integral equation for each element the value of the velocity potential over each element is found. When the velocity potential over the entire surface of the body is known the dynamic pressure can easily be found using the relation:

$$P_{dyn} = -\rho \frac{\mathrm{d}\phi}{\mathrm{d}t} \tag{1.2}$$

Then by applying the Bernoulli equation:

$$\frac{\mathrm{d}\phi}{\mathrm{d}t} + \frac{1}{2}|\nabla\phi|^2 + \frac{P}{\rho} + gz = C \tag{1.3}$$

the velocity over the surface can be found.

Then by integrating the velocity potential over the body one can find potential damping and added mass.

$$A_{kj}(\omega) = \Re\Big[\rho \int_{S_{OB}} \phi_j n_k \mathrm{d}S\Big] \tag{1.4}$$

$$B_{kj}(\omega) = -\omega\Im\Big[\rho \int_{S_{OB}} \phi_j n_k \mathrm{d}S\Big] \tag{1.5}$$

A great advantage of using this procedure is the fact that very accurate results are obtained in relative short time and the computer resources required are not very big. A disadvantage using panel method is the fact that viscous damping can not be found since potential theory assumes irrational, incompressible and inviscid fluid whereas the latter requirement makes finding viscous forces impossible. For a ROV operating far below the surface, potential damping i.e. surface wave damping is very limited, in practice zero for large depths. This means that for ROV's panel methods are not able to say anything about the damping.

There are many programs that uses the panel method mentioned above. A very recognized program is WAMIT(Wave Analysis M.I.T). This program is able to estimate added mass,restoring and potential damping coefficients fairly quick compared to CFD analysis which takes much time and processor power. In this thesis WADAM will be used instead of WAMIT. WADAM is a program in the DNV GL software package SESAM. It is stated in the WADAM software information that the diffration-radiation part of the program is based on WAMIT.[31]

Sink/source method

Sink/Source method build on the same principle as the panel method. Which is to find the velocity potential of the flow domain. In the panel method mentioned in the previous section however a vector with values for each panel is found while in the sink/source method a function for the velocity potential of the entire flow domain is found. This is done by placing a number of sinks, sources and vortices to generate the desired geometry i.e. a ROV shape. It can be shown by using potential flow theory and the principle of continuity that the velocity potential for a source and a sink can be written:(sink is defined as a negative source)

$$\phi_{sink/source} = \frac{Q}{2\pi} ln(r) \tag{1.6}$$

where Q is the volume flow pr. unit time and r is the distance from the source/sink center. Using the same approach it can be shown that the velocity potential for a vortex can be written:

$$\phi_{vortex} = \frac{\Gamma}{2\pi}\theta \tag{1.7}$$

Where Γ is the circulation and θ is the angle relative to the flow or reference coordinate system. In figure 1.8 is a streamline plot of a symmetric foil generated by a sink and a source of equal strength(rankine oval)created in Matlab

Once enough sinks, sources and vortices are created to generate the desired geometry the total velocity potential is analysed and based on this velocity potential velocities and pressures are found using the same approach as for the panel method. The advantages and disadvantages are thus similar for this method as for the panel method.

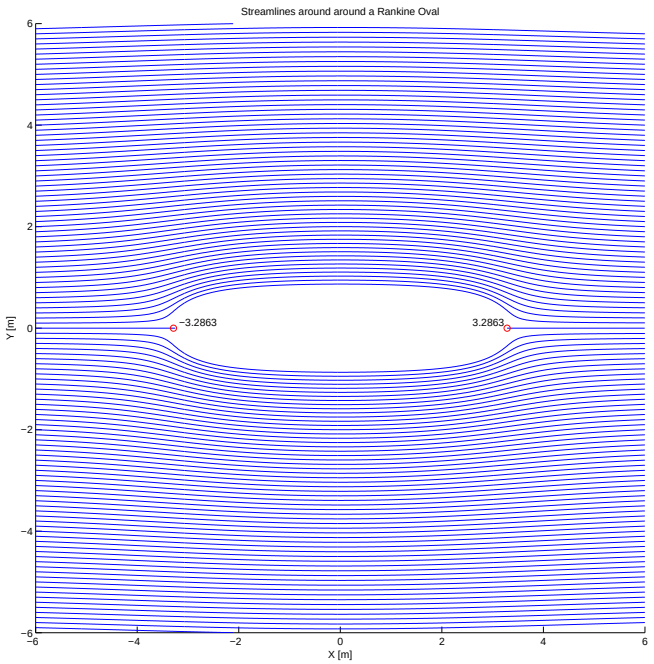

Figure 1.8: Rankine Oval

1.3.3 Experimental Methods

The best way of determining hydrodynamic coefficients are to perform full scale experiments and record the exact results for the ROV. This can be done with a number of different experiments. Sometimes model tests may be the better option due to equipment and cost limitations.

Pendulum Experiments

A pendulum experiment may be performed in different ways but the basis for all experiments are the same. The full or model scale ROV is connected to a string as a pendulum and is displaced and released.[13] By measuring the position of the ROV-pendulum over time the damping and added mass forces can be calculated.

Towing test and rotation test

A regular towing experiment combined with a rotational experiment can give all the diagonal coefficients for a ROV. This is done by first performing a towing test at low speed and increasing the speed until the maximum velocity of the ROV to determine the quadratic damping and linear damping. The resulting damping forces can then be interpolated to obtain both the quadratic and linear damping functions. Then accelerated runs are performed for different accelerations. The force at given velocities are measured and from this it is possible to subtract the already obtained damping and rigid body mass forces. The remaining force will be a result of added mass. This exact same procedure is repeated for the rotational experiment. Here torque is measured and the damping moment and added mass moment can be found. This procedure is fairly easy to perform if a towing tank is available, but can be quite time consuming.

On-board sensor experiment

On-board sensor experiments are a type of experiments where a UUV is equipped with on-board sensors to measure e.g. the acceleration of the vehicle for a given thrust input. The recorded acceleration data is then filtered and used to determine the inertia and damping terms. These methods are described in Caccia et. al[17] and Ridao et. al[20] among others.

These methods have a great advantage in that they can be performed without the use of external equipment and can be performed every time the ROV-setup is changed. The disadvantage is that the accuracy of the results are very dependant on the sensors and test procedures performed. In this method the potential for errors is also quite big. In Conte et. al[21] an approximate inertia of a 200 kg ROV(assuming 100 kg added mass) is found to be almost 700 kg, which is a very large error.

Planar Motion Mechanism Tests

A planar motion mechanism(PMM) is a movement arm which is able to rotate in a given number degrees of freedom.[16] By translating/rotating the ROV while measuring resistance it is possible to obtain the coefficients for the ROV. Since a PMM mounted in a towing tank is able to move in multiple degrees of freedom simultaneously the coupled coefficients are also possible to estimate.[15]
One weakness of this method is the scaling from model scale to full scale. The error from this scaling depends on the scaling procedure being used, but it is usually not very significant. However if the PMM is sufficiently big(or the ROV small enough) a full scale test may be performed for the ROV.

1.3.4 CFD

Computational Fluid Dynamics is a relative new way of working with fluid dynamics. CFD builds on solving the Navier-Stokes equations. The Navier-Stokes equations for 2D incompressible flow can be written[4]:

$$\frac{\partial u}{\partial t} + u\frac{\partial u}{\partial x} + v\frac{\partial u}{\partial y} = \frac{X}{\rho} - \frac{1}{\rho}\frac{\partial P}{\partial x} + v(\frac{\partial^2 u}{\partial x^2} + \frac{\partial^2 u}{\partial y^2}) \tag{1.8a}$$

$$\frac{\partial v}{\partial t} + u\frac{\partial v}{\partial x} + v\frac{\partial v}{\partial y} = \frac{Y}{\rho} - \frac{1}{\rho}\frac{\partial P}{\partial y} + v(\frac{\partial^2 v}{\partial x^2} + \frac{\partial^2 v}{\partial y^2}) \tag{1.8b}$$

where :

Parameter	*Definition*
P	Fluid static pressure
t	Time
u	Fluid velocity in x direction
v	Fluid velocity in y direction
x	Coordinate axis
X	Body force on fluid in x direction
y	Coordinate axis, perpendicular to x
Y	Body force on fluid in x direction
ρ	fluid density
v	kinematic viscosity

Table 1.6: Parameters in 2D incompressible Navier Stokes equations

Due to the nature of these equations CFD requires very much computing power. It was therefore not possible to perform advanced CFD analysis until recent times. Since the average computing power has increased exponentially since the 60's(Moore's Law)[2] it is no doubt that CFD has a bright future.

ANSYS Fluent

It is a very renowned state of the art program used by many prestigious universities such as MIT, Delft and NTNU. Ansys Fluent provides a good number of turbulence models such as RANS(Reynolds Average Navier Stokes) and LES.(Large Eddy Simulation) The validity of this program depends on the problem to be solved and how the problem is solved. The results therefore need as for all CFD programs to be evaluated afterwards to make sure the physics behind is correct.

[2] In 1965 Gordon E. Moore described the trend that the number of transistors in a dense integrated circuit would double approximately every 2 years

OpenFOAM

OpenFOAM is an open source CFD program with over 80 solver functions. It is very versatile and enables the user to modify and extend the existing functionality. OpenFOAM includes RANS solvers,Eddy simulations and direct numerical simulation. The program therefore enables the user to modify the program to fit its need. OpenFOAM may be an alternative to perform CFD calculations or at least to verify established results.

SolidWorks Flow Simulation

SolidWorks is the main CAD-software used in this thesis.It is a 3D-CAD software that contains a number of different functions. One of these is the Flow simulation package. Flow Simulation is a CFD software which is very easy to use, but the limitations are also quite big mainly due to the meshing process. The user has little control over the meshing which can become a problem when performing convergence tests. When benchmarked against established results [4] for a circular cylinder and square rod the drag coefficient were very accurately predicted. It is therefore fair to have reasonable belief in the results obtained by SolidWorks Flow Simulation, but the results still need to be validated against other references. Flow simulation uses k-ϵ-model and Law of the wall to calculate the turbulence properties for the flow[34]. In addition Flow Simulation utilises an adaptive meshing function, which automatically refines the mesh in areas with large gradients during calculations.

1.4 Outline of Thesis

In this thesis a complete procedure for determination the hydrodynamic coefficients of a small scale ROV is presented. The procedure is tested on multiple ROVs to evaluate accuracy and robustness.

The structure of this thesis is as follows:

In chapter 2 the dynamic equation of motion for a typical ocean vessel moving in 6 degrees of freedom is derived. Basic hydrodynamic theory relevant for a ROV is then derived before the equation of motion is applied for a submerged ROV to obtain the relevant hydrodynamic coefficients.

Chapter 3 presents a procedure developed for determining the relevant hydrodynamic coefficients derived in chapter 2. This includes empirical, experimental and numerical estimates.

Chapter 4 presents the results from the parameter estimations discussed in chapter 3 when applied to the different ROVs mentioned in the introduction.

Chapter 5 contains a discussion regarding the obtained results and evaluation of the procedure. Evaluation of the performance and accuracy of the procedure is also discussed.

Chapter 6 is a presentation of the concluding remarks and suggestions for further work

CHAPTER 2

MATHEMATICAL MODELLING

The goal of this chapter is to quantify the different hydrodynamic properties that dictates the behaviour of a typical ROV. The equation of motion connects the external forces such as current, waves and viscous forces with the rigid body mass(inertia) forces. It therefore follows that if the external forces can be estimated accurately the corresponding motion of the ROV can be predicted accurately. It is therefore crucial that the equation is able to describe the relationship between the different external and internal forces. Some forces can be neglected due to size or symmetry condition, but this requires verification that the equation of motion will in fact be able to describe the system properly.

This is done by deriving and evaluating the dynamic equation of motion for a typical offshore vessel moving in 6 degrees of freedom(6DOF). Then basic hydrodynamic theory such as wave theory and vortex shedding theory is introduced to create the hydrodynamic foundation for further work.

Lastly by applying the hydrodynamic theory combined with basic symmetry conditions to the dynamic equation of motion the equation can be used to represent a typical ROV operating far below the free surface. The resulting equation of motion will then describe the properties of the ROV accurately and contain all the parameters of interest. It will hence be the cornerstone for further work in this thesis

2.1 Dynamic Equation of motion

The goal for this section is to establish the equation of motion for a typical ocean vessel. This equation will create a basis for the further work in this thesis. The parameters going into the equation of motion will dictate the behaviour of the vessel. Hence the problem of determining the properties of the vessel actually is the same as finding the parameters in the equation of motion. The theory in this section is mainly taken from Fossen 2011[5]

A rigid body has the ability to move in a total of 6 degrees of freedom(6DOF).
3 translations(surge,sway, heave)and 3 rotations(roll,pitch,yaw)
For marine vessels there are a number of different notations which are used today, one of them is the SNAME notation.(table 2.1) In this thesis the SNAME notation will be used as the standard notation.

DOF	**Forces and Moments**	**Velocities**	**Positions & Euler angles**
Surge	X	u	x
Sway	Y	v	y
Heave	Z	w	z
Roll	K	p	ϕ
Pitch	M	q	θ
Yaw	N	r	ψ

Table 2.1: SNAME-notation[18]

2.1.1 Kinematics

It is natural to begin with the kinematics equations. Kinematics is the science of describing the various types of motion in themselves, leaving out of account the causes which initiates the motion.[12]

When analysing the 6 DOFs motion of a marine vessel it is convenient to define two coordinate systems. An earth-fixed(NED) system and a body fixed(BODY) coordinate system.

NED The North-East-Down (earth fixed) coordinate system is fixed with regards to the earth. It is usually defined as the tangent plane on the surface of the earth moving with the craft, but with axes pointing in different directions than the body-fixed axes of the craft[5]. For slow moving ocean vehicles the motion of the earth has little effect on the vehicles itself. Hence the earth-fixed coordinate system can be considered to be inertial. This again means that Newton's laws still applies.

BODY The body fixed system is a moving reference frame that is fixed to the craft. Usually the x-axis is longitudinal, y-axis transverse and z-axis vertical. The origin of the coordinate system can be set to a point of the body which simplifies the calculations. For surface ships this usually is midship at the waterline. In figure 2.1 the body-fixed coordinate system is defined at the at the center-top side of the ROV.

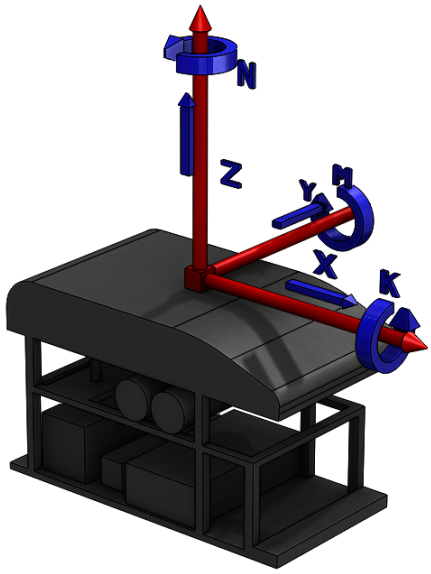

*Figure 2.1: Definition of forces and moments in coordinate system for rigid body motion modes(**BODY**)*

Based on the SNAME notation mentioned in the beginning of this section the general motion of a marine vehicle in 6 DOFs can be described by the following vectors:

Parameter	Total	Linear	Angular
NED position	$\eta = [\eta_1^T, \eta_2^T]^T$	$\eta_1 = [x, y, z]^T$	$\eta_2 = [\phi, \theta, \psi]^T$
BODY Velocity	$\nu = [\nu_1^T, \nu_2^T]^T$	$\nu_1 = [u, v, w]^T$	$\nu_2 = [p, q, r]^T$
BODY force/moment	$\tau = [\tau_1^T, \tau_2^T]^T$	$\tau_1 = [X, Y, Z]^T$	$\tau_2 = [K, M, N]^T$

Table 2.2: Vectors for describing motion of marine vehicles

In Fossen 2011[5](Chapter 2) it is shown that the transformation between the BODY and NED coordinate system can be expressed in vector form:

$$\begin{gathered} \dot{\eta} = \boldsymbol{J}_\Theta(\eta)\nu \\ \Updownarrow \\ \begin{bmatrix} \dot{\boldsymbol{p}}_{b/n}^n \\ \dot{\boldsymbol{\Theta}}_{nb} \end{bmatrix} = \begin{bmatrix} \boldsymbol{R}_b^n(\boldsymbol{\Theta}_{nb}) & \boldsymbol{0}_{3x3} \\ \boldsymbol{0}_{3x3} & \boldsymbol{T}_\Theta(\boldsymbol{\Theta}_{nb}) \end{bmatrix} \begin{bmatrix} \boldsymbol{\nu}_{b/n}^b \\ \boldsymbol{\omega}_{b/n}^b \end{bmatrix} \end{gathered} \tag{2.1}$$

Where :

$$\boldsymbol{R}_b^n(\boldsymbol{\Theta}_{nb}) = \begin{bmatrix} c\psi c\theta & -s\psi c\phi + c\psi s\theta\phi & s\psi s\phi + c\psi c\phi s\theta \\ s\psi c\theta & c\psi c\theta + s\phi s\theta s\psi & -c\psi s\theta + s\theta s\psi c\theta \\ -s\theta & c\theta s\phi & c\theta c\phi \end{bmatrix} \tag{2.2}$$

$$\boldsymbol{T}_\Theta(\boldsymbol{\Theta}_{nb}) = \begin{bmatrix} 1 & s\phi t\theta & c\phi t\theta \\ 0 & c\phi & -s\phi \\ 0 & s\phi/c\theta & c\phi/c\theta \end{bmatrix} \tag{2.3}$$

where $s\cdot = sin(\cdot)$, $c\cdot = cos(\cdot)$ and $t\cdot = tan(\cdot)$

2.1.2 Rigid Body Kinetics

In this section the forces and moments caused by rigid body inertia will be evaluated. From Newton's 2nd law one knows that the force acting on a system is equal to the product of the mass and acceleration of the system.($\Sigma F = ma$). Euler's axioms also states that this is valid for angular momentum as well as linear.[5] Using Newtons law and Euler's axioms the rigid body equations of motion around an arbitrary origin(CO) can be expressed as :

Translational :

$$m\left[\dot{\boldsymbol{v}}^b_{b/n} + \dot{\boldsymbol{\omega}}^b_{b/n} \times \boldsymbol{r}^b_g + \boldsymbol{\omega}^b_{b/n} \times \boldsymbol{v}^b_{b/n} + \boldsymbol{\omega}^b_{b/n} \times (\boldsymbol{\omega}^b_{b/n} \times \boldsymbol{r}^b_g)\right] = \boldsymbol{f}^b_b \tag{2.4}$$

and Rotational:

$$\boldsymbol{I}_b \dot{\boldsymbol{\omega}}^b_{b/n} + \boldsymbol{\omega}^b_{b/n} \times \boldsymbol{I}_b \boldsymbol{\omega}^b_{b/n} + m\boldsymbol{r}^b_g \times (\dot{v}^b_{b/n} + \boldsymbol{\omega}^b_{b/n} \times \boldsymbol{v}^b_{b/n}) = \boldsymbol{m}^b_b \tag{2.5}$$

By introducing the following notation

$\boldsymbol{f}^b_b$	$= [X, Y, Z]^T$	- force through o_b expressed in BODY-coordinate system
$\boldsymbol{m}^b_b$	$= [K, M, N]^T$	- moment about o_b expressed in BODY-coordinate system
$\boldsymbol{v}^b_{b/n}$	$= [u, v, w]^T$	- linear velocity of o_b expressed in BODY-coordinate system
$\boldsymbol{\omega}^b_{b/n}$	$= [p, q, r]^T$	- angular velocity BODY relative to NED expressed in BODY-coordinate system
$\boldsymbol{r}^b_g$	$= [x_g, y_g, z_g]^T$	- vector from o_b to COG expressed in BODY-coordinate system

The rigid body equations of motion can be written the following way:

$$\boldsymbol{M}_{RB}\dot{\nu} + \boldsymbol{C}_{RB}(\nu)\nu = \boldsymbol{\tau}_{RB} \tag{2.6}$$

The matrix $\mathbf{M}_{RB}$ is constant, symmetric and positive definite. It's unique parametrization is in the form[6]:

$$\mathbf{M}_{RB} = \begin{bmatrix} m\mathbf{I}_3 & -m\mathbf{S}(\mathbf{r}^b_c) \\ m\mathbf{S}(\mathbf{r}^b_g) & \mathbf{I}o_b \end{bmatrix} \tag{2.7}$$

The Coriolis matrix on the other hand does not have a unique parametrization, but can always be parametrized such that it is skew symmetrical[6]. Lastly it can be noted by looking at equations (2.4) and (2.5) that equation (2.6) can be greatly simplified if the origin of the body-fixed coordinate system is chosen coincident with the COG i.e $\mathbf{r}^b_g = 0$ and $\mathbf{I}_{ob}$ is a diagonal matrix.(given a symmetric body)

2.1.3 Hydrodynamics

In this subsection the major hydrodynamic effects on a rigid body moving through fluid will be evaluated. The different hydrodynamic aspects discussed here will be thoroughly evaluated in the next section. When evaluating the hydrodynamic forces for ocean vessels it is common to divide the problem into two separate problems, diffraction and radiation. The radiation forces are the forces acting on the body when its forced to oscillate with the wave excitation frequency in the absence of incoming waves. Diffraction forces are the forces that act on the body when its subjected to incident waves but restrained from moving. Hydrodynamic damping can not be completely described by potential theory. This is because the viscosity of water has to be modelled as it can for many ocean vessels affect the damping substantially.

Radiation forces

The radiation forces can be identified as a sum of three components:

- Added mass due to the inertia of the surrounding fluid
- Radiation-induced potential damping due to energy transported away from the body by the generated surface waves
- Restoring forces due to Archimedes principle

The two first terms come from the linear pressure part of the velocity potential of the oscillating body. While the last term come from the hydrostatic pressure term.[1] When the body is oscillating additional damping forces will affect the body in addition to the potential damping caused by generated waves. These contributions are mainly due to skin friction($\mathbf{D}_S$), 2nd order wave drift damping($\mathbf{D}_W$) and damping due to vortex shedding($\mathbf{D}_M$).

The contribution from these components can be expressed mathematically as:

$$\boldsymbol{\tau}_{rad} = -\mathbf{M}_A\dot{\nu} - \mathbf{C}_A(\nu)\nu - \mathbf{D}_{rad}(\nu)\nu - \mathbf{g}(\eta) \tag{2.8}$$

where $\mathbf{D}_{rad}(\nu) = \mathbf{D}_P + \mathbf{D}_W + \mathbf{D}_S + \mathbf{D}_M$

Added Mass

Added mass is the extra inertia mass force/moment added to the system when the body accelerates. According to Fossen 1994[7] added mass should be understood as pressure-induced forces and moments due to the forced motion of the body which are proportional to the acceleration of the body. By using potential theory the expression for the added mass forces can be found as shown below.(the derivation is in large part taken from Korotkin 2007[10])

Using the general equation for kinetic energy:

$$T = \frac{1}{2} m V^2 \tag{2.9}$$

combined with the velocity vector for a potential(irrational,inviscid and incompressible) flow:

$$V = -\nabla\phi \tag{2.10}$$

and evaluate the energy in the fluid between the body surface S and a stationary sphere Σ with radius a that contains the body gives the following expression:

$$T = \frac{1}{2}\rho \iiint_V \left[\left(\frac{\partial\phi}{\partial x}\right)^2 + \left(\frac{\partial\phi}{\partial y}\right)^2 + \left(\frac{\partial\phi}{\partial z}\right)^2 \right] dxdydz \tag{2.11}$$

By applying Green's transformation for two functions(ϕ_1 and ϕ_2) and taking into account that $\phi_1 = \phi_2 = \phi$ and $\Delta\phi = 0$ the kinetic energy can be rewritten to:

$$T = -\frac{\rho}{2} \iint_S \phi \frac{\partial\phi}{\partial n} dS - \frac{\rho}{2} \iint_\Sigma \phi \frac{\partial\phi}{\partial n} dS \tag{2.12}$$

The second term in equation(2.12) goes to zero as the radius of the control volume(stationary sphere) goes to infinity($a \to \infty$) Thus the total kinetic energy of the fluid outside the surface S become:

$$T = -\frac{\rho}{2} \iint_S \phi \frac{\partial\phi}{\partial n} dS \tag{2.13}$$

In Korotkin 2007[10] it can be seen that the velocity potential can be presented as a sum of linear components:

$$\phi = u\phi_1 + v\phi_2 + w\phi_3 + p\phi_4 + q\phi_5 + r\phi_6 \tag{2.14}$$

Inserting the expression for the velocity potential ϕ into equation (3.4) the kinetic energy can be written[10]:

$$T = \frac{1}{2} \sum_{i=1}^{6} \sum_{k=1}^{6} A_{ik} \nu_i \nu_k \tag{2.15}$$

where the values

$$A_{ik} = -\rho \iint_S \frac{\partial\phi_i}{\partial n} \phi_k dS \tag{2.16}$$

are the added mass terms.

The terms in the added mass matrix can be presented in the same manner as the mass in the rigid body motion:

$$\boldsymbol{M}_A \dot{\nu} + \boldsymbol{C}_A(\nu)\nu = \boldsymbol{\tau}_A \tag{2.17}$$

Where the added mass matrix is:

$$\mathbf{M}_A = \begin{bmatrix} X_{\dot{u}} & X_{\dot{v}} & X_{\dot{w}} & X_{\dot{u}} & X_{\dot{p}} & X_{\dot{q}} & X_{\dot{r}} \\ Y_{\dot{u}} & Y_{\dot{v}} & Y_{\dot{w}} & Y_{\dot{u}} & Y_{\dot{p}} & Y_{\dot{q}} & Y_{\dot{r}} \\ Z_{\dot{u}} & Z_{\dot{v}} & Z_{\dot{w}} & Z_{\dot{u}} & Z_{\dot{p}} & Z_{\dot{q}} & Z_{\dot{r}} \\ K_{\dot{u}} & K_{\dot{v}} & K_{\dot{w}} & K_{\dot{u}} & K_{\dot{p}} & K_{\dot{q}} & K_{\dot{r}} \\ M_{\dot{u}} & M_{\dot{v}} & M_{\dot{w}} & M_{\dot{u}} & M_{\dot{p}} & M_{\dot{q}} & M_{\dot{r}} \\ N_{\dot{u}} & N_{\dot{v}} & N_{\dot{w}} & N_{\dot{u}} & N_{\dot{p}} & N_{\dot{q}} & N_{\dot{r}} \end{bmatrix} \tag{2.18}$$

and the Coriolis added mass matrix is:

$$\mathbf{C}_A = \begin{bmatrix} (C_A)_{11} & (C_A)_{12} & (C_A)_{13} & (C_A)_{14} & (C_A)_{15} & (C_A)_{16} \\ (C_A)_{21} & (C_A)_{22} & (C_A)_{23} & (C_A)_{24} & (C_A)_{25} & (C_A)_{26} \\ (C_A)_{31} & (C_A)_{32} & (C_A)_{33} & (C_A)_{34} & (C_A)_{35} & (C_A)_{36} \\ (C_A)_{41} & (C_A)_{42} & (C_A)_{43} & (C_A)_{44} & (C_A)_{45} & (C_A)_{46} \\ (C_A)_{51} & (C_A)_{52} & (C_A)_{53} & (C_A)_{54} & (C_A)_{55} & (C_A)_{56} \\ (C_A)_{61} & (C_A)_{62} & (C_A)_{63} & (C_A)_{64} & (C_A)_{65} & (C_A)_{66} \end{bmatrix} \tag{2.19}$$

Potential Damping

Assuming potential flow theory it is possible to evaluate the forces acting on a body without the presence of friction. As the body moves in the water surface waves will be generated. By evaluating the velocity potential around the body the generated waves can be evaluated. Since the radiation potential can be difficult to determine the Haskind relation can be used to determine the radiation potential. When knowledge of the waves exist the energy transported away from the body is easily found using energy relations. The potential damping is usually given as 6x6 matrix.(Note that it is frequency dependant)

$$\mathbf{D}_P(\omega) = \sum_{k=1}^{6} B_{jk}^P \qquad (j = 1, ..., 6) \tag{2.20}$$

Hydrostatic restoring

Hydrostatic restoring are the forces and moments related to the static pressure term.[1]. Hydrostatic restoring follows from Archimedes principle where the buoyancy force of a submerged body is equal to the displaced volume. Hence the buoyancy-force and gravity-force vectors can be written:

$$f_g^n = \begin{bmatrix} 0 \\ 0 \\ W \end{bmatrix} f_b^n = \begin{bmatrix} 0 \\ 0 \\ B \end{bmatrix} \tag{2.21}$$

where $W = mg$ and $B = \rho g \nabla$, and the forces are relative to the NED-coordinate system.

The restoring forces and moments can be transformed to the BODY-coordinate system by using the same transformation as shown in the section 1. The restoring matrix hence become:[5]

$$\mathbf{g}(\eta) = -\begin{bmatrix} \mathbf{R}_b^n(\mathbf{\Theta}_{nb})^{-1}(\mathbf{f}_g^n + \mathbf{f}_b^n) \\ \mathbf{r}_g^b \times \mathbf{R}_b^n(\mathbf{\Theta}_{nb})^{-1}\mathbf{f}_g^n + \mathbf{r}_b^b \times \mathbf{R}_b^n(\mathbf{\Theta}_{nb})^{-1}\mathbf{f}_b^n \end{bmatrix} \tag{2.22}$$

When expanding this expression the final restoring matrix become:

$$\mathbf{g}(\eta) = \begin{bmatrix} (W-B)sin(\theta) & & \\ -(W-B)cos(\theta)sin(\phi) & & \\ -(W-B)cos(\theta)cos(\phi) & & \\ -(y_gW - y_bB)cos(\theta)cos(\phi) & + & (z_gW - z_bB)cos(\theta)sin(\phi) \\ (z_gW - z_bB)sin(\theta) & + & (x_gW - x_bB)cos(\theta)cos(\phi) \\ -(x_gW - x_bB)cos(\theta)sin(\phi) & - & (y_gW - y_bB)sin(\theta) \end{bmatrix} \tag{2.23}$$

Skin friction

Skin friction is the damping force that arises when a boundary layer is created between the body and the water surrounding it. Due to the no-slip condition the fluid that is close to the body will have 0 velocity relative to the body. This effect gradually decreases as the distance to the body increases. As a result of this tangential forces between the fluid particles in the boundary layer will create damping forces opposite the direction of motion. The skin friction can consist of a turbulent, laminar or combined boundary layers. Turbulent boundary layers are important for high relative velocities and are often referred to as quadratic or nonlinear skin friction.[5] The viscous damping matrix can be presented as:

$$\mathbf{D}_S = \sum_{k=1}^{6} B_{jk}^V \qquad (j = 1, ..., 6) \tag{2.24}$$

Wave drift damping

Wave drift damping is a 2nd order damping phenomenon. It is caused by the interaction between the rapid oscillating behaviour of the incident waves and the slow-drift motion of the body[1]. By evaluating the 2nd order velocity potential this damping force can be evaluated. Usually wave drift damping is only important for large volume structures. The wave drift damping can be presented as a 6x6

matrix:

$$\mathbf{D}_W = \sum_{k=1}^{6} B_{jk}^{WD} \qquad (j = 1, ..., 6) \tag{2.25}$$

Damping due to vortex shedding

The damping due to vortex shedding is also a viscous phenomenon. For Reynolds numbers over a certain limit(depends on geometry) the flow around the body will separate. This separation causes vortices to be generated. As the generation of vortices takes energy away from the body (or wave/current) it will create a damping force opposite the direction of motion. This damping force is usually modelled with the Morison equation.

$$\mathbf{D}_M = \sum_{k=1}^{6} B_{jk}^{M} \qquad (j = 1, ..., 6) \tag{2.26}$$

2.1.4 Diffraction and Froude-Kriloff forces

When a wave/current hits a structure which is restrained from oscillating the unsteady fluid pressure can be divided into two effects. The force due to the undisturbed pressure field is called the Froude-Kriloff force. The force due to the changed pressure field caused by the body's presence is called the diffraction force[1]. For simplicity the waves will be assumed to have a non-rotational velocity vector, hence the Coriolis terms can be neglected in these expressions.

The contributions from these components can be expressed mathematically[7]:

$$\boldsymbol{\tau}_{diff} = \mathbf{M}_{FK}\dot{\boldsymbol{\nu}}_c + \mathbf{M}_A\dot{\boldsymbol{\nu}}_c + \mathbf{D}_{diff}(\boldsymbol{\nu})\boldsymbol{\nu} + \mathbf{N}_V\boldsymbol{\nu}_c \tag{2.27}$$

Where the first term is the Froude-Kriloff force, the two next terms are the added mass and damping caused by the diffracted waves(diffracted waves transport energy away from the body) and the last term is the viscous damping.
The diffraction forces are the combined forces of the first order incident waves scattering of a body that is fixed in space. The diffraction wave potential thus is the sum of the first-order incident wave potential and the scattered potential.
The Froude-Kriloff force is found by integrating the pressure over the wetted surface of the body.(for a circular cylinder the Froude-Kriloff force is equal to the diffraction force)

The viscous damping is a result of the friction between the fluid passing the body as the wave oscillates or the current passes.

2.1.5 Final Equation of Motion

Finally the forces that acts on the rigid body $\boldsymbol{\tau}_{RB}$ will be substituted with the hydrodynamic and hydrostatic forces and moments in addition to the propeller thrust which will be introduced now and for future reference is being called $\boldsymbol{\tau}$:

$$\boldsymbol{\tau}_{RB} = \boldsymbol{\tau}_{rad} + \boldsymbol{\tau}_{diff} + \boldsymbol{\tau} \tag{2.28}$$

Now equation(2.6) can be rewritten to:

$$\boldsymbol{M}_{RB}\dot{\nu} + \boldsymbol{C}_{RB}(\nu)\nu = \boldsymbol{\tau} + \boldsymbol{\tau}_{rad} + \boldsymbol{\tau}_{diff} \tag{2.29}$$

And by substituting the expressions for the hydrostatic and hydrodynamic forces the final equation of motion become:

$$\begin{aligned} &\boldsymbol{M}_{RB}\dot{\nu} + \boldsymbol{C}_{RB}(\nu)\nu + \boldsymbol{M}_{A}\dot{\nu} + \boldsymbol{C}_{A}(\nu)\nu + \boldsymbol{D}_{rad}(\nu)\nu \\ &+\boldsymbol{g}(\eta) + \mathbf{M}_{FK}\dot{\nu}_c + \mathbf{M}_{A}\dot{\nu}_c + \mathbf{D}_{diff}(\nu_c)\nu_c + \mathbf{N}_{V}\nu_c \quad = \boldsymbol{\tau} \end{aligned} \tag{2.30}$$

2.2 Hydrodynamic theory

In this section basic hydrodynamic theory will be discussed. The linearised boundary value problems will be solved and the first order velocity potential will be derived using linear wave theory(Airy) for propagating waves. Afterwards the 2nd order velocity potential will be derived using perturbation. Lastly viscous effects relevant for a typical ROV will be discussed. The wave theory in this section is in large part referenced in Dean and Dalrymple 1991[8]

2.2.1 Bernoulli equation

In this section three important assumptions will be introduced. By assuming that the fluid is inviscid, incompressible and irrotational the Bernoulli equation can be derived.

Continuity equation

By stating that the flow into a specified control volume(dx,dy,dz) given as:

$$\rho u \partial y \partial z \tag{2.31}$$

is equal to the flow out of the control volume given as:

$$\left(\rho + \frac{\partial \rho}{\partial x}\partial x\right)\left(u\rho + \frac{\partial u}{\partial x}\partial x\right)\partial y \partial z \tag{2.32}$$

gives a instantaneous increase of mass of:

$$-\frac{\partial \rho}{\partial t}\partial x \partial y \partial z \tag{2.33}$$

The same applies for y and z directions. By demanding that the instantaneous increase in mass is equal to the difference between flow into the control domain and the flow out of the control domain gives the continuity equation :

$$\frac{\partial \rho}{\partial t} + \frac{\partial \rho u}{\partial x} + \frac{\partial \rho v}{\partial y} + \frac{\partial \rho w}{\partial z} = 0 \tag{2.34}$$

Now by introducing the assumption that water is a incompressible fluid the continuity equation becomes:

$$\frac{\partial u}{\partial x} + \frac{\partial v}{\partial y} + \frac{\partial w}{\partial z} = 0 \tag{2.35}$$

The Euler equations

By again using a reference control volume with sides $dxdydz$ and a flow in the x-direction Newton's 2nd law states that $\sum F_x = ma_x$ and by definition $a_x = du/dt$.

Since the velocity is a function of space its total derivative is:

$$\frac{Du}{Dt} = \frac{\partial u}{\partial t} + \frac{\partial u}{\partial x}\frac{dx}{dt} + \frac{\partial u}{\partial y}\frac{dy}{dt} + \frac{\partial u}{\partial z}\frac{dz}{dt} \tag{2.36}$$

The inertia force in x-direction is:

$$-\rho\Big(\frac{\partial u}{\partial t} + \frac{\partial u}{\partial x}\frac{dx}{dt} + \frac{\partial u}{\partial y}\frac{dy}{dt} + \frac{\partial u}{\partial z}\frac{dz}{dt}\Big)dV = -\rho\frac{Du}{Dt}dV \tag{2.37}$$

Now the assumption that shear stresses between fluid particles can be neglected is introduced. In water wave mechanics this assumption is valid for most problems[8]. The pressure resultant in the x-direction on the control volume becomes:

$$pdydz - \Big(p + \frac{\partial p}{\partial x}dx\Big)dydz = -\frac{\partial p}{\partial x}dV \tag{2.38}$$

The body force in the x-direction becomes: $\rho X dV$
Which leads to the euler equation

$$\frac{Du}{Dt} = X - \frac{1}{\rho}\frac{\partial p}{\partial x} \tag{2.39}$$

and applying similar procedure in y and z direction gives:

$$\frac{Dv}{Dt} = Y - \frac{1}{\rho}\frac{\partial p}{\partial y} \quad \& \quad \frac{Dw}{Dt} = Z - \frac{1}{\rho}\frac{\partial p}{\partial z} \tag{2.40}$$

Velocity Potential

First the velocity vector **V** is introduced. **V** is given by :

$$\boldsymbol{V}(x, y, z, t) = u\hat{\boldsymbol{i}} + v\hat{\boldsymbol{j}} + w\hat{\boldsymbol{k}} \tag{2.41}$$

Now if the velocity potential ϕ is introduced as the line integral of **V** it can be shown[8] that the following relations apply:

$$u = \frac{\partial \phi}{\partial x} \quad \& \quad v = \frac{\partial \phi}{\partial y} \quad \& \quad w = \frac{\partial \phi}{\partial z} \tag{2.42}$$

By introducing the last main assumption which is that the fluid is irrational(vorticity or curl of V is zero) the vector **V** can be represented as :

$$\mathbf{V} = \nabla\phi \tag{2.43}$$

Bernoulli equation

The Bernoulli equation is an important tool in wave mechanics because it connects the kinematics and the pressure field. The Bernoulli equation is simply an integrated form of the Euler equations. By taking the Euler equations in the XZ-plane and inserting the acceleration of gravity as the body force in the z-axis they can be written :

$$\frac{\partial u}{\partial t} + u\frac{\partial u}{\partial x} + w\frac{\partial u}{\partial z} = -\frac{1}{\rho}\frac{\partial p}{\partial x}$$
$$\frac{\partial w}{\partial t} + u\frac{\partial w}{\partial x} + w\frac{\partial w}{\partial z} = -\frac{1}{\rho}\frac{\partial p}{\partial z} - g$$

by introducing the vorticity condition in two dimensions($\nabla \times \boldsymbol{V} = 0$) the equations can be rewritten as:

$$\frac{\partial u}{\partial t} + \frac{\partial (u^2/2)}{\partial x} + \frac{\partial (w^2/2)}{\partial x} = -\frac{1}{\rho}\frac{\partial p}{\partial x}$$
$$\frac{\partial u}{\partial t} + \frac{\partial (u^2/2)}{\partial z} + \frac{\partial (w^2/2)}{\partial z} = -\frac{1}{\rho}\frac{\partial p}{\partial z} - g$$

and by introducing the velocity potential the equations become:

$$\frac{\partial}{\partial x}\left[\frac{\partial \phi}{\partial t} + \frac{1}{2}(u^2 + w^2) + \frac{p}{\rho}\right] = 0$$
$$\frac{\partial}{\partial z}\left[\frac{\partial \phi}{\partial t} + \frac{1}{2}(u^2 + w^2) + \frac{p}{\rho}\right] = -g$$

Integrating the equations yields:

$$\frac{\partial \phi}{\partial t} + \frac{1}{2}(u^2 + w^2) + \frac{p}{\rho} = C_1(z,t)$$
$$\frac{\partial \phi}{\partial t} + \frac{1}{2}(u^2 + w^2) + \frac{p}{\rho} = -gz + C_2(x,t)$$

It now follows by observing that the the left hand sides are equal that :

$$C_1(z,t) = -gz + C_2(x,t)$$

C_1 cannot be a function of x as neither C_2 or gz are. Hence it follows that $C_2(z,t) = -gz + C(t)$ which finally leads to the Bernoulli equation in 2-D:

$$\frac{\partial \phi}{\partial t} + \frac{1}{2}(u^2 + w^2) + \frac{p}{\rho} + gz = C(t) \tag{2.44}$$

2.2.2 Boundary value problems

By solving the two-dimensional periodic water wave boundary value problem it is possible to find a linear velocity potential ϕ that describes the fluid motion in waves. The boundary value problems consists of 3 boundary conditions(in addition to the governing equation) that must be satisfied. Figure 2.2 illustrates the boundary value problem. Note that the two lateral boundary conditions(LBC) are identical.

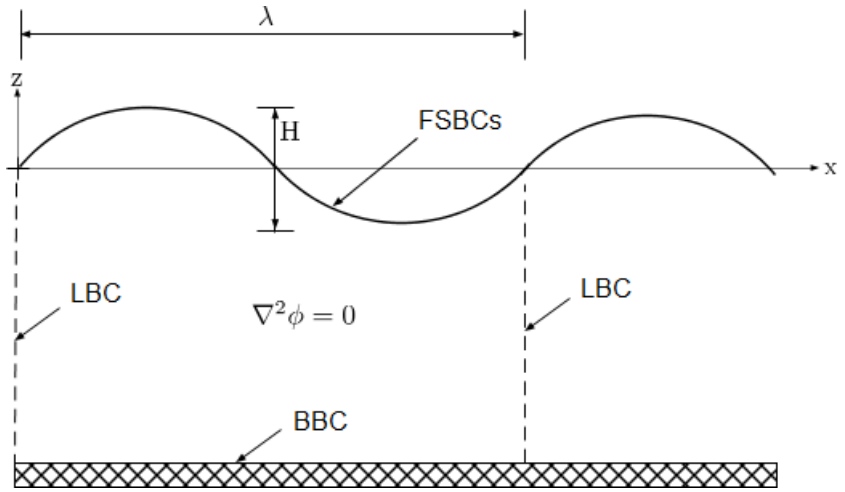

Figure 2.2: Illustration of the two-dimensional water waves boundary value problem

Laplace Equation

The governing equation of the fluid inside the domain is called the Laplace equation. It can be derived by inserting the expression for the velocity vector(assuming irrotational flow)(2.43) into the continuity equation for incompressible flow(2.35).

$$\nabla \boldsymbol{V} = 0 \quad \Longrightarrow \quad \nabla\nabla\phi = 0 \quad \Longrightarrow \quad \nabla^2\phi = \frac{\partial^2\phi}{\partial x^2} + \frac{\partial^2\phi}{\partial y^2} + \frac{\partial^2\phi}{\partial z^2} = 0 \tag{2.45}$$

Bottom Boundary Condition(BBC)

When assuming an impermeable bottom it is expected that the flow velocity through the bottom is zero. This condition is known as the bottom boundary condition. By assuming a horizontal bottom the normal vector simplifies to $\boldsymbol{n} = [0\hat{\boldsymbol{i}} + 0\hat{\boldsymbol{j}} + 1\hat{\boldsymbol{k}}]$. Expressed mathematically:

$$\boldsymbol{V}\cdot\boldsymbol{n}\Big|_{z=-h}=0\Longrightarrow\quad\Big[\frac{\partial\phi}{\partial x}*0+\frac{\partial\phi}{\partial y}*0+\frac{\partial\phi}{\partial z}*1\Big]\Big|_{z=-h}=0\Longrightarrow\quad\Big(\frac{\partial\phi}{\partial z}\Big)_{z=-h}=0 \tag{2.46}$$

Kinematic Free Surface Boundary Condition (KFSBC)

By requiring no fluid to pass through the free surface the same condition as for the bottom can be used. However now the normal vector becomes a function of both time and position. The free surface can be described by the function $F(x,y,z,t)=z-\zeta(x,y,t)$. The normal vector to F hence become:

$$\boldsymbol{n}=\frac{\nabla F}{|\nabla F|}=\frac{\frac{d\zeta}{dx}\hat{\boldsymbol{i}}+\frac{d\zeta}{dy}\hat{\boldsymbol{j}}+1\hat{\boldsymbol{k}}}{\sqrt{(\frac{d\zeta}{dx})^2+(\frac{d\zeta}{dy})^2+1}} \tag{2.47}$$

This in turn gives the kinematic free surface boundary condition:

$$\boldsymbol{V}\cdot\boldsymbol{n}\Big|_{z=\zeta(x,y,t)}=0\Longrightarrow\quad\frac{\partial\phi}{\partial z}=\frac{\partial\zeta}{\partial t}+\frac{\partial\phi}{\partial x}\frac{\partial\zeta}{\partial x}+\frac{\partial\phi}{\partial y}\frac{\partial\zeta}{\partial y}\Big|_{z=\zeta(x,y,t)} \tag{2.48}$$

As seen above the kinematic free surface boundary condition is nonlinear. By using Taylor expansion and linearising the expression at $z=0$ the kinematic free surface boundary condition simplifies to.

$$\frac{\partial\phi}{\partial z}=\frac{\partial\zeta}{\partial t}\Big|_{z=0} \tag{2.49}$$

This linear approximation is only valid when wave amplitudes are small relative to the characteristic wave length.[1]

Dynamic Free Surface Boundary Condition (DFSBC)

The dynamic boundary condition prescribes the pressure distribution in the interface between the water and the air. It is found by evaluating the three dimensional Bernoulli equation at the free surface and hence become:

$$\frac{\partial\phi}{\partial t}+\frac{1}{2}\Big(\Big(\frac{\partial\phi}{\partial x}\Big)^2+\Big(\frac{\partial\phi}{\partial y}\Big)^2+\Big(\frac{\partial\phi}{\partial z}\Big)^2\Big)+\frac{p|_{z=\zeta(x,y,t)}}{\rho}+g\zeta=0 \tag{2.50}$$

By performing Taylor expansion and evaluating the expression around the mean surface $z=0$ the linearised equation can be written :

$$\frac{\partial\phi}{\partial t}+g\zeta=0 \tag{2.51}$$

Where the pressure at the surface(ambient pressure) is set to be zero. This linear approximation is also only valid when wave amplitudes are small relative to the characteristic wave length.[1]

Lateral Boundary Condition

For waves that are periodic in time and space, the lateral boundary conditions can be expressed as a periodicity condition:

$$\phi(x,t) = \phi(x+\lambda,t) \quad \& \quad \phi(x,t) = \phi(x,t+T) \tag{2.52}$$

where λ is the wavelength and T is the wave period.

2.2.3 Wave Velocity Potential

The boundary conditions discussed in the previous subsection can be applied on the general solution to the Laplace equation(governing equation) to find the first and second order velocity potential. Higher order velocity potentials can also be found using perturbation, but higher order terms will not be discussed in this thesis as higher order effects are neglected.

First order velocity potential

The general solution for the governing equation can be found to be[8]:

$$\phi(x,z,t) = (Acos(kx) + Bsin(kx))(Ce^{kx} + De^{-kz})sin(\omega t)$$

By applying the bottom boundary condition and dynamic free surface boundary condition the velocity potential become[8]:

$$\phi = \frac{\zeta_a g}{\omega}\frac{cosh(k[h+z])}{cosh(kh)}cos(kx)sin(\omega t - kx) \tag{2.53}$$

If finally a right going progressive wave form is assumed the velocity potential can be written :

$$\phi = \frac{\zeta_a g}{\omega}\frac{cosh(k[h+z])}{cosh(kh)}cos(\omega t - kx) \tag{2.54}$$

The remaining boundary conditions can be used to prove two important wave relations:

$$k = \frac{2\pi}{\lambda} \quad \& \quad \omega^2 = kgtanh(kh) \tag{2.55}$$

Second order velocity potential

By using stokes expansion a second order velocity potential can be developed. It is assumed that the wave steepness is much smaller than one i.e. $\epsilon = \zeta_a k \ll 1$. The

firs step is to nondimensionalize all quantities. Then it will be assumed that the solution depend on ϵ. Therefore all quantities will be decomposed(perturbed) into power series in ϵ e.g:

$$\begin{aligned} \mathbf{\Phi} &= \mathbf{\Phi}_1 + \epsilon\mathbf{\Phi}_2 + \epsilon^2\mathbf{\Phi}_3 + ... \\ \boldsymbol{\omega} &= \boldsymbol{\omega}_1 + \epsilon\boldsymbol{\omega}_2 + \epsilon^2\boldsymbol{\omega}_3 + ... \end{aligned} \tag{2.56}$$

where $\mathbf{\Phi}$ and $\boldsymbol{\omega}$ is the nondimensionalized velocity potential and frequency respectively. The surface boundary conditions are expanded about $z = 0$, as done earlier, however now all terms up to second order will be retained. Now by collecting all terms which are not dependant of ϵ gives an equation set identical to the first order potential, and the solution become the first order velocity potential obtained in the previous subsection. The remaining terms are related to ϵ, i.e. of second order, and collecting these terms gives the following set of equations.[8]

$$\begin{aligned} \nabla^2\mathbf{\Phi}_2 &= 0 & & \\ \frac{\partial\mathbf{\Phi}_2}{\partial\boldsymbol{Z}} &= 0 & on \quad & Z = -kh \\ \frac{\partial\mathbf{\Pi}}{\partial\boldsymbol{T}} &= \frac{\partial\mathbf{\Phi}_2}{\partial\boldsymbol{Z}} - \frac{\partial\mathbf{\Phi}_1}{\partial\boldsymbol{X}}\frac{\partial\mathbf{\Pi}_1}{\partial\boldsymbol{X}} + \Pi_1\frac{\partial^2\mathbf{\Phi}_1}{\partial\boldsymbol{Z}^2} & on \quad & Z = 0 \\ \frac{\partial\mathbf{\Phi}_2}{\partial\boldsymbol{T}} &= -\Pi_2 - \frac{1}{2}\left[\left(\frac{\partial\mathbf{\Phi}_1}{\partial\boldsymbol{X}}\right)^2 + \left(\frac{\partial\mathbf{\Phi}_1}{\partial\boldsymbol{Z}}\right)^2\right] - \Pi_1\frac{\partial^2\mathbf{\Phi}_1}{\partial\boldsymbol{T}\partial\boldsymbol{Z}} & on \quad & Z = 0 \end{aligned} \tag{2.57}$$

where $\Pi = \frac{\zeta}{\zeta_a}$

Solving this equation set gives the general solution of the 2^{nd} order velocity potential[8]:

$$\phi_2 = \frac{3}{8}\omega\zeta_a^2\frac{cosh(2k[z+h])}{sinh^4(kh)}sin(2kx - 2\omega t) \tag{2.58}$$

2.2.4 Boundary Layers

In the derivation of the Euler equations the assumption that shear stresses between the fluid particles could be neglected was introduced. This assumption is valid for at least two flow situations. For high Reynolds number flow regions the viscous forces are known to be negligible compared to the inertial and/or pressure forces.(known as inviscid flow regions). The other situation occurs when the vorticity of the flow is negligible small.(known as irrotational flow)[9] For other flow conditions than these two cases the shear stress between fluid particles can introduce important phenomenons such as boundary layers. In this section the different boundary layer properties will be discussed.

No-Slip

The no-slip condition is an important phenomenon in fluid mechanics. By evaluating the flow through a stationary pipe all experimental observations indicate that the fluid comes to a complete stop at surface of the pipe.[9]. As the fluid has zero velocity relative to the surface and thus sticks to the surface it gives rice to the name No-slip condition. The viscosity of the fluid is the physical property that creates this phenomenon. No slip conditions can be found on any stationary surface exerted to fluid flow. For moving objects in calm water the same phenomenon also happens as it is the relative velocity between the surface and the fluid that is of relevance.

Boundary layer region

When the fluid at the surface comes to a complete still shear stresses between the fluid particles will be created. The further away the fluid particles are from the surface the bigger will the in relative velocity be. This happens until the fluid particle is so far away from the surface that its velocity is the same as for the rest of the flow. For a flat plate moving at 1 m/s in surge in still water this would translate to a velocity between a fluid particle velocity of 1 m/s relative to the ROV. Figure 2.3 shows how the fluid velocity in the boundary layer varies.

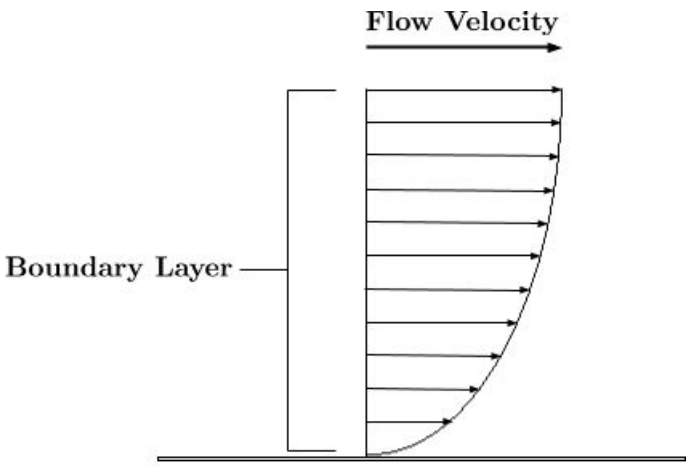

Figure 2.3: Flow Velocity in the Boundary Layer of a flat Surface

The region from the surface to where the fluid particles have velocity close to that of the flow is called the boundary layer region. A number of different approaches exists when determining the thickness of the boundary layer region, but it is dependant on a number of factors. One definition is that the boundary layer thickness is equal to the normal distance from the surface to the point where the tangential velocity of the fluid is 99% of the local upstream velocity.[1]

Skin Friction

The skin friction comes from the molecular resistance that arise when fluid is moving along the surface of a body. As the variation of velocity throughout the boundary layer induces shear stresses on the surface of the body the net shear force will act at the tangential direction on the surface opposite the direction of motion(or parallel to the current). This net tangential shear force will in turn create a damping force on the body moving through the fluid. It is normal to denote this damping as skin friction. The shear stress on a flat plate can be expressed as[8]:

$$\tau_{xy} = \mu\Big[\frac{\partial u}{\partial y} + \frac{\partial v}{\partial x}\Big] \tag{2.59}$$

Where μ is the friction of coefficient between the surface and the fluid. To determine the linear skin friction can be a very challenging task and it is often more practical to use empirical estimates.

Reynolds Number

An important quantity when it comes to boundary layers is the Reynolds number. Reynolds number is a dimensionless coefficient that describes the relation between intertial forces and viscous forces and is expressed mathematically as:

$$R_N = \frac{V * L}{\nu} \tag{2.60}$$

Where ν is the kinematic viscosity, L is the characteristic length of the body and V is the flow velocity. For the flow around a circular cylinder the Reynolds number is important as it governs where the boundary layer becomes turbulent and where flow separation occurs. As roughness and imperfections of a cylinder will in real life affect boundary layer turbulence and flow separation Reynolds number will not give exact knowledge of the boundary layer, but will in many cases give a good approximation. For any boundary layer flow there exists a Reynolds number for which below the boundary layer is laminar and above the boundary layer is turbulent. [4] For a Square cylinder the separation points are not dependant of Reynolds number. The separation points will not change(given constant angle of attack) and will be constantly located at the corners. See figure 2.4. This gives an approximately constant drag curve for all Reynolds numbers[27]. For cylinders/spheres on the other hand the separation point will move forward for higher Reynolds numbers and thus increase the turbulent boundary layer region and give a drop in the drag for Reynolds numbers 10^3-10^5.

2.2.5 Vortex Shedding

Vortex shedding is another viscous fluid phenomenon. When fluid passes a body, depending on the Reynolds number vortices will be shed. Von Karman studied vortex shedding on circular cylinders and found out that the vortices could only be arranged in two ways. Either stacked exactly opposite of each other or staggered[1]. The first of which is highly unstable. The staggered arrangement is generally unstable, but become stable for a definite ratio between the vortex street width h and distance l between two adjacent vortices in the same row. A staggered vortex street can be seen in figure 2.4.

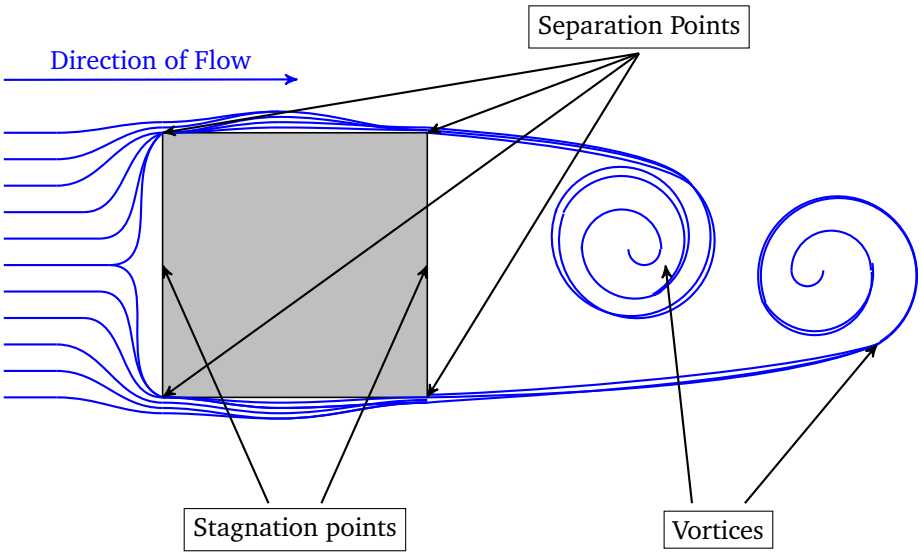

Figure 2.4: Vortex shedding around square cylinder

Reynolds Number

The Reynolds number is an important parameter for vortex shedding as it can indicate how the vortices are shed or if vortices will shed. As drag forces are highly dependant on vortex shedding the Reynolds number can indicate the drag forces on a body.

Strouhal Number

As mentioned earlier a stable train of vortices is a staggered train with a given distance between vortices and a given height. The Strouhal number gives the relationship between the vortex shedding frequency, body length and flow velocity.

It is expressed mathematically as:

$$St = \frac{f_v L}{U_\infty} \tag{2.61}$$

Where f_v is the vortex shedding frequency, U_∞ is the free stream velocity and L is the characteristic length. It should be noted that for critical and supercritical flows there are a spectrum of vortex shedding frequencies rather than one single frequency[1].

Lift Force

When vortices are shed they inflict fluctuating lift forces on the body. As the fluid velocity of a vortex is larger than the surrounding fluid it follows from Bernoulli equation(2.44) that the pressure will drop. The pressure will vary in the transverse(as well as longitudinal) direction and thus generate lift forces. If there is a single vortex shedding frequency f_v the lift force can be written[1]

$$F_L(t) = \left|F_L\right| cos(2\pi f_v t + \alpha) \tag{2.62}$$

For a body symmetric to the direction of flow(for an offshore vessel and also a ROV this will mean symmetry in XZ-plane) the lift forces will have a zero mean value as the vortices shed on each side are of equal strength. Lift forces are therefore not always relevant. Lift force is usually presented as a non-dimensional lift coefficient C_L:

$$C_L = \frac{\left|F_L\right|}{\frac{1}{2}\rho U_\infty^2 D} \tag{2.63}$$

Drag Force

The drag force is the result of the pressure drop in longitudinal direction due to vortex shedding. The drag force has as opposed to the lift force a time independent constant. The time independent drag comes as a result of the constant pressure drop behind the body. The drag force can therefore be written mathematically as :

$$F_D(t) = \overline{F}_D + A_D cos(4\pi f_v t + \beta) \tag{2.64}$$

As seen in the expression for the drag force the frequency of oscillation is twice the frequency of oscillation of the lift force. This is simply due to the fact that the lift force needs two vortices to complete one cycle whilst the drag force complete 1 cycle for each vortex. The oscillating drag force component A_D is typically 20% of the constant term F_D and is thus not the dominating factor.[1]

It is normal to define the drag force for cylinders and offshore structures using the constant drag term as it is the dominating term(the mean value of the oscillating term is zero). The drag can similarly to the lift force be non-dimensionalised :

$$C_D = \frac{|\overline{F}_D|}{\frac{1}{2}\rho U_\infty^2 D} \tag{2.65}$$

2.2.6 Morison Equation

The Morison equation was first presented in Morison et. al, 1950[14] The equation builds on the fact that the forces on a cylinder is expressed by two terms, the drag and the mass terms. The equation is expressed mathematically as:

$$F = \rho C_m V \dot{u} + \frac{1}{2}\rho C_D A u|u| \tag{2.66}$$

Where V is the volume of the cylinder, A is the reference area, u is the flow velocity, C_m is the mass coefficient and C_D is the drag coefficient.

Mass force

The mass force is governed by the mass coefficient as seen in the equation above. This force is a result of the radiation force(added mass) and Froude-Kriloff force. For a circular cylinder accelerated in calm water the mass coefficient can be found fairly easy using potential theory:

The velocity potential of a cylinder in calm water can be found by solving the governing equation with the boundary condition:

$$V * n = 0 \tag{2.67}$$

which gives the following velocity potential :

$$\phi(r,\theta) = -u(t)(r + \frac{R^2}{r})cos(\theta)$$

Now the dynamic pressure is found using Bernoulli equation(2.44):

$$p = -\rho\frac{\partial\phi}{\partial t} = \rho\dot{u}(t)(r + \frac{R^2}{r})cos(\theta) \tag{2.68}$$

The pressure on the cylinder surface hence become:

$$p\big|_{r=R} = \rho\ddot{u}cos(\theta)R + \rho\dot{u}cos(\theta)R$$

Where the first term is the Frodue-Kriloff pressure and the latter is the diffraction pressure. These pressure terms gives a force in the x-direction of:

$$F_x = \int_0^{2\pi} cos(\theta)(\rho \dot{u} cos(\theta) R + \rho \dot{u} cos(\theta) R) R d\theta$$

Where $cos(\theta)$ is the normal vector and $\int_0^{2\pi} R d\theta$ is the area of the cylinder.

Carrying out the integral gives a total force in the x-direction of:

$$F_x = \dot{u}\rho R^2 \pi + \dot{u}\rho R^2 \pi = 2\dot{u}\rho R^2 \pi = 2\rho V \dot{u}$$

By comparing this result with the mass term in Morison equation(2.66) it is seen that the mass coefficient C_m for a circular cylinder is exactly 2. For other geometries the mass term can be calculated using potential flow theory(computer programs should be used for advanced geometries) or by empirical tables.

Drag Force

It can now be noted that the expression for the drag force is identical to the term presented in (2.65). Inserting the correct drag coefficient can hence give the drag forces for a cylinder. It now follows that the equation can be modified to estimate the drag forces on e.g. a square cylinder as long as the correct drag coefficient can be found. This relation can be transformed to any given geometry as long as the correct drag coefficient for that specific geometry can be found. Morrison III et. al [19] proved experimentally that this relation also applies for underwater vehicles. Many publications and standards have empirical drag coefficients for a variety of shapes e.g. DNV-standard[29] and Applied fluid dynamics handbook by Blevins[4].

2.3 Determining Relevant Coefficients

In section 1. the dynamic equation of motion was derived. In this section the different terms in the equation will be evaluated with respect to a typical work class ROV.

$$\begin{aligned} &\boldsymbol{M}_{RB}\dot{\nu} + \boldsymbol{C}_{RB}(\nu)\nu + \boldsymbol{M}_A\dot{\nu} + \boldsymbol{C}_A(\nu)\nu + \boldsymbol{D}_{rad}(\nu)\nu \\ &+\boldsymbol{g}(\eta) + \mathbf{M}_{FK}\dot{\nu}_c + \mathbf{M}_A\dot{\nu}_c + \mathbf{D}_{diff}(\nu_c)\nu_c + \mathbf{N}_V\nu_c \quad = \boldsymbol{\tau} \end{aligned} \tag{2.69}$$

2.3.1 Rigid Body Mass and Coriolis

In this subsection the two first terms of equation (2.69) will be evaluated. As basic symmetry principles can be applied both matrices can be simplified greatly

Mass

The complete Matrix looks like :

$$M = \begin{bmatrix} m_{11} & m_{12} & m_{13} & m_{14} & m_{15} & m_{16} \\ m_{21} & m_{22} & m_{23} & m_{24} & m_{25} & m_{26} \\ m_{31} & m_{32} & m_{33} & m_{34} & m_{35} & m_{36} \\ m_{41} & m_{42} & m_{43} & m_{44} & m_{45} & m_{46} \\ m_{51} & m_{52} & m_{53} & m_{54} & m55 & m_{56} \\ m_{61} & m_{62} & m_{63} & m_{64} & m_{65} & m_{66} \end{bmatrix}$$

Now symmetry in 2 of 3 planes will be assumed. This is a valid assumption for most underwater vehicles. If the ROV does not have 2 planes of symmetry its manoeuvring capabilities are poor as it would not be able to hold a steady course without having to use thrusters. In addition it will be assumed that the center of gravity(COG) will be located in the symmetry planes.Stating that the ROV has symmetry in the xz-plane and xy-planes gives the following mass matrix:

$$M = \begin{bmatrix} m & 0 & 0 & 0 & mz_g & 0 \\ 0 & m & 0 & -mz_g & 0 & 0 \\ 0 & 0 & m & 0 & 0 & 0 \\ 0 & -mz_g & 0 & I_4 & 0 & 0 \\ mz_g & 0 & 0 & 0 & I_5 & 0 \\ 0 & 0 & 0 & 0 & 0 & I_6 \end{bmatrix}$$

This is easily verified by referring to figure 2.1. As the CO is set in the COG in the horizontal direction and symmetry around COG applies in two planes the simplification can be justified.

By looking at the surge DOF, the rigid body equation become:

$$m_{11}\dot{u} + m_{12}\dot{v} + m_{13}\dot{w} + m_{14}\dot{p} + m_{15}\dot{q} + m_{16}\dot{r} = X \tag{2.70}$$

Now due to lateral symmetry in XZ-plane m_{12} is zero, this because an acceleration in sway direction would not cause any inertia forces in surge. The same happens with m_{13} due to symmetry in YZ-plane.

Moving on to the forces due to angular accelerations. A rotation in roll(p) or yaw(r) will not produce any inertia force in surge DOF. This is because the moment-arm from the origin to the center of gravity will always be zero. For rotation in pitch(q) however there will still be an inertia force, given that the BODY-coordinate system origin(CO) has a vertical distance to the COG. This becomes apparent when studying figure 2.5.

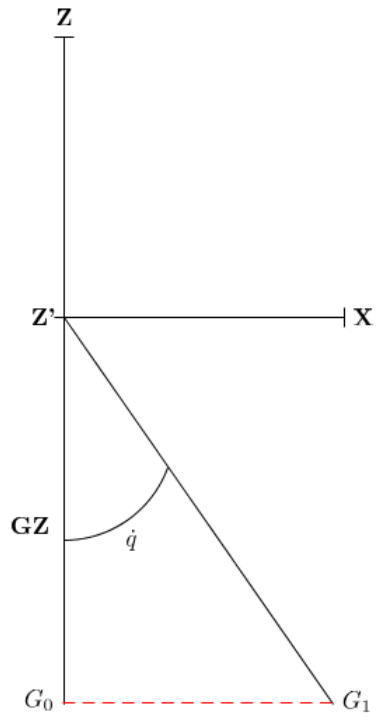

Figure 2.5: Mass moment in surge-direction

therefore :$m_{15} = mz_g$
The final mass equation for surge therefore becomes :

$$m\dot{u} + mz_g\dot{q} = X \tag{2.71}$$

The arguments used can also be used on sway and heave DOF, but these proofs will not be shown here as they are identical. Instead a rotational degree of freedom will be analysed.

By using the same approach for the roll DOF as was used for the surge DOF the mass matrix can be further simplified. In roll the rigid body equation of motion become

$$m_{41}\dot{u} + m_{42}\dot{v} + m_{43}\dot{w} + m_{44}\dot{p} + m_{45}\dot{q} + m_{46}\dot{r} = K \tag{2.72}$$

Now m_{41} and m_{43} are zero since accelerations in surge and heave would not cause any forces in roll.(again because of symmetry)
For m_{42} however there will be a contribution. This contribution comes from the fact that when the body is moved in the positive y-direction(Sway) it will generate a moment around the x-axis. The lever of this moment will become the distance from the the origin on the z-axis to the center of gravity. The sign of this moment will become negative since a positive translation would result in a clockwise moment. For future reference counter-clockwise rotation will be denoted as positive.

Figure 2.6 illustrates how this moment arises:

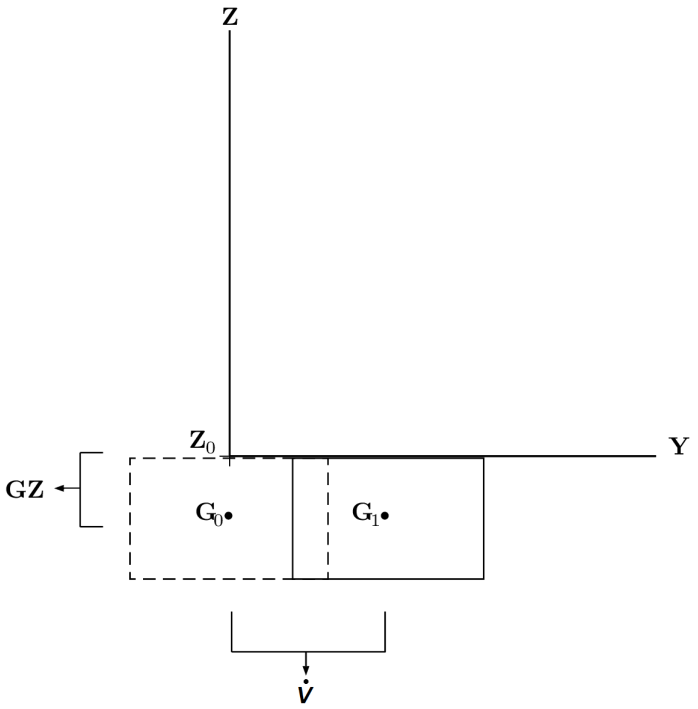

Figure 2.6: Mass moment in roll DOF due to sway acceleration

Furthermore there is an additional term in the equation for roll. This is due to moment of inertia. The term is the moment of inertia in roll due to the roll motion itself. It is simply expressed as:

$$m_{44}\dot{p} = I_x\dot{p} \tag{2.73}$$

Combining all the 6 simplified equations grants the mass matrix shown in the beginning of this section

$$M = \begin{bmatrix} m & 0 & 0 & 0 & mz_g & 0 \\ 0 & m & 0 & -mz_g & 0 & 0 \\ 0 & 0 & m & 0 & 0 & 0 \\ 0 & -mz_g & 0 & I_x & 0 & 0 \\ mz_g & 0 & 0 & 0 & I_y & 0 \\ 0 & 0 & 0 & 0 & 0 & I_z \end{bmatrix}$$

Since the matrix is symmetric about the diagonal it can be written:

$$M = \begin{bmatrix} m & 0 & 0 & 0 & mz_g & 0 \\ & m & 0 & -mz_g & 0 & 0 \\ & & m & 0 & 0 & 0 \\ & \text{Sym} & & I_x & 0 & 0 \\ & & & & I_y & 0 \\ & & & & & I_z \end{bmatrix}$$

It can now be noted that by defining the origin of the body fixed coordinate system at the center of gravity the mass matrix would further simplify to a purely diagonal matrix. The origin of the Body-fixed coordinate system will therefore be set to the COG. The rigid body mass matrix can therefore be presented as a vector containing only the diagonal mass terms:

$$M = \left[m, m, m, I_x, I_y, I_z\right]^D \tag{2.74}$$

Rigid body Coriolis Matrix

As shown in section 1 the rigid body Coriolis matrix does not have a unique parametrization. One skew-symmetrical representation is shown in Fossen 1994[7] and is presented on the next page. It should be noted that for design of nonlinear control systems it can be quite beneficial to exploit the dynamic properties of the nonlinear equation. However as the focus in this thesis is on the hydrodynamic properties rather than the control theory of ROVs the choice of parametrizations and representations of the different matrices will not be discussed further.

$$\boldsymbol{C_{RB}}(\nu) = \begin{bmatrix} 0 & 0 & 0 \\ 0 & 0 & 0 \\ 0 & 0 & 0 \\ -m(y_g q + z_g r) & m(y_g p + w) & m(z_g p - v) \\ m(x_g q - w) & -m(z_g r + x_g p) & m(z_g q + u) \\ m(x_g r + v) & m(y_g r - u) & -m(x_g p + y_g q) \end{bmatrix}$$

$$\begin{bmatrix} m(y_g q + z_g r) & -m(x_g p - w) & -m(x_g r + v) \\ -m(y_g p + w) & m(z_g r + x_g p) & -m(y_g r - u) \\ -m(z_g p - v) & -m(z_g q + u) & m(x_g p + y_g q) \\ 0 & -I_{yz} q - I_{xz} p + I_z r & I_{yz} r - I_{xy} p + I_y q \\ I_{yz} q + I_{xz} p - I_z r & 0 & -I_{xz} r - I_{xy} q + I_x p \\ -I_{yz} r - I_{xy} p + I_y q & I_{xz} r + I_{xy} q - I_x p & 0 \end{bmatrix} \tag{2.75}$$

As already stated the r_g is the vector from center of origin of the body-fixed coordinate system(CO) to the center of gravity(COG) given in body coordinates and can be written:

$$\boldsymbol{r}_g = \begin{bmatrix} x_g \\ y_g \\ z_g \end{bmatrix} \tag{2.76}$$

As it has been stated that the CO and COG have the same location it follows by inserting the expression for r_g into the matrix(2.77) that the Coriolis matrix can be be simplified. In addition due to symmetry in the xz- and yz-planes the products of inertia are zero. This gives the following representation of the Coriolis matrix:

$$\boldsymbol{C_{RB}}(\nu) = \begin{bmatrix} 0 & 0 & 0 & 0 & -m(-w) & -m(v) \\ 0 & 0 & 0 & -m(w) & 0 & -m(-u) \\ 0 & 0 & 0 & m(v) & -m(u) & 0 \\ 0 & m(w) & -m(v)0 & I_z r & I_y q & \\ m(-w) & 0 & m(u) & -I_z r & 0 & I_x p \\ m(v) & m(-u) & 0 & -I_y q & -I_x p & 0 \end{bmatrix} \tag{2.77}$$

It can now be noticed that the Coriolis matrix only contains products of mass-coefficients and velocity-components. It therefore follows that for parameter identification only mass terms are needed. This because the Coriolis matrix is represented with the same mass terms. This again means that no parameter estimation is needed explicitly for the Coriolis matrix to determine its coefficients.

2.3.2 Radiation Forces

As seen in the last section the radiation forces consist of 3 main contributions,the added mass, damping and restoring forces and moments. In this section it will be shown that for a general ROV in operating conditions most of these contributions can be greatly simplified or even neglected.

Added mass

By assuming that the body is far below the surface and thus independent of the surface waves it can be assumed that the added mass coefficients are constant and independent of wave frequency. The added mass hence become dependant of only the acceleration of the rigid body. The added mass can be found by evaluating the kinetic energy of the fluid using potential theory. [5]:

$$
\begin{aligned}
X_A = \quad & X_{\dot{u}}\dot{u} + X_{\dot{w}}(\dot{w} + uq) + X_{\dot{q}}\dot{q} + Z_{\dot{w}}wq + Z_{\dot{q}}q^2 \\
& + X_{\dot{v}}\dot{v} + X_{\dot{p}}\dot{p} + X_{\dot{r}}\dot{r} - Y_{\dot{v}}vr - Y_{\dot{p}}rp - Y_{\dot{r}}r^2 \\
& - X_{\dot{v}}ur - Y_{\dot{w}}wr \\
& + Y_{\dot{w}}vq + Z_{\dot{p}}pq - (Y_{\dot{q}} - Z_{\dot{r}})qr \\
Y_A = \quad & X_{\dot{v}}\dot{u} + Y_{\dot{w}}\dot{w} + Y_{\dot{q}}\dot{q} \\
& Y_{\dot{v}}\dot{v} + Y_{\dot{p}}\dot{p} + Y_{\dot{r}}\dot{r} + X_{\dot{v}}vr - Y_{\dot{w}}vp + X_{\dot{r}}r^2 + (X_{\dot{p}} - Z_{\dot{r}})rp - Z_{\dot{p}}p^2 \\
& X_{\dot{w}}(up - wr) + X_{\dot{u}}ur - Z_{\dot{w}}wp \\
& Z_{\dot{q}}pq + X_{\dot{q}}qr \\
Z_A = \quad & X_{\dot{w}}(\dot{u} - wq) + Z_{\dot{w}}\dot{w} + Z_{\dot{q}}\dot{q} - X_{\dot{u}}uq - X_{\dot{q}}q^2 \\
& X_{\dot{v}}up + Y_{\dot{w}}wp \\
& X_{\dot{v}}vq - (X_{\dot{p}} - Y_{\dot{q}})pq - X_{\dot{r}v}qr \\
K_A = \quad & X_{\dot{p}}\dot{u} + Z_{\dot{v}}\dot{w} + K_{\dot{q}}\dot{q} - X_{\dot{v}}wu + X_{\dot{r}}uq - Y_{\dot{w}}w^2 - (Y_{\dot{q}} - Z_{\dot{r}})wq + M_{\dot{r}}q^2 \\
& Y_{\dot{p}}\dot{v} + K_{\dot{p}}\dot{p} + K_{\dot{r}}\dot{r} + Y_{\dot{w}}v^2 - (Y_{\dot{q}} - Z_{\dot{r}})vr + Z_{\dot{p}}vp - M_{\dot{r}}r^2 - K_{\dot{q}}rp \\
& X_{\dot{w}}uv - (Y_{\dot{v}} - Z_{\dot{w}})vw - (Y_{\dot{r}} + Z_{\dot{q}})wr - Y_{\dot{p}}wp - X_{\dot{q}}ur \\
& (Y_{\dot{r}} + Z_{\dot{q}})vq + K_{\dot{r}}pq - (M_{\dot{q}} - N_{\dot{r}})qr \\
M_A = \quad & X_{\dot{q}}(\dot{u} + wq) + Z_{\dot{q}}(\dot{w} - uq) + M_{\dot{q}}\dot{q} - X_{\dot{w}}(u^2 - w^2) - (Z_{\dot{w}} - X_{\dot{u}})wu \\
& Y_{\dot{q}}\dot{v} + K_{\dot{q}}\dot{p} + M_{\dot{r}}\dot{r} + Y_{\dot{p}}vr - Y_{\dot{r}}vp - K_{\dot{r}}(p^2 - r^2) + (K_{\dot{p}} - N_{\dot{r}})rp \\
& Y_{\dot{w}}uv + X_{\dot{v}}vw - (X_{\dot{r}} + Z_{\dot{p}})(up - wr) + (X_{\dot{p}} - Z_{\dot{r}})(wp - ur) \\
& - M_{\dot{r}}pq + K_{\dot{q}}qr \\
N_A = \quad & X_{\dot{r}}\dot{u} + Z_{\dot{r}}\dot{q} + M_{\dot{r}}\dot{q} + X_{\dot{v}}u^2 + Y_{\dot{w}}wu - (X_{\dot{p}} - Y_{\dot{q}})uq - Z_{\dot{p}}wq - K_{\dot{q}}q^2 \\
& Y_{\dot{r}}\dot{v} + K_{\dot{r}}\dot{p} + N_{\dot{r}}\dot{r} - X_{\dot{v}}v^2 M_{\dot{r}}rp + K_{\dot{q}}p^2 \\
& - (X_{\dot{u}} - Y_{\dot{v}})uv - X_{\dot{w}}vw + (X_{\dot{q}} + Y_{\dot{p}})up + Y_{\dot{r}}ur + Z_{\dot{q}}wp \\
& - (X_{\dot{q}} + Y_{\dot{p}})vq - (K_{\dot{p}} - M_{\dot{q}})pqK_{\dot{r}}qr
\end{aligned}
\tag{2.78}
$$

These parameters can furthermore be divided into an added mass matrix and an added mass Coriolis matrix[5]

The added mass matrix become :

$$\mathbf{M}_A = \begin{bmatrix} X_{\dot{u}} & X_{\dot{v}} & X_{\dot{w}} & X_{\dot{u}} & X_{\dot{p}} & X_{\dot{q}} & X_{\dot{r}} \\ Y_{\dot{u}} & Y_{\dot{v}} & Y_{\dot{w}} & Y_{\dot{u}} & Y_{\dot{p}} & Y_{\dot{q}} & Y_{\dot{r}} \\ Z_{\dot{u}} & Z_{\dot{v}} & Z_{\dot{w}} & Z_{\dot{u}} & Z_{\dot{p}} & Z_{\dot{q}} & Z_{\dot{r}} \\ K_{\dot{u}} & K_{\dot{v}} & K_{\dot{w}} & K_{\dot{u}} & K_{\dot{p}} & K_{\dot{q}} & K_{\dot{r}} \\ M_{\dot{u}} & M_{\dot{v}} & M_{\dot{w}} & M_{\dot{u}} & M_{\dot{p}} & M_{\dot{q}} & M_{\dot{r}} \\ N_{\dot{u}} & N_{\dot{v}} & N_{\dot{w}} & N_{\dot{u}} & N_{\dot{p}} & N_{\dot{q}} & N_{\dot{r}} \end{bmatrix} \tag{2.79}$$

and the added mass Coriolis matrix:

$$\mathbf{C}_A(\nu) = \begin{bmatrix} 0 & 0 & 0 & 0 & -a_3 & a_2 \\ 0 & 0 & 0 & a_3 & 0 & -a_1 \\ 0 & 0 & 0 & -a_2 & a_1 & 0 \\ 0 & -a_3 & a_2 & 0 & -b_3 & b_2 \\ a_3 & 0 & -a_1 & b_3 & 0 & -b_1 \\ -a_2 & a_1 & 0 & -b_2 & b_1 & 0 \end{bmatrix} \tag{2.80}$$

where:

$$\begin{aligned} a_1 &= X_{\dot{u}}u + X_{\dot{v}}v + X_{\dot{w}}w + X_{\dot{p}}p + X_{\dot{q}}q + X_{\dot{r}}r \\ a_2 &= Y_{\dot{u}}u + Y_{\dot{v}}v + Y_{\dot{w}}w + Y_{\dot{p}}p + Y_{\dot{q}}q + Y_{\dot{r}}r \\ a_3 &= Z_{\dot{u}}u + Z_{\dot{v}}v + Z_{\dot{w}}w + Z_{\dot{p}}p + Z_{\dot{q}}q + Z_{\dot{r}}r \\ b_1 &= K_{\dot{u}}u + K_{\dot{v}}v + K_{\dot{w}}w + K_{\dot{p}}p + K_{\dot{q}}q + K_{\dot{r}}r \\ b_2 &= M_{\dot{u}}u + M_{\dot{v}}v + M_{\dot{w}}w + M_{\dot{p}}p + M_{\dot{q}}q + M_{\dot{r}}r \\ b_3 &= N_{\dot{u}}u + N_{\dot{v}}v + N_{\dot{w}}w + N_{\dot{p}}p + N_{\dot{q}}q + N_{\dot{r}}r \end{aligned} \tag{2.81}$$

In ROV applications it can furthermore often be assumed low speeds(this is generally not the case for AUVs). In addition it will be assumed three planes of symmetry. This last assumption is for many ROVs not completely correct, but as the coupling terms can be very difficult to determine especially using empirical estimates this assumption will be enforced. Whether this assumption is valid will be dependant of the ROV, but if the ROV is close to the typical prismatic shape the assumption should be valid. However it would still need validation. These two assumptions makes the coupling terms zero and the added mass and added mass Coriolis matrices greatly simplifies. As the added mass matrix now only contains diagonal terms it can be presented as a diagonal vector:

$$M_A = \left[X_{\dot{u}}, Y_{\dot{v}}, Z_{\dot{w}}, K_{\dot{p}}, M_{\dot{q}}, N_{\dot{r}}\right]^D \tag{2.82}$$

And the added mass Coriolis matrix become:

$$\mathbf{C}_A(\nu) = \begin{bmatrix} 0 & 0 & 0 & 0 & -Z_{\dot{w}}w & Y_{\dot{v}}v \\ 0 & 0 & 0 & Z_{\dot{w}}w & 0 & -X_{\dot{u}}u \\ 0 & 0 & 0 & -Y_{\dot{v}}v & X_{\dot{u}}u & 0 \\ 0 & -Z_{\dot{w}}w & Y_{\dot{v}}v & 0 & -N_{\dot{r}}r & M_{\dot{q}}q \\ Z_{\dot{w}}w & 0 & -X_{\dot{u}}u & N_{\dot{r}}r & 0 & -K_{\dot{p}}p \\ -Y_{\dot{v}}v & X_{\dot{u}}u & 0 & -M_{\dot{q}}q & K_{\dot{p}}p & 0 \end{bmatrix} \tag{2.83}$$

Again it is seen that the Coriolis matrix only contains products of mass (added mass) terms and velocity components. It therefore follows that no parameter identification is needed to determine the coefficients in this matrix as they are determined by the added mass matrix.

Potential Damping

As stated earlier potential damping is the energy transported away from the body due to the generation of surface waves. By assuming that the ROV is far below the free surface the ROV will not generate any waves. This implies that the potential damping is negligible. When the ROV is close to the surface this approximation will not be valid, but the operational condition is usually not in this range.

Hydrostatic Restoring

For underwater vehicles the buoyancy force is usually slightly larger than the weight in water. This precaution is made to ensure that in case of power loss or other problems the ROV will eventually resurface. However this net buoyancy force is usually small and will in this thesis be neglected. Figure 2.7 shows the physical concept behind the restoring moment in pitch, note that roll would be identical.

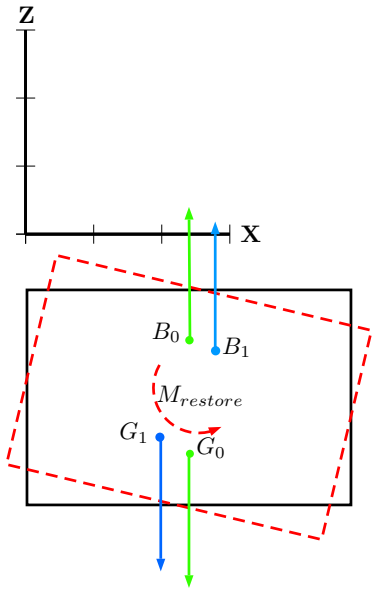

Figure 2.7: Restoring moment in pitch

The hydrostatic restoring matrix can therefore be simplified to:

$$\boldsymbol{g(\eta)} = \begin{bmatrix} 0 \\ 0 \\ 0 \\ -(z_g * W - z_b * B) * cos(\theta) sin(\phi) \\ -(z_g * W - z_b * B) * sin(\theta) cos(\phi) \\ 0 \end{bmatrix} \tag{2.84}$$

Skin Friction

The off diagonal terms of the skin friction will be assumed to be negligible compared to the diagonal terms. This approximation will in many cases not be correct, as off diagonal terms can be quite big. However the diagonal terms are usually dominant and this approximation is done to simplify the matrix enough to be able to estimate the terms. The more symmetric the body is the more accurate this approximation becomes. The skin friction matrix can hence be rewritten to a vector of diagonal terms:

$$D_S = \left[B_{11}^V, B_{22}^V, B_{33}^V, B_{44}^V, B_{55}^V, B_{66}^V\right]^D \tag{2.85}$$

Wave drift damping

As stated earlier wave drift damping is a 2nd order phenomenon that is caused by interaction between rapid oscillating behaviour of the incident waves and the slow-drift motion of the body. It was shown in section 2 that the 2nd order velocity potential for surface waves could be given as:

$$\phi_2 = \frac{3}{8}\omega\zeta_a^2 \frac{cosh(2k[z+h])}{sinh^4(kh)} sin(2kx - 2\omega t) \tag{2.86}$$

It can now be seen that the dynamic pressure and velocities of the surface waves will decay with the factor of e^{2kz} at deep water. It therefore follows that for a ROV at 100 meters depth the pressure amplitude experienced by the ROV will only be 0.0003% of that at the surface. Hence the ROV is not subjected to wave drift damping and:

$$\boldsymbol{D}_W = 0 \tag{2.87}$$

Damping due to vortex shedding

The vortex shedding phenomenon is an important damping contribution for ROVs. For the typical ROV shape(prismatic) the drag coefficients in Morison equation will be more or less independent of Reynolds number(for Reynolds numbers above 10^4[4]) which simplifies the damping matrix as it can be set to be constant for all

velocities. The off diagonal terms will be assumed to be negligible which again is a question of symmetry. If the body is perfectly symmetric this approximation is valid. However the more unsymmetrical the body is the less accurate this approximation gets. As a fairly symmetric body is already assumed the vortex shedding damping will be written as a vector of diagonal terms:

$$D_M = \left[B_{11}^M, B_{22}^M, B_{33}^M, B_{44}^M, B_{55}^M, B_{66}^M\right]^D \tag{2.88}$$

2.3.3 Froude-Kriloff and Diffraction Forces

It will in this section be shown that the diffraction can for underwater vehicles often be neglected due to the relative large distance to the free surface. In addition the Froude-Kriloff force will be evaluated for a ROV.

Froude-Kriloff

As stated earlier the Froude-Kriloff force is the force resulting from the undisturbed pressure field caused by e.g. current. As proven in section 2 the Froude-Kriloff mass on a cylinder is equal to the displaced mass of the cylinder. By assuming that the ROV is neutrally buoyant with uniformly distributed mass the Froude-Kriloff mass matrix become equal to the rigid body mass matrix[7] i.e. $M_{FK} = M_{RB}$. If then the acceleration of the current(wave acceleration is assumed negligible) is $\dot{\nu}_c$ the acceleration of the ROV can be written $\dot{\nu}_{rel} = \dot{\nu} + \dot{\nu}_c$. By inserting the relative velocity in the equation of motion instead of the ROV velocity it then follows that the Froude-Kriloff force will become a part of the rigid body mass matrix since :

$$M_{RB}\dot{\nu} + M_{FK}\dot{\nu}_c = M_{RB}\dot{\nu} + M_{RB}\dot{\nu}_c = M_{RB}\dot{\nu}_{rel} \tag{2.89}$$

Hence the relative velocity of the ROV will be used for future reference. Note that the relative velocity will simply be denoted ν and thus be used as the BODY-velocity.

Diffraction Forces

As the diffraction forces are a result of a body's interaction with surface waves they can be neglected for ROVs. The assumption that the body is independent of surface waves were used for the radiation problem and also for the Froude-Kriloff force. This can easily be proofed as the 1st order velocity potential is :

$$\phi = \frac{\zeta_a g}{\omega}\frac{cosh(k[h+z])}{cosh(kh)}cos(\omega t - kx)$$

By assuming deep water i.e. :

$$\lim_{h\to\infty}\frac{cosh(k[h+z])}{cosh(kh)} = \lim_{h\to\infty}\frac{\frac{e^{kh}e^{kz}+e^{-kh}e^{-kz}}{2}}{\frac{e^{kh}+e^{-kh}}{2}} = \frac{e^{\infty}e^{kz}+0}{e^{\infty}+0} \approx e^{kz}$$

It follows that the wave effects diminishes rapidly with the depth. For instance a wave at 100 meters depth will have a pressure/velocity amplitude of approximately 0.2% of that at the surface. In other words for ROVs operating on relative large depths the diffraction forces are fair to neglect. If the ROV comes close to the free surface the approximation to neglect diffraction forces may however still be valid. This because according to Faltinsen [1] the relative importance of diffraction forces is small when the wave length or height is much larger then the length of the body. The importance of diffraction for a ROV close to the surface is therefore dependant on the actual sea state.

2.3.4 Simplified equation of motion

In this chapter it was shown that the many coefficients in the equation of motion can be neglected. By enforcing the approximations and simplifications mentioned in this chapter the dynamic equation of motion can be written as:

$$\boldsymbol{M}_{RB}\dot{\nu} + \boldsymbol{C}_{RB}(\nu)\nu + \boldsymbol{M}_{A}\dot{\nu} + \boldsymbol{C}_{A}(\nu)\nu + \boldsymbol{D}_{S}(\nu)\nu + \boldsymbol{D}_{M}(\nu)\nu + \boldsymbol{g}(\eta) = \boldsymbol{\tau} \tag{2.90}$$

CHAPTER 3

PROPOSED PROCEDURE

In this chapter the proposed procedure for determining the hydrodynamic parameters evaluated in chapter 2 is presented. The procedure consists of a empirical estimate, an experimental estimate and a numerical estimate. The procedure hence consists of 3 different methods for obtaining the hydrodynamic parameters.

The 3 methods proposed in this chapter have very different characteristics. Especially the expected accuracy and time consumption of the methods are important factors. The empirical procedure can obtain estimate much faster than both numerical and experimental estimates which both take much time to complete. However the numerical and especially experimental procedures are meant to give very accurate estimates. The experimental procedure proposed requires little time and equipment. As the setup is very basic it remains to see whether the results produced will be accurate or not.

3.1 Empirical Estimates

In this section a method for estimating the hydrodynamic parameters for a typical work class ROV will be shown. The procedure for estimating hydrodynamic mass, damping, restoring and rigid body mass is presented. The results of the method applied on the reference ROVs can be found in chapter 4. The method is built on basic empirical and analytical data available and can be used on any geometrical shape. When developing this method the focus was to create a basic estimate that can be performed quickly with reasonable accuracy. The method therefore requires little knowledge of the ROV.

3.1.1 Mass

The terms in the mass matrix are very simple geometric quantities. If a CAD-model exists the exact value of the coefficients can easily be found. If a CAD-model does not exist the coefficients can be found by use of integration and parallel axis theorem. It will in these estimations be assumed that the ROV is a prism with mass of m kg

Translations

When calculating the translational terms it is assumed that the mass is evenly distributed over the entire volume of the ROV. As the weight in air is already known for the ROV the translational terms are already known,$M_{11} = m$ kg, $M_{22} = m$ kg, $M_{33} = m$ kg. Note that M_{15} and M_{34} are zero since z_g is zero due to the definition of the coordinate system.

Rotations

The rotational degrees of freedom coefficients are defined as the moments and products of inertia. The diagonal terms are called moments of inertia and are calculated by the formula:

$$I_P = \int_V \rho(r) * r^2 \mathrm{dV} = m * r^2 \tag{3.1}$$

This gives the following values for the moments of inertia (around the center of gravity) when the ROV is assumed to be prismatic shaped:

$$I_4 = \frac{m}{12}(W^2 + H^2) = \frac{m\,[kg]}{12}((W\,[m])^2 + (H\,[m])^2) = I_4[kgm^2]$$

$$I_5 = \frac{m}{12}(L^2 + H^2) = \frac{m\,[kg]}{12}((L\,[m])^2 + (H\,[m])^2) = I_5[kgm^2]$$

$$I_6 = \frac{m}{12}(W^2 + L^2) = \frac{m\,[kg]}{12}((W\,[m])^2 + (L\,[m])^2) = I_6[kgm^2]$$

If the ROV is a perfect prism this means that the center of gravity will be in the geometrical center which again will make the coupling terms zero.

3.1.2 Hydrostatic Restoring

Using simple trigonometry it is possible to find the restoring moments in roll and pitch. Since the distance between the COB and COG is fixed the moment arm will only be dependant of the displacement.

As stated earlier it is normal for ROVs to have a buoyancy force slightly larger than the weight in water. This is because in the event of a power loss or other problems the ROV will eventually resurface. This net buoyancy force is usually very small and can be neglected when calculating the restoring moments. In other words it is assumed that the weight is equal to the buoyancy. The distance between the center of gravity and the center of buoyancy is a very important parameter for estimating the restoring moments. Simultaneously it is a parameter which is very hard to estimate analytically. CAD-softwares like Rhinoceros or HydroD are able to find the center of gravity and buoyancy fairly quick. For the point of this exercise it is assumed that position of the center of buoyancy will be known.

The restoring moments for a ROV thus becomes:

$$B = W = m * G = m\,[kg] * 9.81\frac{m}{s^2} = 9.81 * m\,[N]$$

$$C_{44} = -(z_g * W - z_b * B) * cos(\theta)sin(\phi) \approx W * \overline{BG} * 1 * \phi$$

and:

$$C_{55} = -(z_g * W - z_b * B) * cos(\phi)sin(\theta) \approx W * \overline{BG} * 1 * \theta$$

Where the z-axis is positive upwards and $\overline{BG}$ is the distance(vertical) between COG and COB. As z_g is zero and small angles are assumed the expressions simplifies to:

$$C_{44} \approx (9.81 * m) * (\overline{OB})\phi\,[Nm]$$

$$C_{55} \approx (9.81 * m) * (\overline{OB})\theta\,[Nm]$$

Where $\overline{OB}$ is the distance from CO to COB.

3.1.3 Added Mass

Introduction

To estimate the added mass for the ROV analytical data must be used. There are many sources for added mass data, but in this thesis the DNV standard will be used as reference[29][1]. The DNV-standard uses a rectangular prism where 2 of 3 sides are equal as reference. This assumption is valid for SF-30k, AC-ROV 100, Seabotics LBV600-6 and Videoray PRO-4 as all these ROVs have approximately equal height and width. (For ROV Neptunus this assumption is not valid and may therefore give rice to a possible error in the estimates) The mean value of the height and width will therefore be used to find empirical values.
Since the reference values assumes a solid prism the results need to be adjusted to account for penetrating flow as the ROV is not completely solid. This will be done by including a scaling coefficient C_p^{mn}. This coefficient is the projected area in the superscripted plane divided by the area of the referenced prism i.e. $C_p^{mn} = A_p^{mn}/A^{mn}$. In the table below the local coordinate system used to obtain the relevant projected area coefficients is presented.

DOF	m	n	o
Surge & roll	X	Y	Z
Sway & Pitch	Y	Z	X
Heave & Yaw	Z	X	Y

Table 3.1: Projected area coefficient superscript
(used in empirical calculations)

The added mass data for a rectangular prism is according to DNV[29] :

Body shape	*Dimensions(B/A)*	*Added mass coefficient*
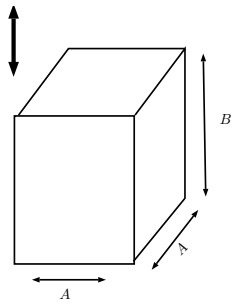	1.0	0.68
	2.0	0.36
	3.0	0.24
	4.0	0.19
	5.0	0.15
	6.0	0.13
	7.0	0.11
	10.0	0.08

Table 3.2: Added mass coefficients
[29]

[1]The DNV standard is based on Applied fluid dynamics handbook by Blevins 1984

For the rotational degrees of freedom empirical 3D data was not found. A different approach therefore had to be used. Using knowledge about similar shapes one knows that the difference in added mass for a sphere (3D) and an infinitely long cylinder of same radius(2D) is 50%[2]. By converting this relation to the problem at hand it is possible to create a procedure for the rotational degrees of freedom.

A possible procedure is described below:

- Find added mass for tranlational DOF using empirical 3D data.
- Find added mass for translational DOF using 2D data and strip theory.
- Calculate the difference in the two methods.(Scaling factor)
- Find added mass for rotational DOF using 2D data and strip theory.
- Scale the results.

By using this method it is possible to find all the diagonal terms in the added mass matrix.

Projected Area

In order to utilize the empirical data in the reference[29] it is important that a good scaling procedure exists to take into account the deviation of the ROV against the referenced prism. This can be done in many different ways, but it is important to use a method in which all the quantities can be obtained with relative ease. In this thesis the added mass coefficients will be scaled using the projected area as mentioned earlier. These values are found by creating a model in SolidWorks and measuring the projected area in all 3 planes. The projected area can also be found by measuring the full size ROV manually. The projected area is then used to calculate the coefficients C_p^{mn}.

$$C_p^{XY} = \frac{A_p^{XY}}{A} = \frac{A_p^{XY}}{L * W}$$
$$C_p^{YZ} = \frac{A_p^{YZ}}{A} = \frac{A_p^{YZ}}{H * W}$$
$$C_p^{ZX} = \frac{A_p^{XZ}}{A} = \frac{A_p^{XZ}}{L * H}$$

Translations

The procedure will first be performed on the surge DOF. It can be seen in table 3.2 that the minimum (B/A) value referenced is 1.0. This means that the 3D-data is only available for surge DOF when it is assumed that the length is larger than both the width and height of the ROV. This is usually the case and is also the case for all the five ROVs used as reference in this thesis.

The first step is to find the empirical 3D coefficients for A_{11}. To look up the table values the width over height relation of the ROV is needed(b/a). As the table only contains a given number of data points the dataset is linearised between the two values in which the (b/a) value lies.

Linearising the distance between the points gives the following formula to obtain the empirical value:

$$C_a(b/a) = \frac{C_a(2) - C_a(1)}{X_2 - X_1} * (X - X_2) + C_a(2) \tag{3.2}$$

Then the reference volume needs to be calculated:

$$V_R = b * a^2$$

The modified formula for added mass is hence written:

$$A_{ij} = C_a V_R \rho_{water} (C_p^{no})^2 (C_p^{mo})(C_p^{mn}) \tag{3.3}$$

A_{11} is now calculated using 3D data and should therefore give a reasonable estimate.

Now the same coefficient will be estimated using strip theory with 2D coefficients given in Newman 1977[2] on page 145 and DNV rp-h103[29] on page 139. The first step is again to find the width over height relation (b/a). Inserting this value into equation (3.2) gives the added mass coefficient. As strip theory is used the reference area rather than the reference volume needs to be calculated:

$$A_R = \pi * (a)^2$$

The 2-D added mass coefficient in Surge then becomes:

$$A_{11}^{2D} = \rho * C_a A_r (C_p^{no})^2 (C_p^{mo})(C_p^{mn})$$

Then by applying strip theory the 2D added mass is integrated over the entire length of the body. The 3D added mass using strip theory therefore becomes:

$$A_{11} = \int_{-L/2}^{L/2} A_{11}^{2D} dx$$

It is now possible to find the difference between the strip theory and 3D calculations:

$$\lambda = \frac{A_{11}^{empirical-3D}}{A_{11}^{strip-theory}}$$

The scaling factor λ is the relationship between the two methods. It therefore becomes apparent that if this relationship is valid for all DOFs the added mass can be calculated using strip theory and then scaled to obtain the correct added mass estimate.

Rotations

For the rotational degrees of freedom strip theory will be used and scaled the same way as the translational degrees of freedom. The 2D added mass coefficient is again found from DNV[29]. The general formula for the 2D added mass for rotational DOFs is:

$$A_{ii}^{2D} = \rho * C_a * \pi * a^4 (C_p^{no})(C_p^{mo})(C_p^{mn}) \tag{3.4}$$

Integrating over entire length of the body:

$$A'_{ii} = \int_{-(L,B,H)/2}^{(L,B,H)/2} A_{ii}^{2D} dx$$

and finally scale the result:

$$A_{ii} = A'_{ii}\lambda[kgm^2]$$

3.1.4 Damping

Introduction

The Damping of the ROV are forces related to the velocity. As the damping is a highly non-linear phenomenon it is very hard to estimate correctly.
To analyse the damping forces on the ROV the concept of damping must first be understood. As seen in chapter 2 the relevant damping contributions acting on a submerged ROV are: linear and quadratic skin friction in addition to damping due to vortex shedding. As stated in chapter 2 the damping due to vortex shedding can be modelled as a 2nd order function(Morison Equation). It therefore follows that the main damping contributions for a ROV can be described by a linear and a 2nd order damping coefficient.

$$B = B^{LIN} + B^{NL} \tag{3.5}$$

The linear part of the damping therefore consists of linear skin friction. The non-linear damping consists of all higher order terms such as turbulent skin friction and drag due to vortex shedding. For low velocities there will be less turbulence and vortex shedding which will make the linear damping the dominating term. Likewise will the non-linear term dominate for larger velocities. It therefore becomes apparent that both terms are crucial to describe the damping behaviour of the ROV over the entire operational domain.

Quadratic Damping

As stated earlier the quadratic damping represents all higher order damping contributions, but mainly vortex shedding and turbulent boundary layer skin friction. One might think its more logical to start with the linear damping, but for empirical estimates the quadratic damping is easier to find by utilizing Morison equation.
The quadratic damping can not be found using potential theory this because potential theory assumes that water is an irrotational,incompressible and inviscid fluid. This assumption can for many applications be sufficient, but when it comes to damping the viscosity of water is important.

Just as for added mass the only available 3D-parameters are the 3D drag coefficients in the surge DOF.(again assuming that the ROV has a length which is larger than width and height) The procedure will therefore be similar to that of the added mass. The quadratic damping will be estimated using 3D coefficient and then by using Morison equation. The result will afterwards be scaled. The same scaling number will then be applied for the remaining degrees of freedom.

The drag coefficients are, as established earlier, purely empirical coefficients meant to describe the viscous drag forces of a specific geometry. As the dimensions for the ROV are known the 3D and 2D drag coefficients can be found in table 10-19 and 10-20 in Blevins 2003[4] respectively.

The drag coefficients for the translational DOFs can for the ROV Seabotix LBV6-600 be found in the table below.

DOF	***L/D***	$C_D(2D)$	$C_D(3D)$
$Surge$	1.81	1.65	0.90
$Sway$	1.10	2.04	NA
$Heave$	0.91	2.17	NA

Table 3.3: Drag Coefficients for Seabotix LBV600-6

It should be noted that the drag coefficients in the reference [4] are given as :

$$C_D = \frac{F_D}{\frac{1}{2}\rho * A * u|u|} \tag{3.6}$$

Which is the same non-dimensional expression as was found in chapter 2.

Using equation (2.66) a general expression for the translational quadratic damping coefficients can be written:

$$B_{jj}^{NL} v_j|v_j| = \frac{\rho}{2} C_D A v_j|v_j| \lambda(C_p^{no}) \qquad j = 1,2,3 \tag{3.7}$$

Note that the reference area in Morison equation is scaled using the projected area. The difference between strip theory(2D) and the 3D drag coefficient then needs to be calculated. For e.g. Seabotix LBV600-6 the ratio is found to be:

$$\lambda = \frac{C_D(3D)}{C_D(2D)} = \frac{0.90}{1.65} = 0.53 \tag{3.8}$$

All the necessary terms going into the modified Morison equation are now found and the quadratic damping in the translational DOFs can therefore be calculated using equation (3.7).

To estimate the nonlinear damping in the rotational DOFs is quite challenging, mainly because good empirical methods were not found. As the author were not able to find a reliable method for estimating the nonlinear damping for rotational DOFs a new method had to be established. This method builds on the fact that for small rotations a rotational motion can be evaluated as a translational motion.

Firstly the ROV is divided into a total of 4 quadrant around each axis.(Will add up to 12 quadrants for all 3 axes) Furthermore it will be assumed that each quadrant only moves in the horizontal or vertical direction. By looking at figure 3.1 this

means that the solid quadrants will move horizontally and the stapled quadrants will move vertically. The most important assumption here is that the quadrants have small angular rotations.

As the quadratic damping is a quadratic function with respect to velocity the drag will be zero at the center corner of the quadrants and have a maximum value at the outer end, again see figure 3.1. It then follows that the torque-arm attacks at a distance $\frac{3}{4}$ quadrant width from the center of rotation. The rotational damping in all rotational DOFs can thus be expressed by the drag coefficient of each quadrant and the local translational velocity at the endpoints.

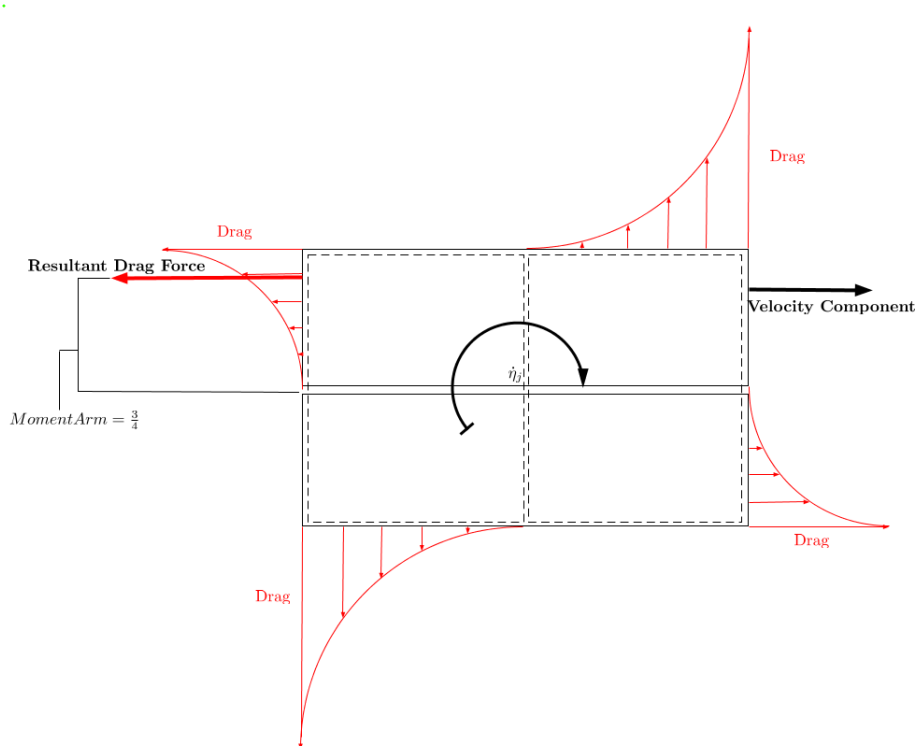

Figure 3.1: Discretization of ROV

Now an expression for the translational velocity for the different quadrant must be found. The points of interest are the outer corners. The translational velocity for these points can be described using the relation below:(The choice of L,B or H depends on the degree of freedom)

$$\overline{v_2}[m/s] = v_2[rad/s] * \frac{(L/B/H)}{2}[m] \tag{3.9}$$

Lastly the drag coefficients for each quadrant are needed. From Blevins 2003 table 10-20[4] these can be found. The general equation for the drag force of each

quadrant can be written:(Note that the correct C_P value is "om" for horizontal quadrants and "mn" for vertical quadrants)

$$F^j_{quadrant} = \frac{1}{2} * \frac{1}{3} * \rho * C_D * A * C_P^{om/mn} * \lambda * \overline{v_2}\left| * \overline{v_2}\right| \qquad j = 4,5,6 \qquad (3.10)$$

Note that the total integrated force of a 2nd order force function from 0 to 1 is 1/3 since:

$$F = \int_0^1 x^2 \, dx = \frac{1}{3}$$

Multiplying with the distance 3/4 from the center of rotation to get the moment around the axis:

$$\overline{M}^j_{quad} = F^j_{quadrant} * \frac{3}{4} \frac{L,B,H}{2}$$

Again L,B or H depends on the degree of freedom and whether it is a horizontal or vertical quadrant.

Finally the translational velocity terms need to be inserted:

$$M^j_{quad} = \overline{M}^j_{quad} * \left(\frac{L,B,H}{2}\right)^2$$

Now the damping for the horizontal and vertical quadrants are added together. For all 4 quadrants this gives a total damping moment of :

$$M_{tot} = 2 * M^j_{quad-Horizontal} + 2 * M^j_{quad-Vertical}$$

Linear Damping

The linear damping can be very hard to estimate analytically. A number of general approximations exists, though most of them are for surface vessels. Fossen 2011[5] page 125 suggests the following empirical estimates for the linear skin friction damping of a floating vessel:

$$B_{11}^{LIN} = \frac{M_{11} + A_{11}}{T_{surge}} \tag{3.11a}$$

$$B_{22}^{LIN} = \frac{M_{22} + A_{22}}{T_{sway}} \tag{3.11b}$$

$$B_{33}^{LIN} = 2\Delta\zeta_{heave}\omega_{heave}[M_{33} + A_{33}(\omega_{heave})] \tag{3.11c}$$

$$B_{44}^{LIN} = 2\Delta\zeta_{roll}\omega_{roll}[I_{44} + A_{44}(\omega_{heave})] \tag{3.11d}$$

$$B_{55}^{LIN} = 2\Delta\zeta_{pitch}\omega_{pitch}[I_{55} + A_{55}(\omega_{pitch})] \tag{3.11e}$$

$$B_{66}^{LIN} = \frac{I_{66} + A_{66}}{T_{yaw}} \tag{3.11f}$$

Where:

$$T_{DOF} = \frac{T_{n(DOF)}}{2\pi\zeta} \tag{3.12}$$

In this thesis a similar approach will be used. Starting with the equation of motion for a viscously damped(linear damped) free vibration linear 1DOF system :

$$(m + m_a)\ddot{\overline{X}} + K_L\dot{\overline{X}} + g\overline{X} = 0 \tag{3.13}$$

Dividing by the mass term gives:

$$\ddot{\overline{X}} + \frac{K_L}{m}\dot{\overline{X}} + \omega_n^2\overline{X} = 0 \tag{3.14}$$

According to Kreyzsig 2010[11] the equation has the roots:

$$\begin{Bmatrix}\lambda_1\\ \lambda_2\end{Bmatrix} = -\frac{K_L}{2m} \pm \sqrt{K_L^2 - 4mg} \tag{3.15}$$

It can now be seen that the critical damping occurs when K_L equals $2m\omega_n$. By introducing the critical damping to equation (3.14) it can be rewritten:

$$\ddot{\overline{X}} + 2\zeta\omega_n\dot{\overline{X}} + \omega_n^2\overline{X} = 0 \tag{3.16}$$

where

$$\zeta = \frac{K_L}{K_{Lcrit}} = \frac{K_L}{2m\omega_n} \tag{3.17}$$

It therefore follows that the linear damping can be estimated by three parameters. The mass and the natural frequency can be calculated whilst for the damping ratio a value must be assumed. For surface vessels the damping ratio in roll usually lies in the range of $2-10\%$ [5] [30]. The damping ratio will in this thesis be set to 2.5% for all ROVs. It may prove to be to big or to small, but should at least be in

the correct range.

As the natural frequency is given :

$$\omega_n = \sqrt{\frac{g}{m + m_a}}$$

(3.17) can be rewritten to :

$$K_L = 2\zeta m \sqrt{\frac{g}{m + m_a}} \tag{3.18}$$

The restoring matrix only have non-zero values in roll and pitch. The linear damping is therefore only possible to calculate in these two DOFs by the use of this method.

It will for the remaining DOFs be assumed that a linear relationship between the quadratic and linear damping exists. In other words it will be assumed that the ratio between the linear and quadratic damping coefficients in pitch will be equal to that of yaw. The scaling factor for yaw will hence be obtained from the pitch or roll results. While for the translational DOFs the scaling factor of 0.16 is obtained from Eng et. al 2009 [15].

Complete Damping Matrix

Now the linear and nonlinear damping terms can be added together to create the complete damping matrix. In appendix A a Matlab script performing the mentioned routine can be found.

3.1.5 Summary

An empirical procedure to determine the coefficients in the dynamic equation of motion is presented. The empirical procedure presented can be applied to any ROV shape, size or geometry.

In the further work of this thesis two of the coefficient matrices will be left out. These are the rigid body mass matrices and restoring matrices. Since these coefficients can fairly easy be obtained from CAD-drawings or estimations as performed in this section the interest in these parameters is small. The focus will instead be put on the added mass and damping coefficients as these parameters are more difficult to obtain and present a more interesting challenge.

3.2 Experiment

In this thesis the experimental method of choice is a towing/rotation test. The test is designed to be fairly cheap and can be performed in relative little time. The experiment will be performed on two ROVs with completely different geometries, ROV Neptunus and Videoray PRO-4.

3.2.1 Theory

The experiment will be performed using a towing and rotation rig. The towing cart can move at a given speed in the horizontal direction whilst the rotation rig can rotate with a given angular velocity. The ROV and mounting bracket will be towed for different velocities/Reynold numbers and based on these results using least squares interpolation a drag/damping curve in each degree of freedom can be calculated. As the ROV is towed in full scale there is no need for scaling procedures, this removes a potentially large source for errors.
An important assumption used in this experiment is that the damping contribution from the mounting bracket can be linearly superimposed to the damping from the ROV. Hence by measuring the damping force of the bracket alone the damping force of the ROV can be found using the relation :

$$F_{ROV} = F_{Tot} - F_{Bracket} \tag{3.19}$$

In addition is bottom and free surface effects neglected as the ROV is located approximately 60 cm from the bottom as well as the free surface.

3.2.2 Setup

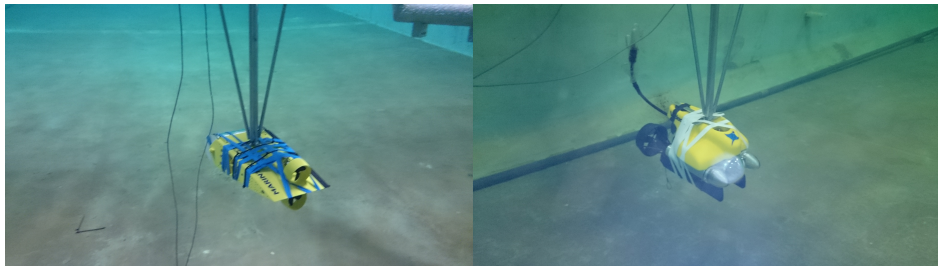

Figure 3.2: Underwater photos ROV Neptunus(left) and Videray PRO-4(right) mounted to bracket with strips, tape and screws for tests in heave/pitch(left) and surge/yaw(right).

The experimental setup is simple and the costs involved are small, however the experiment requires a towing/rotation rig to be present. The Experiment is peformed in the Marine Cybernetics laboratory(MC-Lab) at ntnu. This test facility have a towing rig that can move in 4 DOFs. More Information about the experimental facility can be found in Appendix G. In addition to a towing rig are two load cells

and a mounting bracket needed to perform this experiment.

The first step is to design the mounting bracket. As the mounting bracket must fit both the ROV and the towing/rotation rig exact measurements have to be taken. The mounting bracket also have to be the correct length to avoid bottom and free surface effects. As the depth of the pool is 1.5 m and the height from the surface to the rotation rig is 40 cm the mounting bracket has to be between 80 cm to 120 cm to avoid large free surface or bottom effects. The bracket is designed in Solidworks before it is cut and welded in the workshop. Figure 3.3 shows the CAD-model and the finished bracket. In addition a base plate has to be created. This base plate is screwed directly to the towing/rotation rigs already existing mounting system. The load cells are in turn connected to this base and the bracket. In that way all forces exerted on the bracket is absorbed by the loadcells. The base plate can be seen in figure 3.3 to the left of the bracket, and the load cells can be seen in figure 3.9

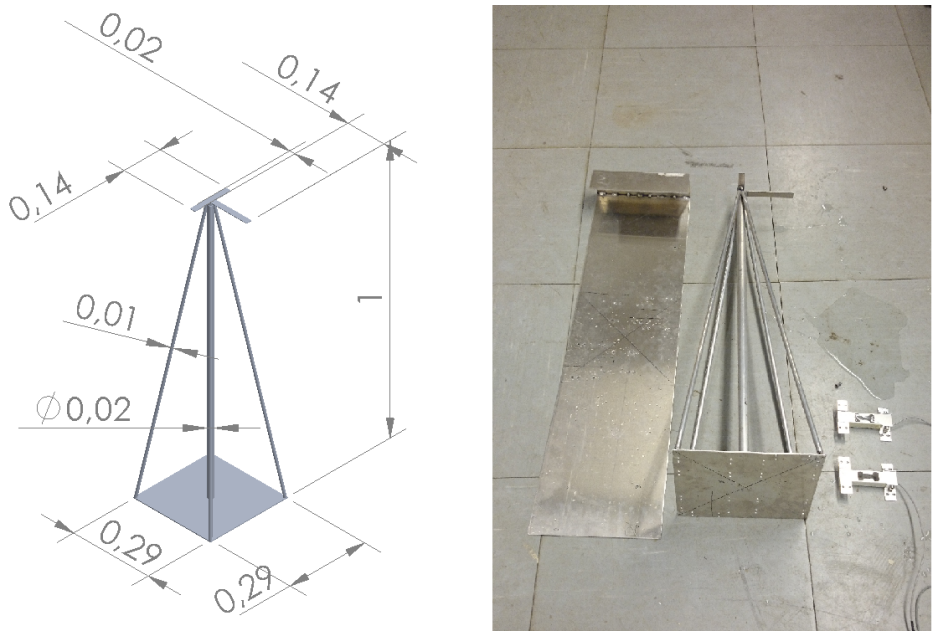

Figure 3.3: CAD-model of the custom bracket and picture of the final bracket

On top of the mounting bracket the load cells are fastened. The two 18 kg load cells are mounted diagonally with a distance of 0.12 m from the center of rotation. This setup enables both translational and rotational degrees of freedom to be measured without having to disassemble and reassemble the mounting bracket. The load cells are in turn mounted to the towing/rotation cart. The load cells are connected to a computer to record the horizontal force. At the bottom of the bracket the ROV is attached. The ROV is attached to the mounting bracket using screws and strips as shown in figure 3.4a. For the roll DOF waterproof tape also

has to be applied in order to completely lock the ROVs to the mounting bracket. For all DOFs the bracket is centered at the COG of the ROV which as stated in chapter 2 also is the center of origin of the body fixed coordinate system.

For all test runs the following quantities are recorded:

- Time step
- Force from both load cells
- Angular position
- Horizontal position

The data is recorded with a sampling rate of 200 Hz and stored in .ascii-file format. Each run is stored as a separate file which is automatically opened when the Matlab script found in appendix A.2 is run.

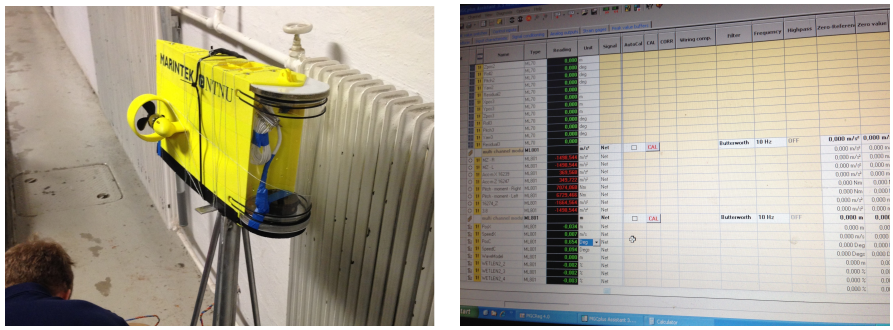

(a) ROV Neptunus mounted for surge and yaw tests)

(b) Recording computer setup

Figure 3.4: Test Setup ROV Neptunus

3.2.3 Experimental procedure

The towing cart is accelerated up to a given horizontal/rotational velocity and the corresponding forces are recorded. In this thesis, MATLAB has been used to write a program script to extract the relevant values(force and position) and calculate the linear and quadratic damping terms(K_L and K_Q) using least squares algorithm. Due to large oscillations(especially for small velocities) the script takes the average values over the relevant domain.
An example of this can be seen in figure 3.5 where the relevant domain is between 25 and 50 seconds.

For the rotational DOFs the measured force is converted to angular moment by multiplying the measured force with the distance from center of rotation(0.12m) and $\sqrt{2}$ see figure 3.9

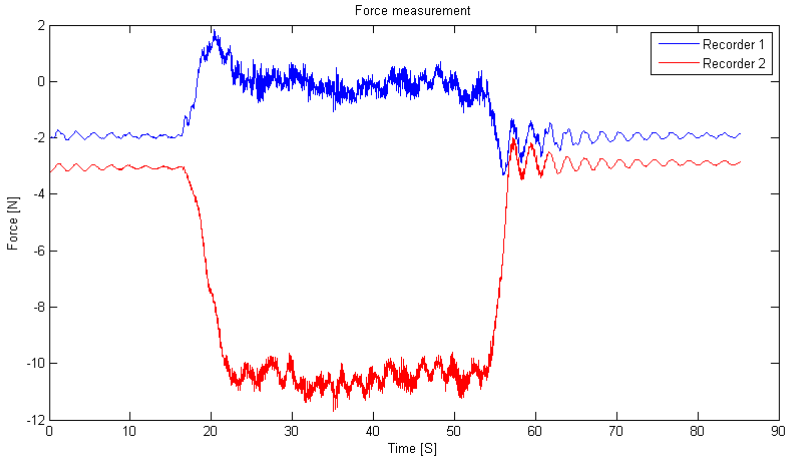

Figure 3.5: Example of experiment force recordings. Note that the total force is the sum of the two recordings

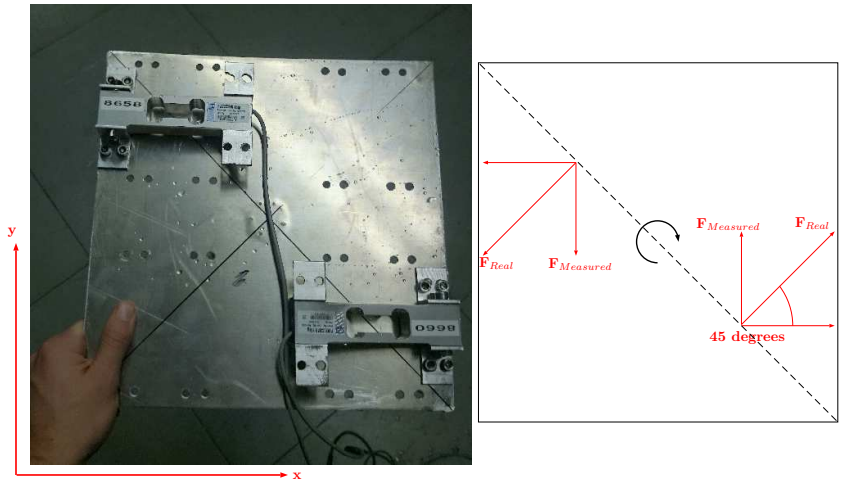

Figure 3.6: Picture and sketch of load cells setup seen in the horizontal plane

For each degree of freedom the tests are performed for about 10-14 different speeds, ranging from 0 to about 1.2 m/s or 0.4 rad/s. This results in approximately 10-14 data points to generate damping functions. After two DOFs have been run the bracket and ROV needs to be disassembled and reassembled with a different configuration to measure two new DOFs.(see figure 3.8) The DOFs that can be run simultaneously are surge/yaw, sway/roll and Heave/pitch.

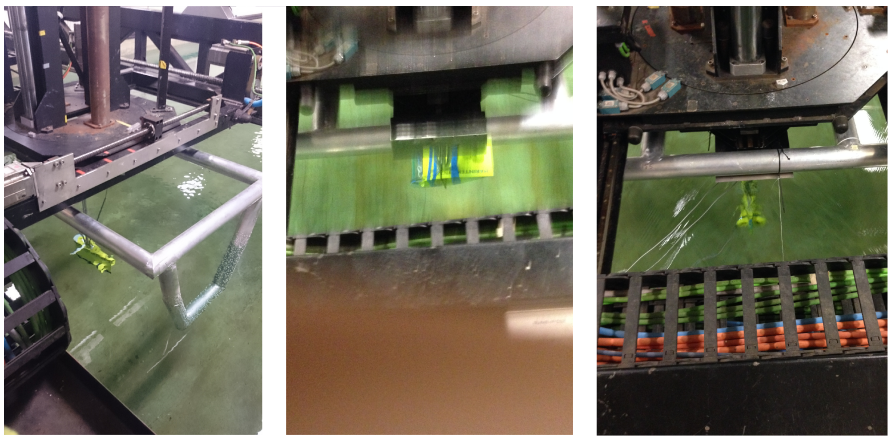

Figure 3.7: ROV Neptunus during sway, Heave and surge tests

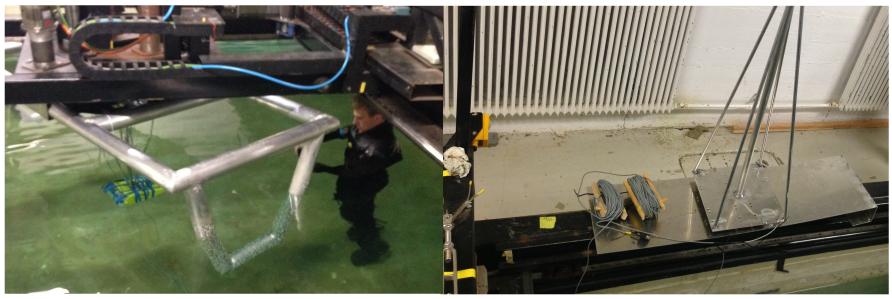

Figure 3.8: Disassembling Mounting bracket and ROV from towing cart

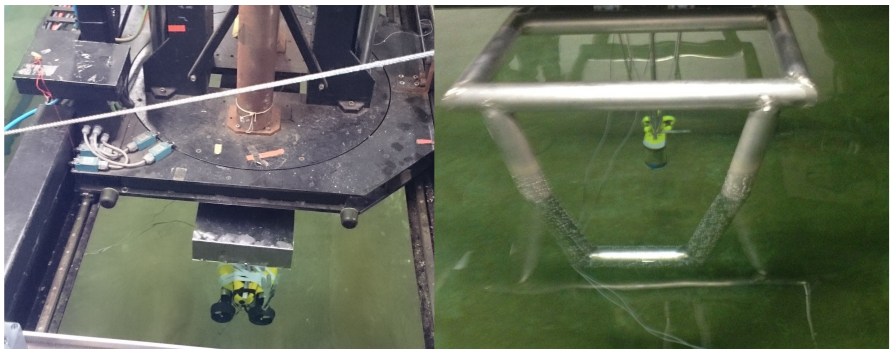

Figure 3.9: Towing test of VideoRay Pro-4(left) and Neptunus(right)

Lastly translation tests and rotation tests are performed for the bracket without the ROV.(see figure 3.10) Then damping functions for the bracket in the rotation and translation DOFs are computed using least squares interpolation.

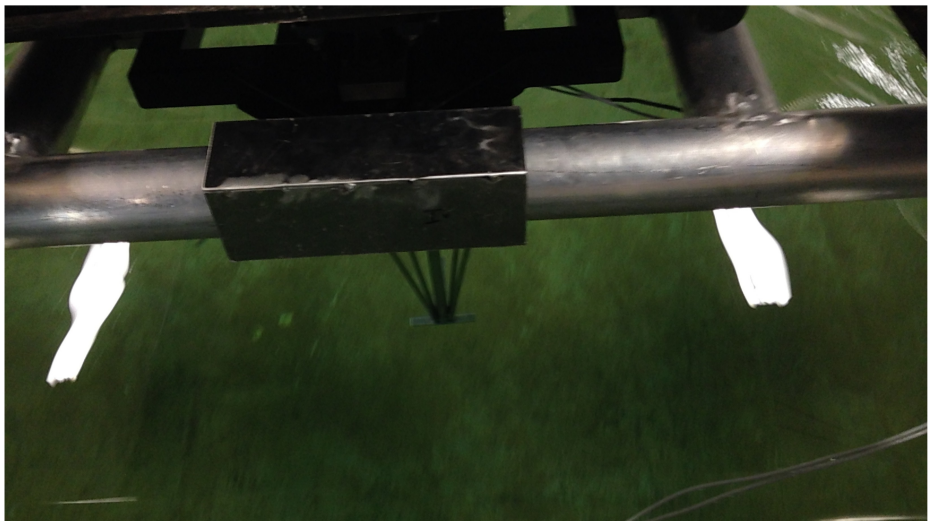

Figure 3.10: Mounting Bracket Towing test

3.3 Numerical Calculations

In this section the procedure used to obtain the numerical results will be explained. This procedure consists of using two types of programs. A Potential flow program(WADAM) is used to obtain the added mass and a CFD program is used to obtain the damping forces(SolidWorks Flow Simulation)

3.3.1 WADAM

As stated earlier WADAM is an extension to the HydroD program found in the DNV's Sesam Package which is based on WAMIT. WADAM can only import geometries hence other meshing tools have to be used. In this thesis Rhinoceros 3D is used as meshing software.

Meshing

The geometry imported in WADAM first have to be manually created. This is done in Solidworks. In SolidWorks the geometry is first sketched in 2D and then extruded in 3D. To create the geometry for the different ROVs is a very time consuming task. This because the different dimensions of the ROVs first have to be measured and then drawn in SolidWorks before a 3D body can be extruded. (the Model for Sf-30k did not have to be created as it could be found in Berg 2012[25]) After a complete ROV geometry is created the file needs to be exported as a .STEP file. As WADAM can only process .gdf files(WAMIT file format) another meshing software has to be used. Rhinoceros imports .STEP files and can create a mesh fairly quick using the "from NURBS object" function. This function takes the shape of any circle, arc or curve and convert them to Non-Uniform Rational B-Splines(Nurbs)[35]. The meshed file is then saved in .gdf file format. (All meshing files can be found in appendix D) The meshing procedure is illustrated in figure 3.12.

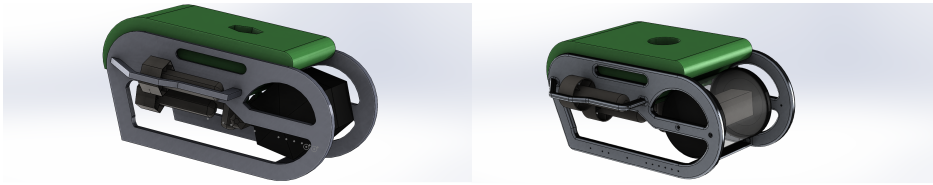

Figure 3.11: Simplified LBV600-6(left) and original LBV600-6(right)

A problem that can frequently occur is that the analysis takes to much time or the mesh files become to big.(WADAM has a limit of 20000 elements) It can therefore be necessary to simplify the mesh generated in Rhinoceros in order to be able to perform the analysis. A problem that can occur when a courser

mesh is applied is that the geometry becomes inconsistent. As circular shapes are converted to triangles or quadrilaterals it is given that a minimum number of mesh elements can be used before the shapes become disfigured. One way to avoid this problem is to create a simplified model in SolidWorks where some circular elements are converted to e.g hexagonal elements. This can be seen in figure 3.11 and in appendix D where "simplified" models have a reduced number of circular elements. However as this procedure both gives error in the estimates and takes much time it is not done unless needed.

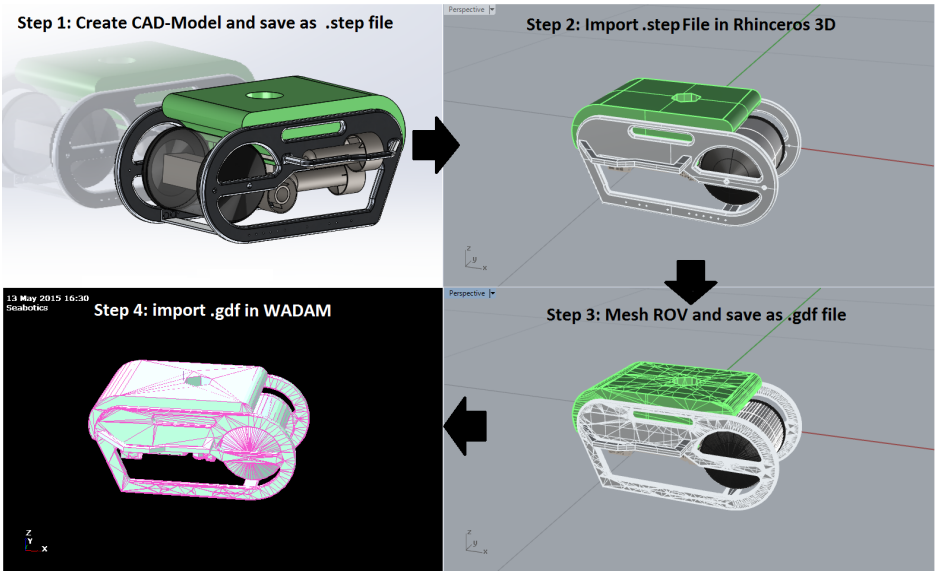

Figure 3.12: Meshing procedure for WADAM runs

Analysis

When performing the analysis the HydroD program first have to be booted. The WADAM-wizard is then run. As the quantity of interest in this analysis is only the frequency independent added mass(no wave interaction) the body is dislocated a distance of 100 meters from the surface and the surface waves are set to have a length of 0.15 meters(frequency of 20 rad/s). The ROV is hence unaffected by the surface waves. The mass model assumes that the mass is evenly distributed over the entire body when it calculates the moments and products of inertia, this should be a reasonably fair assumption. The center of buoyancy can be calculated using Rhinoceros. As all the inputs are given the analysis can be run.

WADAM furthermore uses a radius of gyration in pitch and roll equal the vertical dislocation. This become a problem since the roll and pitch added mass moments then become incorrect. This is solved by performing the analyses 3 times with different coordinate axis. The coefficients for surge, sway, heave and yaw are

found by setting surge as the x-axis, sway as the y-axis and heave as the z-axis(which is the correct orientation of the ROV). The Roll DOF is found by setting the surge as the z-axis, sway as the y-axis and heave as the x-axis. And finally the pitch DOF is found by setting surge as the x-axis, sway as the z-axis and heave as the y-axis. This procedure hence creates a total of 3 WADAM runs for each ROV.

Output

When the WADAM analysis is finished the results are stored in a .LIS file. The file can be opened by the Notebook text program, which is a standard Windows text editor. Normally the results can be read directly from this file. However the added mass data needs to be merged from three different result files. This because when dislocating the ROV 100 meters vertically the radius of gyration given as input in WADAM is set to be 100 meters in roll and pitch. The results are therfore taken from the three result files which can be found in appendix C.2 and can for all ROVs be found in an Excel spreadsheet located in the same appendix

3.3.2 Flow Simulation

SolidWorks was the main design tool used in this thesis, using the built in CFD package was therefore very practical. The damping forces can be found by evaluating the forces acting on the ROV when exposed to a uniform current with a given velocity. These forces are recorded and saved. Flow Simulation has the ability to run parallel computing which significantly reduces the computation time. As each CFD run generated approximately 120 MB of data the runs were not stored. However all the project files can be found in appendix D and the results from the CFD calculations can be found in appendix C.1.

Meshing

Creating CAD-models of the ROVs is the first step in the CFD analysis. The CAD-models are then meshed using the built in meshing tool in Flow Simulation. The mesh tool has two user inputs. First the mesh refinement can be modelled with a refinement from 1 to 8 where 8 is the most refined mesh. This simply means that two neighbouring blocks can have difference of maximum 8(1 block can be maximum 8 times or minimum 1/8 of the size of the other). A fine initial mesh is used for all ROVs except for Sf-30k. This because the other ROVs are very small and the computational domain is hence small and number of elements does not become to big. For SF-30k the finest mesh resolution is not chosen due to time constraints. As this ROV is much larger than the other ROVs the computational domain and element number become very big.

SolidWorks Flow Simulation has as of 2014 an adaptive mesh refinement function. [34] This function refines the mesh during calculations to give a more refined

mesh in important regions. This function therefore greatly simplifies the user inputs, but it also remove some of the user control. The adaptive mesh refinement is in this thesis limited to approximate 13 850 000 elements. This to make sure that the number of elements would not become larger then the computational resources(RAM and CPU) can handle. In figure 3.13 the mesh refinement process is illustrated for the verification test performed on a sphere with a diameter of 1 meter.

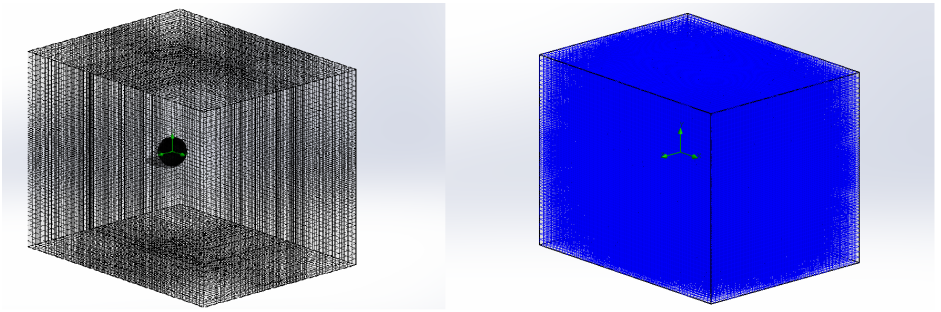

Figure 3.13: Initial mesh(left) and final refined mesh(right) with 353648 elements

Analysis

As stated earlier the drag-coefficients for prisms are approximately constant for high Reynold numbers(above 10^4). For spheres and cylinder this is however not the case as separation points and instability points will vary with Reynold numbers. As the ROVs consists of both prismatic and spherical elements it is fair to assume that the drag coefficients will vary over the operational domain. To find accurate damping forces multiple simulations will be run for each DOF with varying flow velocities. A damping function will based on these result be generated using least square interpolation.

The translational DOFs can be run fairly easy. The ambient flow is set to vary between 0.1 m/s to 1.0 m/s with an increment of 0.1 or 0.2 m/s. A total of 5 or 6 simulations are therefore done for each DOF.

The rotational DOFs need to be run with a different setup as the ambient flow cannot be set to rotate. This is done by creating a circular body that encloses the entire ROV. The body is given a rotational velocity and the corresponding torque acting on the ROV is measured. Figure 3.14 illustrates this concept. Different angular velocities are applied and the damping function is again found using least squares interpolation.

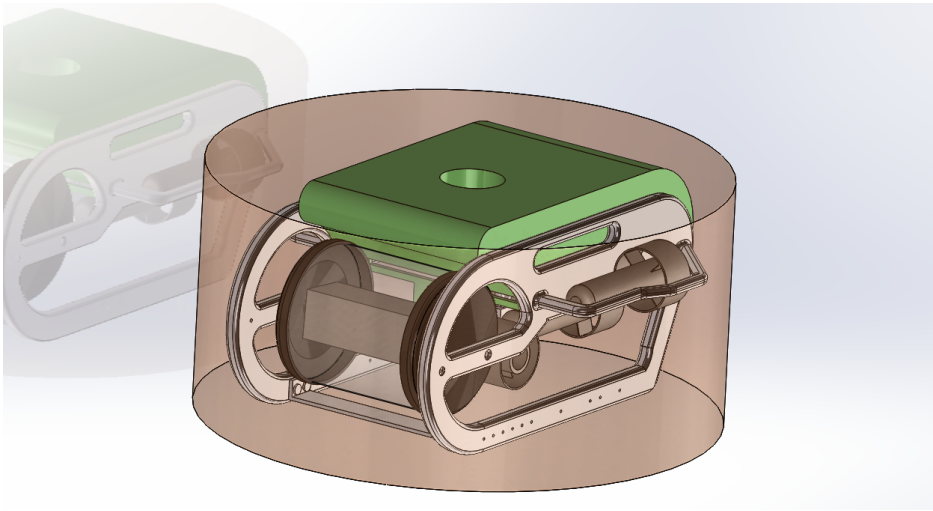

Figure 3.14: Rotational CFD setup of ROV LBV-600-6 to find damping torque in yaw

Output

The output from the CFD simulations can be set by the user. E.g. skin friction, torque, force, velocity and pressure are quantities that can be given as output. In the simulations done in this thesis only forces and torques are given as output. The output values are interpolated and the resulting damping functions are found.

Verification

In order to verify the CFD-program a simple verification using basic shapes and reference drag coefficients found in Blevins 03[4] is performed.

A verification test is performed on a square rod parallel to the flow. The Rod has dimensions of 1 meter diameter and 2 meter length. The Reynold number is set to be $1.7 * 10^5$ which is the Reynold number given in the reference. It would in this case result in a flow velocity of $0.085\,m/s$.(assuming a kinematic viscosity of water of $1 * 10^{-6} m^2/s$). The reference drag coefficient for this analysis is $C_D = 0.87$[4]. The simulation done in SolidWorks Flow simulation gives a drag coefficient of 0.8552 which is very close to the referenced value.

Another verification test is performed on a sphere with diameter 1 m. The analysis is performed using Reynold number 10^6 which results in a flow velocity of 1 m/s.(again using a kinematic viscosity of $10^{-6} m^2/s$) The reference drag coefficient for this analysis is $C_D = 0.12$[4]. The simulation done in SolidWorks Flow Simulation gives a drag coefficient of 0.1130 which is fairly close to the referenced value. This proves to show that for at least simple geometries and flow

conditions the CFD simulation should be able to produce results in the correct range and can thus can be used as reference.

CHAPTER 4

RESULTS

In this chapter the results from empirical, experimental and numerical estimates will be presented. For some ROVs only empirical and numerical estimates exists. The results are presented as:

- Numerical presentation of added mass
- Numerical presentation of Damping
- Graphical presentation of the damping
- Summary of Results

No graphical presentation will be performed on added mass since it is already proven that the added mass is frequency independent and thus only consists of constant terms. The added mass WADAM results furthermore can be found in appendix C.2.
The added mass results will be presented as the relative difference between the empirical estimates and the WADAM results given as: $D = \frac{Empirical}{WADAM} - 1$

No difference is calculated for the damping terms K_L and K_Q. This is because the linear interpolation functions found from CFD and experimental analysis are just 2nd order functions containing a linear and quadratic term. To compare the linear and quadratic terms separately does therefore not make sense.

The experimental procedure were only performed on 2 ROVs. ROV Neptunus and VideoRay Pro-4. Experimental results are therefore only presented for these two ROVs, these results can be found in appendix E.[1]

[1] AC-ROV 100 and Seabotix LBV600-6 were not able for testing at the time of this thesis

4.1 Sf-30k

4.1.1 Added mass

Added Mass

DOF	Empirical	WADAM	Unit	Difference
Surge(1)	932.9	780.2	kg	19.6%
Sway(2)	1516.5	1145.4	kg	32.4%
Heave(3)	3100.8	3717.0	kg	-16.6%
Roll(4)	201.9	512.2	kgm^2	-60.6%
Pitch(5)	657.0	926.8	kgm^2	-29.1%
Yaw(6)	515.1	219.2	kgm^2	135.0%

Table 4.1: Added mass diagonal values for SF-30k

4.1.2 Damping

Linear Damping[K_L]

DOF	Empirical	CFD	Unit
Surge(1)	126.9	19.9	kg/s
Sway(2)	175.0	33.0	kg/s
Heave(3)	315.9	-131.9	kg/s
Roll(4)	124.8	1.17	kgm/s
Pitch(5)	177.1	41.13	kgm/s
Yaw(6)	107.4	6.8	kgm/s

Table 4.2: Linear damping Sf-30k

Quadratic Damping[K_Q]

DOF	Empirical	CFD	Unit
Surge(1)	792.7	377.0	kg/m
Sway(2)	1093.6	604.0	kg/m
Heave(3)	1974.2	1374.0	kg/m
Roll(4)	275.4	358.57	kgm/s
Pitch(5)	943.6	826.66	kgm/s
Yaw(6)	572.1	521.2	kgm/s

Table 4.3: Quadratic damping Sf-30k

4.1.3 Graphical representation

Below are the damping forces and moments presented graphically.

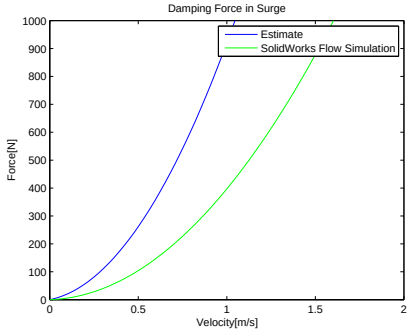

(a) Surge Damping Forces

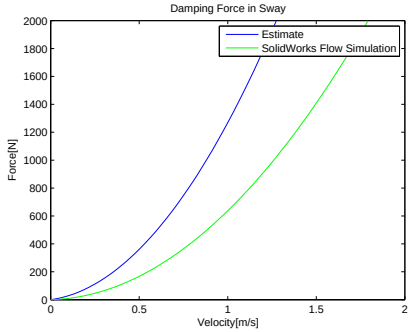

(b) Sway Damping Forces

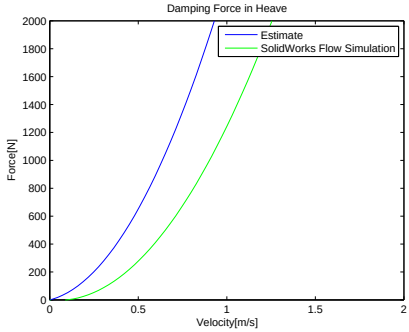

(c) Heave Damping Forces

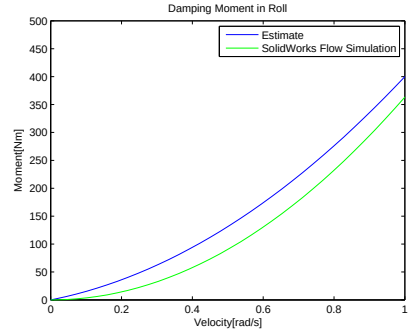

(d) Roll Damping Moments

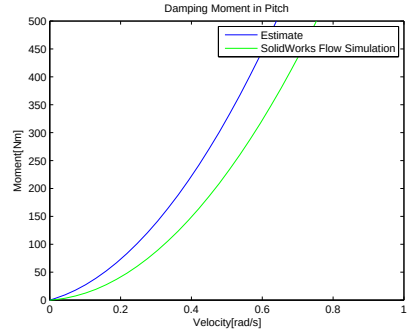

(e) Pitch Damping Moments

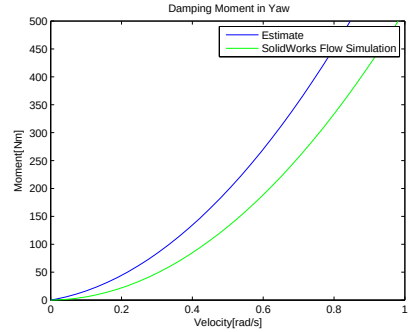

(f) Yaw Damping Moments

Figure 4.1: Damping forces and moments for SF-30k

4.2 ROV Neptunus

4.2.1 Added Mass

Added Mass

DOF	Empirical	WADAM	Unit	Difference
Surge(1)	1.926	1.867	kg	3.2%
Sway(2)	18.840	14.489	kg	30.0%
Heave(3)	5.993	2.706	kg	121.5%
Roll(4)	0.014	0.186	kgm^2	-92.4%
Pitch(5)	0.052	0.075	kgm^2	-30.7%
Yaw(6)	0.091	0.315	kgm^2	-71.1%

Table 4.4: Added mass diagonal values for ROV Neptunus

4.2.2 Damping

Linear Damping[K_L]

DOF	Empirical	CFD	Experiment	Unit
Surge(1)	1.993	-0.053	2.2907	kg/s
Sway(2)	13.139	0.539	4.8904	kg/s
Heave(3)	3.081	0.0403	15.1897	kg/s
Roll(4)	0.008	-0.0002	0.0025	kgm/s
Pitch(5)	0.012	0.0011	0.0093	kgm/s
Yaw(6)	0.0368	-0.0013	0.2605	kgm/s

Table 4.5: Linear damping ROV Neptunus

Quadratic Damping[K_Q]

DOF	Empirical	CFD	Experiment	Unit
Surge(1)	12.459	3.3804	4.077	kg/m
Sway(2)	83.2442	43.7230	35.2159	kg/m
Heave(3)	16.2536	14.3730	10.3037	kg/m
Roll(4)	0.022	0.0207	0	kgm/s
Pitch(5)	0.0552	0.0412	0	kgm/s
Yaw(6)	0.1698	0.1800	0.3196	kgm/s

Table 4.6: Quadratic damping ROV Neptunus

4.2.3 Graphical representation

Below are the damping forces and moments presented graphically.

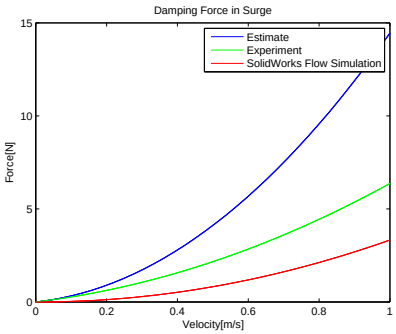

(a) Surge Damping Forces

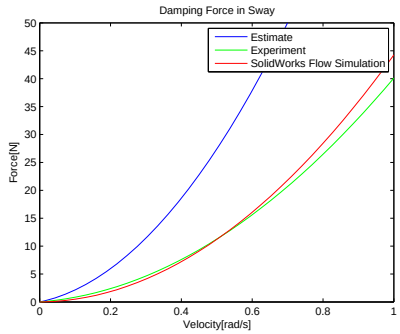

(b) Sway Damping Forces

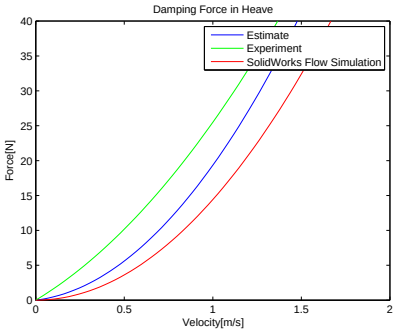

(c) Heave Damping Forces

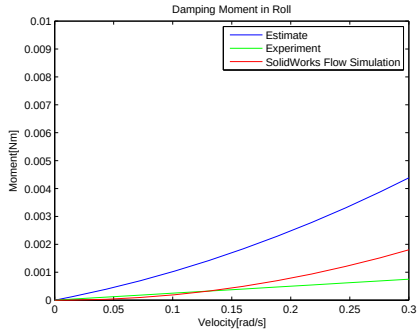

(d) Roll Damping Moments

Figure 4.2: Damping forces and moments for ROV Neptunus

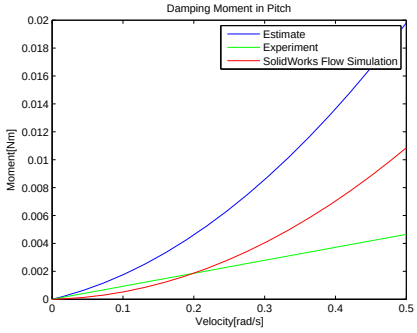

(a) Pitch Damping Moments

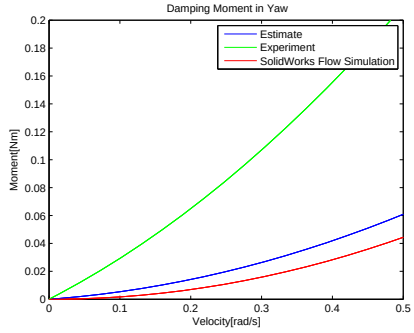

(b) Yaw Damping Moments

Figure 4.3: Damping forces and moments for ROV Neptunus

4.3 VideoRay PRO-4

4.3.1 Added Mass

Added Mass

DOF	Empirical	WADAM	Unit	Difference
Surge(1)	2.210	2.5028	kg	-11.7%
Sway(2)	5.814	7.1401	kg	-18.6%
Heave(3)	5.857	8.0125	kg	-26.9%
Roll(4)	0.007	0.0283	kgm^2	-90.0%
Pitch(5)	0.040	0.0371	kgm^2	+7.8 %
Yaw(6)	0.0288	0.0395	kgm^2	-27.1%

Table 4.7: Added mass diagonal values for VideoRay PRO-4

4.3.2 Damping

Linear Damping[K_L]

DOF	Empirical	CFD	Experiment	Unit
Surge(1)	2.3170	0.3572	20.55	kg/s
Sway(2)	5.0326	0.0515	NA	kg/s
Heave(3)	6.6261	0.0450	25.00	kg/s
Roll(4)	0.0189	0.0005	NA	kgm/s
Pitch(5)	0.0313	-0.0005	0.79	kgm/s
Yaw(6)	0.0286	-0.0026	0.05	kgm/s

Table 4.8: Linear damping VideoRay PRO-4

Quadratic Damping[K_Q]

DOF	Empirical	CFD	Experiment	Unit
Surge(1)	14.473	6.5482	30.60	kg/m
Sway(2)	31.454	27.4530	NA	kg/m
Heave(3)	41.413	31.0980	89.16	kg/m
Roll(4)	0.033	0.0255	NA	kgm/s
Pitch(5)	0.057	0.0549	0	kgm/s
Yaw(6)	0.048	0.0561	0	kgm/s

Table 4.9: Quadratic damping VideoRay PRO-4

4.3.3 Graphical representation

Below are the damping forces and moments presented graphically.

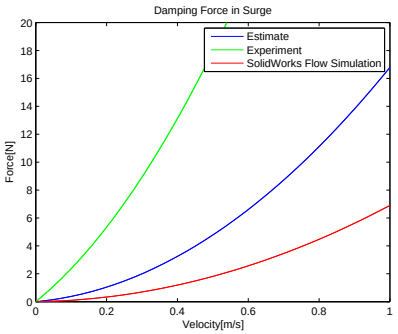

(a) Surge Damping Forces

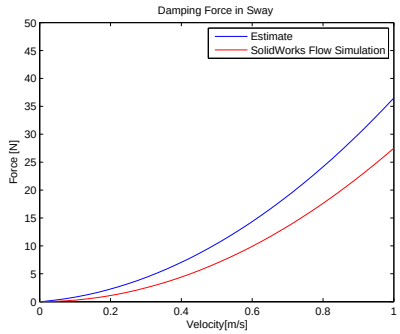

(b) Sway Damping Forces

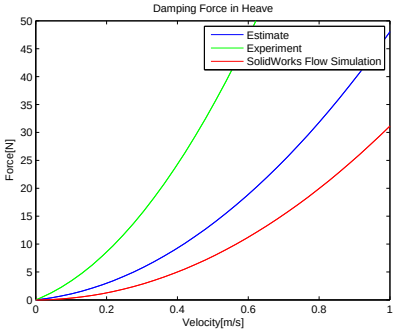

(c) Heave Damping Forces

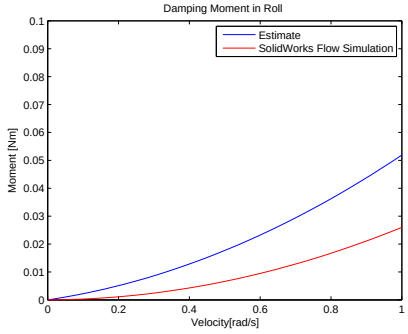

(d) Roll Damping Moments

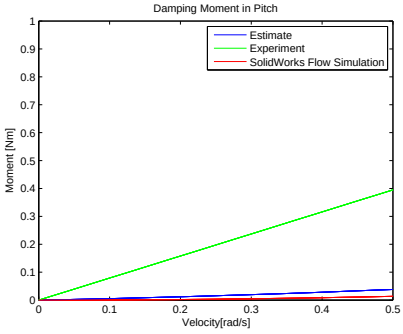

(e) Pitch Damping Moments

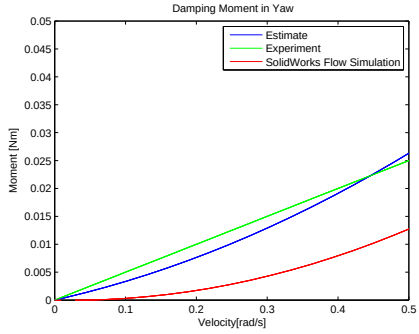

(f) Yaw Damping Moments

Figure 4.4: Damping forces and moments for VideoRay PRO-4

4.4 Seabotix LBV600-6

4.4.1 Added Mass

Added Mass

DOF	Empirical	WADAM	Unit	Difference
Surge(1)	10.6322	14.3173	kg	-25.7%
Sway(2)	23.5517	22.3744	kg	17.7%
Heave(3)	32.7863	29.9081	kg	9.6%
Roll(4)	0.0719	0.4814	kgm^2	-85.1%
Pitch(5)	0.2925	0.6471	kgm^2	-54.7 %
Yaw(6)	0.2736	0.5509	kgm^2	-50.3%

Table 4.10: Added mass diagonal values for Seabotix LBV600-6

4.4.2 Damping

Linear Damping[K_L]

DOF	Empirical	CFD	Unit
Surge(1)	4.7364	0.1213	kg/s
Sway(2)	8.9463	1.1732	kg/s
Heave(3)	13.2936	-20.1130	kg/s
Roll(4)	0.0544	-0.0282	kgm/s
Pitch(5)	0.0738	-0.0034	kgm/s
Yaw(6)	0.0529	-0.0033	kgm/s

Table 4.11: Linear damping Seabotix LBV600-6

Quadratic Damping[K_Q]

DOF	Empirical	CFD	Unit
Surge(1)	29.6028	23.9000	kg/m
Sway(2)	55.9146	46.2700	kg/m
Heave(3)	83.0852	87.2780	kg/m
Roll(4)	0.0773	0.3664	kgm/s
Pitch(5)	0.4091	0.4547	kgm/s
Yaw(6)	0.2931	0.5489	kgm/s

Table 4.12: Quadratic damping Seabotix LBV600-6

4.4.3 Graphical representation

Below are the damping forces and moments presented graphically.

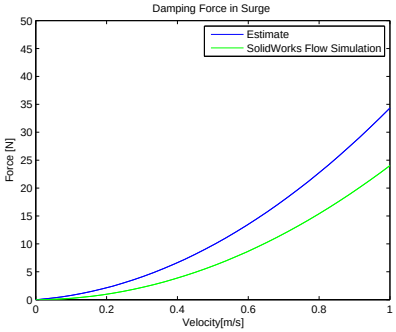

(a) Surge Damping Forces

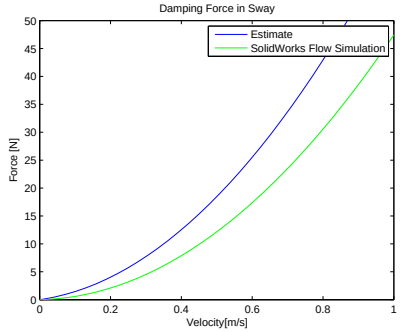

(b) Sway Damping Forces

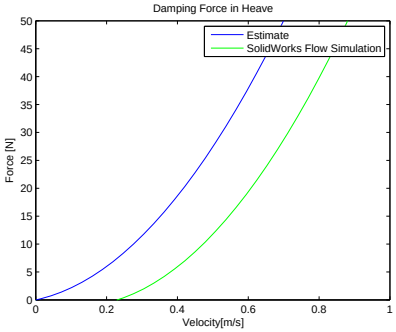

(c) Heave Damping Forces

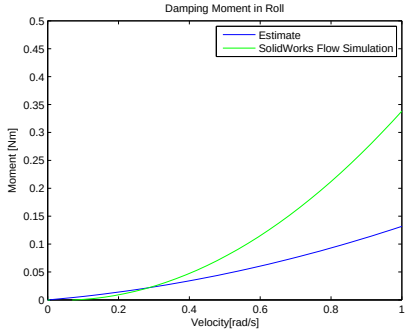

(d) Roll Damping Moments

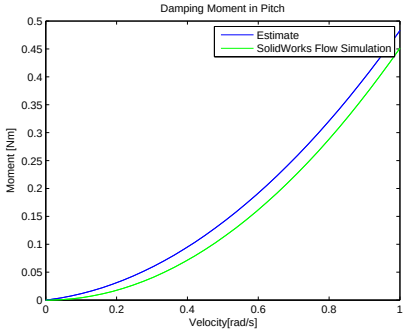

(e) Pitch Damping Moments

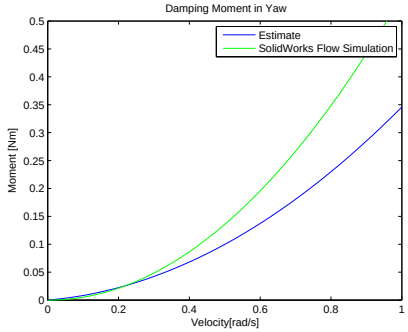

(f) Yaw Damping Moments

Figure 4.5: Damping forces and moments for Seabotix LBV 600-6

4.5 AC-ROV 100

4.5.1 Added Mass

Added Mass

DOF	Empirical	WADAM	Unit	Difference
Surge(1)	1.6875	2.0986	kg	-19.6%
Sway(2)	2.5681	2.2458	kg	14.3%
Heave(3)	2.6531	2.3915	kg	9.6%
Roll(4)	0.0022	0.0018	kgm^2	+22.2%
Pitch(5)	0.0038	0.0023	kgm^2	+65.2 %
Yaw(6)	0.0025	0.0032	kgm^2	-21.9%

Table 4.13: Added mass diagonal values for AC-ROV 100

4.5.2 Damping

Linear Damping[K_L]

DOF	Empirical	CFD	Unit
Surge(1)	1.4604	0.0280	kg/s
Sway(2)	2.1647	0.0088	kg/s
Heave(3)	2.3145	-0.0011	kg/s
Roll(4)	0.0044	-0.0003	kgm/s
Pitch(5)	0.0054	0.0006	kgm/s
Yaw(6)	0.0054	-0.0001	kgm/s

Table 4.14: Linear damping AC-ROV 100

Quadratic Damping[K_Q]

DOF	Empirical	CFD	Unit
Surge(1)	9.1273	9.2871	kg/m
Sway(2)	13.5296	6.3805	kg/m
Heave(3)	14.4655	4.2860	kg/m
Roll(4)	0.0022	0.0012	kgm/s
Pitch(5)	0.0022	0.0037	kgm/s
Yaw(6)	0.0022	0.0057	kgm/s

Table 4.15: Quadratic damping AC-ROV 100

4.5.3 Graphical representation

Below are the damping forces and moments presented graphically.

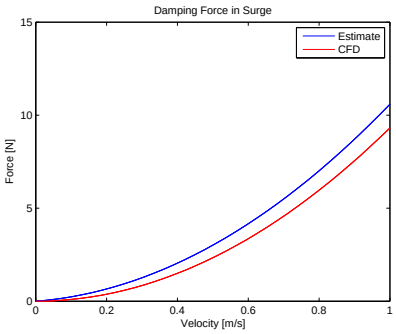

(a) Surge Damping Forces

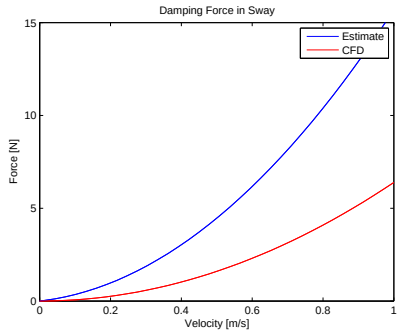

(b) Sway Damping Forces

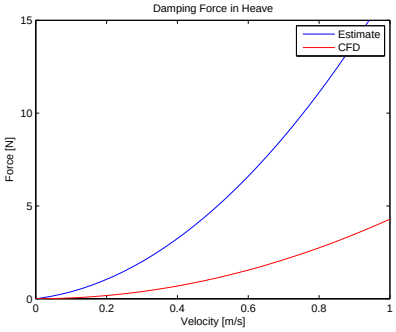

(c) Heave Damping Forces

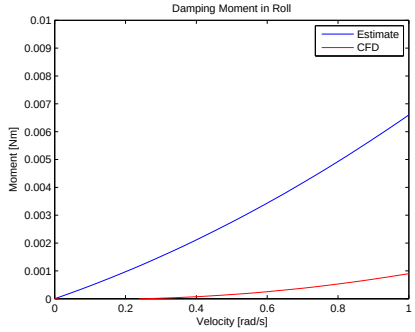

(d) Roll Damping Moments

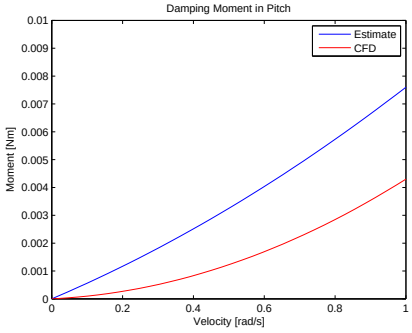

(e) Pitch Damping Moments

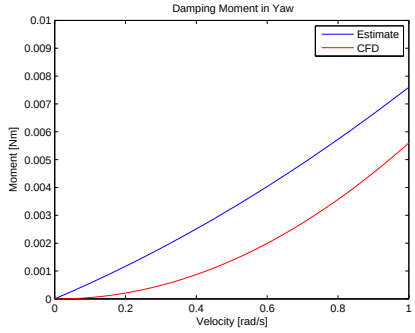

(f) Yaw Damping Moments

Figure 4.6: Damping forces and moments for AC-ROV 100

4.6 Summary

4.6.1 Added Mass

The relative difference between empirical estimate and WADAM anlysis is shown in figure 4.7

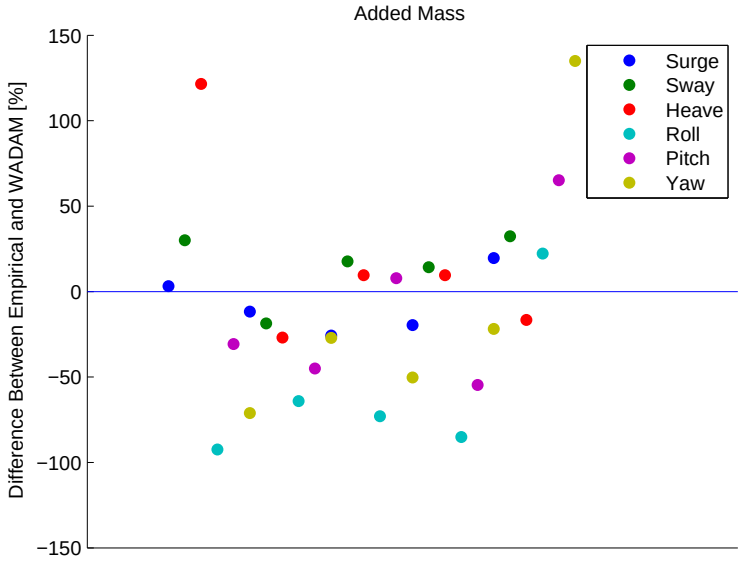

Figure 4.7: Relative difference in added mass between empirical estimate and WADAM analysis

The statistical properties of the added mass difference is then calculated:

DOF	Mean	σ	RMS
Surge	-6.8%	16.4%	17.7 %
Sway	15.2%	18.2%	23.7 %
Heave	19.4%	53.0%	56.6 %
Roll	-58.5%	41.5%	71.7 %
Pitch	-11.5%	43.8%	45.3 %
Yaw	-7.1%	73.2%	73.5 %

Table 4.16: Statistical properties of the relative difference between added mass empirical estimates and WADAM

4.6.2 Damping

Using the CFD estimates as reference the relative difference between empirical estimate and CFD, and experimental estimate and CFD damping can be presented graphically. The Relative difference is calculated as :

$$D^{Emp} = \frac{B^{Emp} - B^{CFD}}{B^{CFD}} \quad \text{and} \quad D^{Exp} = \frac{B^{Exp} - B^{CFD}}{B^{CFD}} \tag{4.1}$$

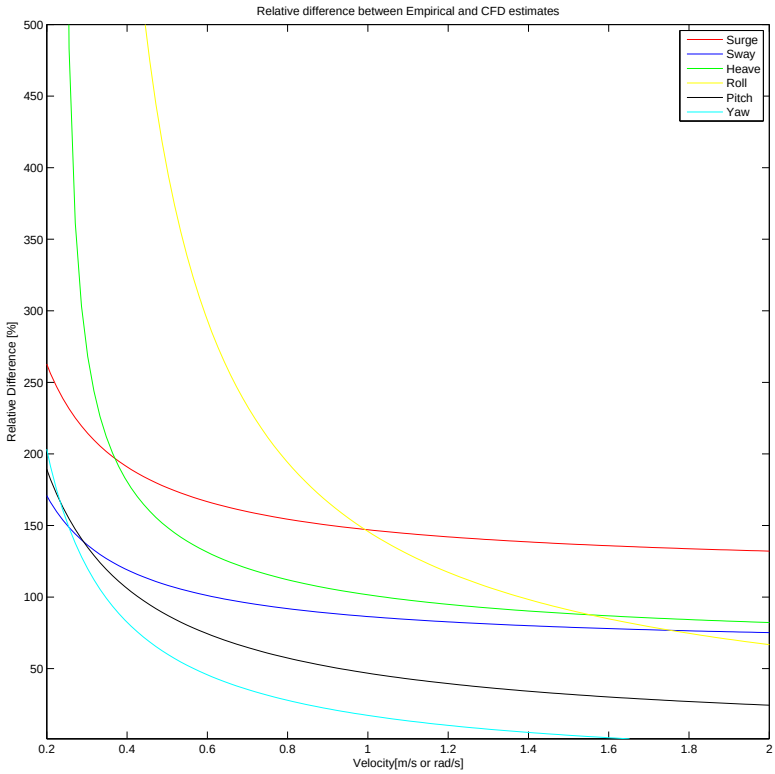

Figure 4.8: Relative Difference in Damping between Empirical estimate and CFD

Similarly the relative difference between the experimental estimate and the CFD damping is found. The results for ROV Neptunus and VideoRay Pro-4 are presented separately. This because the relative errors for the two experiments were very different.

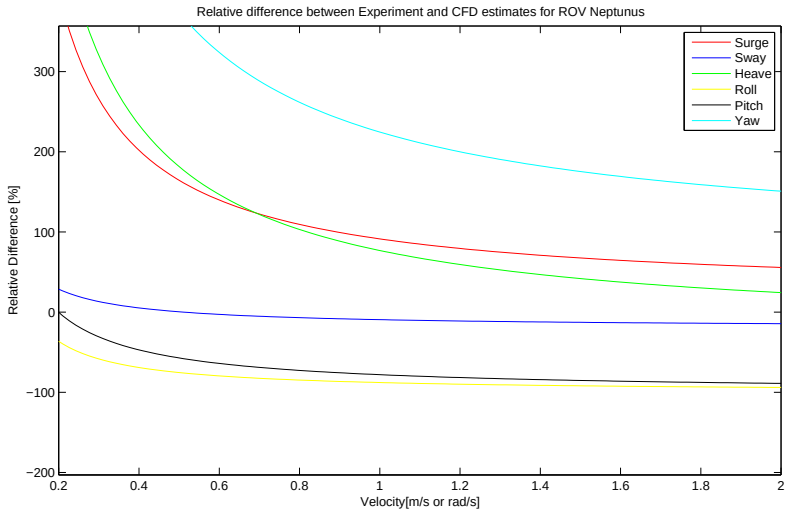

Figure 4.9: Relative Difference in Damping between Experimental estimate and CFD for ROV Neptunus

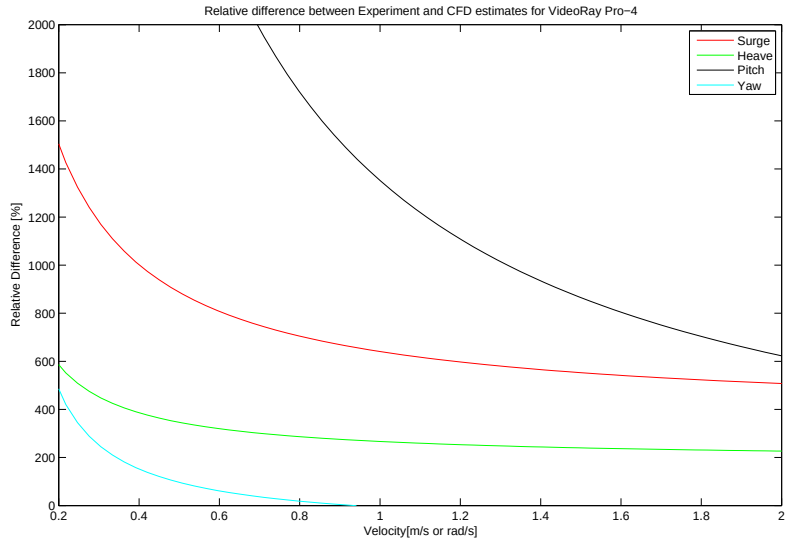

Figure 4.10: Relative Difference in Damping between Experimental estimate and CFD for VideoRay PRO-4

4.6.3 Drag Coefficients

Below are the drag coefficients for the translational DOFs presented. The drag coefficients are calculated using the quadratic damping forces and the characteristic area is defined as the projected area which is the normal way of defining drag coefficients[9]. These coefficients are only valid when assuming that the drag-coefficients are independent of Reynold number.(usually a valid assumption for high Reynold numbers[4])

	Surge			**Sway**			**Heave**		
ROV	**Emp**	**CFD**	**Exp**	**Emp**	**CFD**	**Exp**	**Emp**	**CFD**	**Exp**
Sf-30k	0.94	0.45	NA	1.12	0.62	NA	0.99	0.69	NA
ROV Neptunus	1.08	0.29	0.35	0.85	0.45	0.36	0.38	0.34	0.24
VideoRay PRO-4	0.72	0.32	1.5	0.99	0.86	NA	1.10	0.83	2.37
Seabotix LBV600-6	0.86	0.70	NA	1.08	0.89	NA	1.17	1.22	NA
AC-ROV 100	0.85	0.86	NA	0.89	0.42	NA	0.90	0.27	NA

Table 4.17: Drag coefficients for translational DOFs

CHAPTER 5
DISCUSSION

In the following a discussion about the obtained results is presented. In addition will the experimental, numerical and empirical procedures be evaluated.

5.1 Experimental results

5.1.1 Added Mass

Experimental estimates of added mass were meant to be performed in the scope of this thesis. A complete procedure was tested, but the results were poor and the experimental added mass estimates was therefore left out of this thesis. In appendix E.1 the results from the acceleration tests performed on ROV Neptunus can be found.(No acceleration tests were performed on VideoRay Pro-4 due to the poor results from ROV Neptunus) The matlab script used to extract the damping forces can automatically read out the acceleration tests and calculate the total force or moment for a number of velocities. Figure 5.1 shows the recorded results for one acceleration test performed on ROV Neptunus:(Surge, $0.03 m/s^2$)

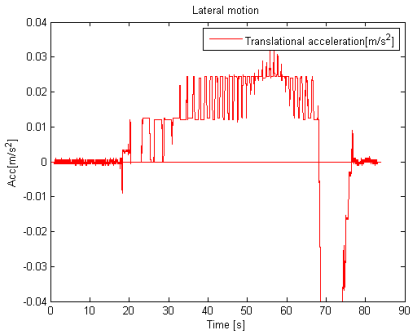

(a) Acceleration

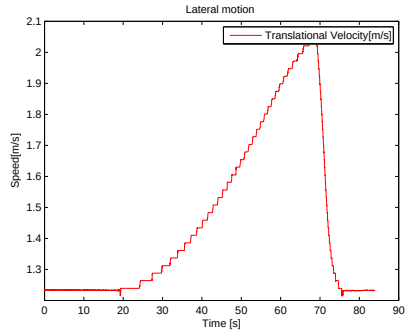

(b) Velocity

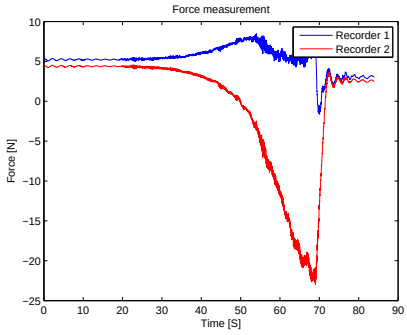

(c) Force Recordings

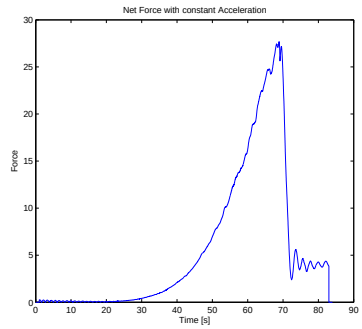

(d) Net force (smoothed)

Figure 5.1: Plots of acceleration test data(Surge, 0.03m/s^2)

When the total force is calculated for a given acceleration the rigid body mass and damping forces can be subtracted. The remaining term will be the added mass. See figure 5.2

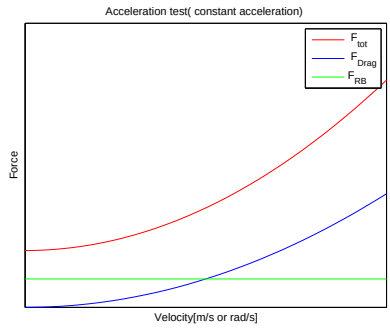

Figure 5.2: Acceleration Test components.
Added mass is found from $A = F_{tot} - F_{drag} - F_{RB}$

When performing this procedure the added mass results obtained were inconsistent and for some values negative. This most likely come from two main contributions. One is the fact that when the towing cart is set to accelerate with a given acceleration the towing cart does not reach the given acceleration for more than a couple of seconds(see figure 5.1a). This because the towing cart uses the input acceleration as a maximum limit. Hence the sample interval is very limited and for some tests non-existent.
The other contribution comes from errors in the measurements. When operating with forces in the range of 1-10 N, rounding-off errors and recording errors become significant. As the Load cells have a range of 0 to 180 N each, forces of 1 to 10 N may be recorded with relative large errors. If large sample intervals exists the error in the recordings can be minimized, but as the sample intervals for the acceleration tests were small this was not possible.

Many improvements can be made to the procedure used in the acceleration tests. One important improvement will be to install an inertial measuring unit(accelerometer) to record the exact acceleration. Another improvement will be to install the load cells directly onto the ROV and hence reduce the measurement error. Using more sensitive load cells can also improve recordings. In addition can more tests performed on the same acceleration give a more accurate representation of the forces(this were not done due to time constraints in the towing tank)

5.1.2 Damping

ROV Neptunus

The experimental damping forces obtained on ROV Neptunus correspond well with the CFD estimate.(except for the yaw DOF). It can be observed that the the experiment gives a slightly larger damping than that of the CFD-anlysis. As the CFD-tool used is very basic the difference in the two estimates may come from both error in the CFD analysis and in the experiment. The Yaw DOF shows a very large damping moment compared to the CFD analysis.(and also empirical estimate) Compared to the results for the pitch and roll DOF it is likely that some errors in the recording are present for the yaw DOF.

When performing the interpolation of the damping functions it was noticed that a linear interpolation gave accurate representation of the damping functions for the rotational DOFs. Linear interpolation was therefore used to describe the rotational damping.(See figure 5.3b) This coincides well with the observations done in Caccia et. al 2004[17].

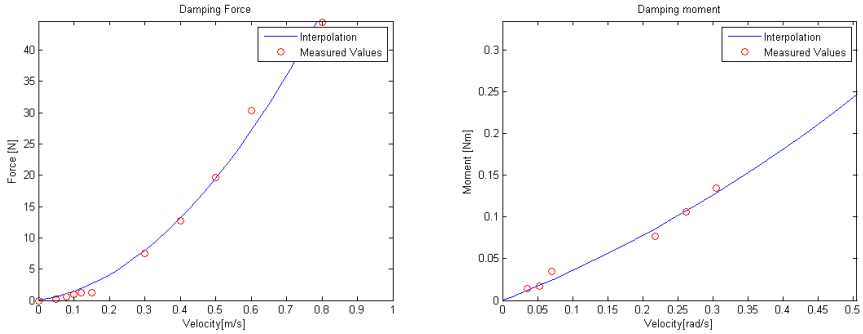

(a) Sway Interpolation *(b) Yaw interpolation*

Figure 5.3: Plot of least square interpolation of force/moment recordings on ROV Neptunus

It was noticed when analysing the data that for the rotational DOFs that the load cells did not always realign with the zero value after the rotation was stopped. This was a big problem when trying to extract the correct damping values, especially the yaw DOF recordings were of poor quality. In addition was the amplitude of oscillation of the recordings very big. The main reason for this was that the rotating disc is gear driven and thus exposes the ROV and load cells for high frequency vibrations. According to Torgeir Wahl (senior engineer, Dept. of Marine Technology) this is a usual problem when performing experiments on small models. An example of both these phenomenons can be seen in figure 5.4.

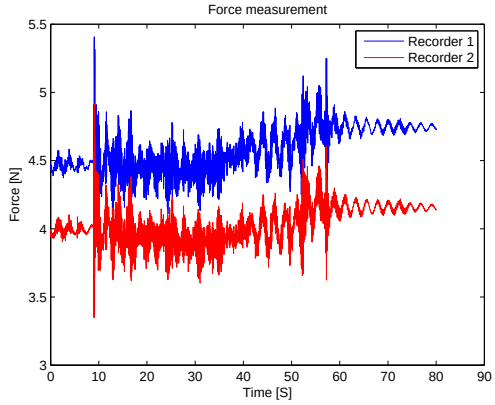

Figure 5.4: Yaw Test

It is observed that the relative difference between the experimental values and the CFD-analysis is quite big for all DOFs except for sway. The reason for this can be a combination of experimental errors and CFD-analysis errors. If a too course mesh is used in the CFD analysis important flow characteristics can be neglected and hence give a lower estimated damping force.

VideoRay Pro-4

The experimental results obtained in the VideoRay Pro-4 experiment is very inconsistent with that of both the CFD and empirical methods. The experimental value is substantially larger then the other two estimates. With a relative difference exceeding 1000% for low velocities. As the difference is so much bigger than for ROV Neptunus it is apparent that some error must be present in this experiment.

One reason for the poor results can be that fact that Videoray Pro-4 was hard to mount perfectly onto the bracket.(ROV Neptunus was mounted with screws, this was not possible with VideoRay Pro-4) The ROV may therefore have rotated slightly during the test which may have increased the drag. Another cause can be the fact that the load cells were not recalibrated before the experiment.
It should also be noted that no exact CAD-model of VideoRay Pro-4 were found(VideoRay were reluctant to give away the CAD-model) and the model had to be created manually. As the geometry of VideoRay Pro-4 is quite complex some error in the CAD-models is therefore expected. This would definitely affect the results from the CFD-analysis. However it can not explain the difference in many orders of magnitude. As the procedure performed on VideoRay Pro-4 was identical to that of ROV Neptunus it is hard to determine what the cause of the problem was.

5.1.3 Summary

The experimental procedure performed were able to be performed in little over a week in the towing tank. Where much of the time were spent installing equipment. As the ROVs were very small some measurement error is bound to occur. Due to the poor results for VideoRay Pro-4 the procedure definitely have some flaws. Compared to the results obtained in Eng. et. al 2009[15] the differences between CFD and experimental results are very big.

5.2 Empirical results

5.2.1 Added Mass

The empirical estimates for the added mass shows promising results. For the different ROVs the relative difference between empirical and WADAM analysis lies for the most case well under 100%. It can be observed that the roll and pitch DOFs have the largest relative differences. (table 4.16) The mean difference for the translational DOFs are just around ±10%. The rotational DOFs shows greater deviation and especially the root mean square is larger for the rotational DOFs. It is noticed that the empirical estimates generally underestimates the rotational added mass moments. This can hence be accounted for in future estimates as it is seen that at least for pitch and yaw the mean relative difference is approximately 10 %. When taking into account the basic methods used to estimate the added mass empirically the results are quite promising. There is much room for improvement on these calculations and the accuracy can be improved, but it is important that the calculation method remains quick and easy to use.

5.2.2 Damping

The empirical damping corresponds well with the CFD-estimates for all DOFs and ROVs. Compared to the CFD results the empirical method always over estimates the damping. One reason for this can be that the reference geometry used is a squared prism which have a larger drag-coefficient(above 2 times more) than a prism with rounded nose section. [4]. This can especially be seen for ROV Neptunus. As ROV Neptunus have rounded corners in surge and sway the empirical estimate overestimates the damping quite much. In the heave DOF on the other hand there are no rounded corners and the empirical estimate is hence more accurate.

5.3 Numerical Results

5.3.1 WADAM

A tremendous amount of effort was made to perform the WADAM analyses. This was mainly due to two things. One was the import of the desired geometry. As WADAM can only handle 15000 elements the CAD-models had to be altered and redone, this became a very time consuming task as the minimum element size imported into WADAM was frequently exceeded. The problem of minimum element size was a very big problem for the smaller ROVs. Another problem was the radius of gyration which could not be modified. The radii of gyration was set by the user to the desired values,but these values were overwritten by WADAM during the calculations. Effort was therefore put into overcoming these challenges.

The results obtained in WADAM shows good correspondence with referenced values estimated by WAMIT(Berg 2012[25]).

5.3.2 Flow Simulation(CFD)

The CFD-analysis performed in this thesis is fairly basic and were performed using parallel computing on an 8-core AMD FX-8150 4.8 GHz CPU. The simulations were done fairly quick with using approximately 2 hours pr. run, or about 12 hours pr DOF. As SolidWorks Flow Simulation has the ability to create batch runs much of the simulations were therefore done without the user being present. The total number of simulations was between 150-180. It therefore follows that the simulation work took months to complete.

The CFD-simulations work as a reference for the other estimates and its noticed that the damping found from CFD is slightly less then both experimental and empirical estimates. As the meshes used are fairly course some important flow characteristics are likely to be missed and this can greatly affect the result. It is therefore fair to assume some error in the CFD analysis. The verification tests performed in chapter 3 gave accurate results compared to the reference values[4] which gives confidence in the obtained CFD results.

CHAPTER 6

CONCLUSIONS AND FURTHER WORK

6.1 Conclusion

The main goal of this thesis was to suggest an accurate and practical procedure for obtaining knowledge of the hydrodynamic properties of ROVs. The main focus was the added mass forces and especially the hydrodynamic drag(damping) forces. As limited empirical or analytical methods existed for estimating these coefficients a substantial amount of effort was put into creating a method for complete estimate of the coefficients based on both analytical and empirical data. The experimental procedure was designed to be low cost and fairly quick and was based on standard experimental methods and the equipment available at the MC-lab at NTNU. The CFD-estimates were mainly used as reference as a complete CFD analysis would need more verification and a series of convergence tests to obtain good confidence in the obtained results.

The empirical method proved to be able to estimate hydrodynamic mass and damping with fairly good accuracy. As the method is built of basic assumptions and is just meant to give a brief estimate a mean added mass difference from the WADAM-analysis of ±10% can be considered good very good. As the tendencies for all the ROVs tested are the same the empirical method can easily be modified to take these differences into account. This goes especially for the rotational DOFs where the relative difference shows that the empirical estimate generally under estimates the added mass. The damping forces are also estimated fairly good, but have the tendency of overestimation. This overestimation probably come as a result of curved edges vs. sharp edges. In Blevins 2003[4] it is stated that a

rounding of the corners of 2.5% of the width of a 2D rectangle can reduce the drag with 10-20%. With this in mind it therefore follows that the empirical estimates are highly dependant of the actual geometry and curvature of the different elements of the ROV. This can especially be seen for ROV Neptunus and AC-ROV 100. There the heave and surge DOF respectively have little to no curvature and the damping forces are hence estimated close to experimental and CFD estimates. For the other DOFs the relevant edges are curved and the empirical estimate thus over estimates the damping forces greatly(see table 4.17)

The experimental method have the advantage over other experimental methods of being quick and easy to perform, but have disadvantages when it comes to accuracy. As the components used in the experiment are very basic(load cells, bracket, mounting-arrangement, etc.)some error can be expected. As mentioned in the discussion many improvement can be made to both the procedure and equipment to increase the accuracy of the experiment.

Some experimental values are in good agreement with the referenced CFD values(ROV Neptunus), however others have little correspondence with the references(VideoRay Pro-4). As the experimental values that correspond well with the references were obtained during a different experiment than the ones that show little agreement experimental errors can therefore be said to be an important factor. One can hence draw the conclusion that even though experimental methods can give very accurate results, referencing values can be important to verify that the obtained results are in fact correct.

The CFD-simulations performed are very basic and require relative little time and knowledge of hydrodynamics to perform. For the verification simulations the CFD-results was very accurate with regards to the referenced values found in Blevins 2003[4]. However the ROVs have a much more complex geometry and the CFD results may therefore be less accurate for the ROV tests.

It is shown in this thesis that empirical and experimental estimations both have positive and negative sides. The main downside with CFD is the time consumption. The CFD simulations performed in this thesis were basic and took very little time compared to more advanced simulations, yet the simulations took weeks to complete.(compared to a couple of minutes for the empirical estimates) As the method is tested on a wide variety of different ROVs with completely different characteristics the advantages and disadvantages of the different methods in the procedure has been uncovered. It is also shown that for the tested ROVs the procedure can produce estimates with a good degree of confidence.

6.2 Further Work

For further work it is suggested that the empirical method is improved to incorporate more parameters which will increase accuracy. The results obtained in this analysis can be also used to modify the empirical method described to produce a more accurate method. It is also suggested that the empirical method can be expanded to estimate coupling coefficients either based on established empirical data or by developing new theory. The method should thereafter be tested and verified.

The experimental procedure can also be improved significantly. Custom design of the mounting bracket to fit the relevant ROV can give more accurate experimental result(the bracket used in this thesis was designed to fit any ROV and thus had to be made fairly basic) The experimental procedure can also be expanded to include the added mass estimates. As the procedure for the experimental added mass had, as mentioned earlier big errors the proposed setup for added mass experiment needs modifications and improvements. The latter probably would require more accurate measurement tools(load cells and IMU(inertial measuring unit).

The CFD results obtained can also be verified and can also be compared to results produced using other CFD programs such as Ansys Fluent or OpenFOAM. As a complete and extensive CFD procedure can be very time consuming it is suggested as a proposal for a master thesis. See e.g. Skorpa 2012[28] for reference.

BIBLIOGRAPHY

[1] **O.M Faltinsen, 1990**
Sea Loads on Ships and Offshore Structures,
Cambridge University Press, New York, 1990.

[2] **John N. Newman, 1977**
Marine Hydrodynamics,
Mitpress, Cambridge, Massachusetts, 1977.

[3] **Sighard F. Hoerner, 1965**
Fluid-Dynamic Drag,
Published by the Author, New York, 1965.

[4] **Robert D. Blevins, 2003**
Applied Fluid Dynamics Handbook,
Krieger Publishing Company, Malabar, Florida, 2003.

[5] **Thor Inge Fossen, 2011**
HandBook of Marine Craft Hydrodynamics and Motion Control ,
Wiley ,Sussex, United Kingdom, 1st Edition, 2011.

[6] **Gianluca Antonelli, 2006**
Underwater Robots : Motion and Force Control of Vehicle-Manipulator Systems ,
Springer, 2nd Edition, Berlin, 2006.

[7] **Thor I. Fossen, 1994**
Guidance and Control of Ocean Vehicles,
John Wiley & sons, West Sussex, England, 1994.

[8] **Robert G. Dean and Robert A. Dalrymple, 1991**
Water Wave Mechanics for Engineers & Scientists(Advanced Series on Ocean Engineering - Volume 2),
World Scientific Pub Co Inc , Singapore, 1991.

[9] **Yunus A. Cengel & John M. Cimbala, 2010**
Fluid Mechanics: Fundamentals and Applications - 2nd Edition ,
McGraw Hill Higher Education , New York, USA 2010.

[10] **Alexandr I. Korotkin, 2007**
Added mass of ship structures,
Springer , St. Petersburg, Russia, 2007.

[11] **Erwin Kreyszig, 2011**
Advanced engineering mathematics,
10th Edition, Hoboken, N.J: Wiley,2011

[12] **E. T. Whittaker, 1988**
A Treatise on the Analytical Dynamics of Particles and Rigid Bodies,
Press syndicate of the university of Cambridge , Cambridge, US, 1988.

[13] **Chin, Cheng and Lau, Michael, 2012**
Modeling and testing of hydrodynamic damping model for a complex-shaped remotely-operated vehicle for control,
Harbin Engineering University, Harbin, China, 01.06.2012.

[14] **J. R. Morison, M. P. O'Brien, J. W. Johnson AND S. A. Schaff, 1950**
THE FORCE EXERTED BY SURFACE WAVES ON PILES ,
University of California ,Berkeley, California, Vol. 189, 1950.

[15] **Eng YH, Lau WS, Low E., Seet GGL and CS Chin, 2009**
Estimation of The Hydrodynamic Coefficients of an ROV using Free Decay Pendulum Motion,
Engineering Letters, 3rd Edition, 16.03.09.

[16] **David Millan; Thornburn, Paul, 2010**
A Planar Motion Mechanism (PMM) for Ocean Engineering Studies,
18th Newfoundland Electrical and Computer Engineering Conference, Canada,2010.

[17] **M. Caccia, G. Indiveri, and G. Veruggio, 2000**
Modeling and identification of open-frame variable configuration unmanned underwater vehicles,
P IEEE Journal of Oceanic Engineering, Vol. 25, pp. 227-240, 2000.

[18] **Khac Duc Do and Jie Pan, 2009**
Control of Ships and Underwater Vehicles : Design for Underactuated and Nonlinear Marine Systems,
Springer, London, 2009

[19] **Archie T. Morrison III & Dana R. Yoerger, 1993**
Determination of the Hydrodynamic Parameters of an Underwater Vehicle During Small Scalle, Nonuniform, 1-Dimensional Translation ,
OCEANS '93. Engineering in Harmony with Ocean. Proceedings , Victoria, BC, Canada, 1993.

[20] **P. Ridao, J. Batlle and M. Carreras, 2001**
Model identification of a low-speed UUV
Proceedings of IFAC Conference on Control Applications in Marine Systems(CAMS 2001) Glasgow, Scotland UK, 2001.

[21] **G. Conte, S. M. Zanoli, D. Scaradozzi and A. Conti, 2004**
Evaluation of Hydrodynamics parameters of a UUV. A preliminary study.
Presented at International Symposium on Control, Communications and Signal Processing, ISCCSP, Hammamet, 2004.

[22] **Azis, F.A, Aras M.S.M, Rashid, M.Z.A, Othman M.N, Abdullah, S.S, 2012**
Problem Identification for Underwater Remotely Operated Vehicle(ROV): A Case Study ,
International Symposium on Robotics and Intelligent Sensors, 2012

[23] **Fredrik Dukan, 2014**
ROV Motion Control Systems,
Phd Thesis, IVT, NTNU, August 2014.

[24] **Thor Inge Fossen, 1991**
Nonlinear modelling and control of underwater vehicles,
Doctoral dissertation, Fakultet for informasjonsteknologi, matematikk og elektronikk(NTNU), Trondheim, Norway, 1991

[25] **Viktor Berg, 2012**
Development and Commissioning of a DP system for ROV SF 30k,
Master Thesis, IVT, NTNU,2012.

[26] **Marianne Kirkeby, 2010**
Comparisson of Controllers for Dynamic Positioning and Tracking of ROV Minerva,
Master thesis, IVT, NTNU,2010.

[27] **Sindre Dahl, 2014**
Unsteady RANS Simulation of Flow around Rectangular Cylinders with different Aspect Ratios at High Reynolds Number ,
Master thesis, IVT, NTNU,2014.

[28] **Steinar Skorpa, 2012**
Numerical Simulation of Flow Around Remotely Operated Vehicle (ROV),
Master thesis, IVT, NTNU,2012.

[29] **DNV-RP-H103, 2010**
Modelling and Analysis of Marine Operations,
https://exchange.dnv.com/publishing/Codes/download.asp?url=2010-04/rp-h103.pdf, 25.09.2014.

[30] **SHIP STRUCTURE COMMITTEE, 1991**
Hydrodynamic Hull Damping,
Ship Structure Committee, 1991.

[31] **Det Norske Veritas, 2005**
WADAM User Manual,
DNV Software Report No.: 94-7100, Rev. 5, 2005.

[32] **Sperre ROV technology**
Product specifcations SUB-fighter 30k,
https://sites.google.com/site/sperrerov/sperre-support-files , 24.09.2014.

[33] **ROV Minerva**
Information about the ROV Minerva,
www.ntnu.edu/oceans/minerva, 24.09.2014.

[34] **Dassault Systems, 2014**
TECHNICAL REFERENCE SolidWorks Flow Simulation 2014,
Dassault Systems ,2014

[35] **Robert McNeel & Associates, 2014**
http://www.rhino3d.com/nurbs,
12.05.2015

[36] **openROV, 2015**
http://www.openrov.com/products/2-7.html,
19.05.2015

[37] **Seabotix, 2015**
http://www.seabotix.com/products/lbv600-6.htm,
20.05.2015

[38] **AC-cess, 2015**
http://www.ac-cess.com/products/acrov/acrov-technicalspecifications,
24.05.2015

[39] **VideoRay, 2015**
http://www.videoray.com/images/specsheets/2014
/2014PRO4STANDARDBASEFINAL.pdf,
24.05.2015

APPENDIX A
MATLAB SCRIPTS

A.1 Added mass

The digital version of this script is located in the folder:
"appendices/appendix A/ A.A - Empirical"

Contents


```
clear all
clc
close all
% ------------Empirical Added Mass estimator for ROV-----

%=========================================
```

```
% This program estimates the added mass diagonal terms
%for an ROV of varying size and shapes.
%Due to the simplicity program the added mass matrix will
% be assumed to be diagonal.

% In addition will the program only compute Added mass for
 %ROVs where two of the sides are somewhat equal,
 % i.e +- 10% difference
%
% The Program will also estimate the cross coupling terms based on
% empirical data from other ROV's.
%============================================
```

Input Values

```
L=404;                          % Length of ROV [mm]
H=214;                          % Height of ROV [mm]
W=108;                          % Width  of ROV  mm]
rho=1000;                        % Density fluid [kg/m^3]
PF= 22256;                      % Projected Area front [mm^2]
PS= 86456;                      % Projected Area side  [mm^2]
PT= 27500;                      % Projected Area top   [mm^2]
A=zeros(6,6);                     % Added mass Matrix
```

Empirical 3D data(DNV)————————————————

```
EMP3D=[1,0.68;2,0.36;3,0.24;4,0.19;5,0.15;6,0.14;7,0.11];
CA3D=spline(EMP3D(:,1),EMP3D(:,2));
%................................
```

Empirical 2D-data (DNV)

```
EMP2D=[10,1.14,0.125;5,1.21,0.15;2,1.36,0.15;1,1.51,0.234;...
       0.5,1.7,0.15;0.2,1.98,0.15;0.1,2.23,0.147];
CA2DT=spline(EMP2D(:,1),EMP2D(:,2));
CA2DR=spline(EMP2D(:,1),EMP2D(:,3));


.................
```

Coefficients

```
H3D=(H+W)/2;                    % Averaged Height( For 3D-est)
W3D=H3D;                        % Averaged Width ( For 3D-est)
CpXY=PT/(L*W);                  % Projected Area Coefficient XY
CpYZ=PF/(H*W);                  % Projected Area Coefficient YZ
CpXZ=PS/(L*H);                  % Projected Area Coefficient XZ
%.....................................................................
```

Surge Direction

3D————————————————

```
B=L/H3D;
Ca=ppval(CA3D,(B));
V=L*H3D^2;
A(1,1)= Ca*V*10^(-9)*rho*(CpYZ)^2*CpXZ*CpXY;
```

2D————————————————

```
B=W/L;
Ca=ppval(CA2DT,B);
Ar=pi*((W*0.5)^2);
A2D=rho*Ca*Ar*10^(-6)*(CpYZ)^2*CpXZ*CpXY;
At=H*10^(-3)*A2D;
lambda=sqrt(A(1,1)/At);
A(1,1)=At*lambda;
```

Sway and heave

```
B=L/W;
Ca=ppval(CA2DT,B);
Ar=pi*(L*0.5)^2*10^-6;
A2D=rho*Ca*Ar*CpXZ^2*CpXY*CpYZ;
At=A2D*H*10^-3;
A(2,2)=At*lambda;
A2D=rho*Ca*Ar*CpXY^2*CpXZ*CpYZ;
At=A2D*W*10^-3;
A(3,3)=At*lambda;
```

Roll

```
B=H/W;
Ca=ppval(CA2DR,B);
if (B<=1)
  A2D=rho*Ca*pi*(W*0.5*10^(-3))^4*CpYZ*CpXY*CpXZ;
else
 A2D=rho*Ca*pi*(H*0.5*10^(-3))^4*CpYZ*CpXY*CpXZ;
end
At=L*A2D*10^-3;
A(4,4)=At*lambda;
```

Pitch

```
B=L/H;
Ca=ppval(CA2DR,B);
if(B>=1)
A2D=rho*Ca*pi*(L*0.5*10^(-3))^4*CpYZ*CpXY*CpXZ;
else
A2D=rho*Ca*pi*(H*0.5*10^(-3))^4*CpYZ*CpXY*CpXZ;
end
At=W*10^-3*A2D;
A(5,5)=At*lambda;
```

Yaw

```
B=W/L;
Ca=ppval(CA2DR,B);
if(B>=1)
    A2D=rho*Ca*pi*(W*0.5*10^(-3))^4*CpYZ*CpXY*CpXZ;
else
    A2D=rho*Ca*pi*(L*0.5*10^(-3))^4*CpYZ*CpXY*CpXZ;
end
At=A2D*H*10^-3;
A(6,6)=At*lambda;
```

A.2 Damping

The digital version of this script is located in the folder:
"appendices/appendix A/ A.A - Empirical"

Contents

- Input Values
- Coefficients
- Drag Coefficients (2D)
- Drag Coefficients (3D)
- Nonlinear damping
- Roll
- Pitch
- Yaw
- Linear Viscous Damping

```
clear all
clc
close all
% -------------Empirical Damping estimator for ROV-------------

%================================================
% This program estimates the damping diagonal terms for an ROV of
% varying size and shapes. Due to the simplicity program the damping
% matrix will be assumed to be diagonal.

%================================================
```

Input Values

```
L=2500;                     % Length of ROV [mm]
H=1500;                     % Height of ROV [mm]
W=1600;                     % Width  of ROV  mm]
rho=1025;                   % Density fluid [kg/m^3]
PF= 1678091;                % Projected Area front [mm^2]
PS= 1956253;                % Projected Area side  [mm^2]
PT= 3384000;                % Projected Area top   [mm^2]
lambda=0.16;                % scaling linear/quadratic
I44 = 525;                  % Moment of inertia in roll
I55 = 794;                  % Moment of inertia in pitch
A44= 356;                   % Added mass in roll
A55= 980;                   % Added mass in pitch
C=7073;                     % Restoring coefficient (pitch=roll)
%.............................................................
```

Coefficients

```
CpXY=PT/(L*W);                  % Projected Area Coefficient XY
```

```
CpYZ=PF/(H*W);                    % Projected Area Coefficient YZ
CpZX=PS/(L*H);                    % Projected Area Coefficient XZ
%.....................................................
```

Drag Coefficients (2D)

```
Data2D =[0.5,2.5;1.5,1.8;2.5,1.4;6,0.89];
 % Blevins table 10.20 page 343
Drag2D=spline(Data2D(:,1),Data2D(:,2));
```

Drag Coefficients (3D)

```
Data3D =[0,1.25;0.5,1.25;1,1.15;1.5,0.97;2,0.87;...
         2.5,0.9;3,0.93;4,0.95;5,0.95];
Drag3D=spline(Data3D(:,1),Data3D(:,2));
```

Nonlinear damping

```
% Surge 3D
LD=L/((H+W)/2);
BQ3D =ppval(Drag3D,(LD));
% Surge 2D
LD=L/W;
BQ2D=ppval(Drag2D,(LD));

lambda = BQ3D/BQ2D;

% Final Surge nonlinear damping
LD=L/((H+W)/2);
BQ(1,1)=0.5*rho*ppval(Drag2D,(LD))*H*W*10^-6*CpYZ*lambda;
% Sway
LD=W/H;
BQ(2,2)=rho*0.5*ppval(Drag2D,(LD))*L*H*10^-6*CpZX*lambda;
%Heave
LD=H/W;
ppval(Drag2D,(LD));
BQ(3,3)=rho*0.5*ppval(Drag2D,(LD))*L*W*10^-6*CpXY*lambda;
```

Roll

```
LD=W/(H/2);
Fh=rho*(1/6)*ppval(Drag2D,(LD))*(H/2)*L*10^-6*CpZX*lambda;
Mh=Fh*(3/4)*((H/2)*10^-3)^3;
LD=H/(W/2);
Fv=rho*(1/6)*ppval(Drag2D,(LD))*(W/2)*L*10^-6*CpXY*lambda;
Mv=Fv*(3/4)*((W/2)*10^-3)^3;
BQ(4,4)= (2*Mv+2*Mh);
```

Pitch

```
LD=L/(H/2);
Fh=rho*(1/6)*ppval(Drag2D,(LD))*(H/2)*W*10^-6*CpYZ*lambda;
```

```
Mh=Fh*(3/4)*((H/2)*10^-3)^3;
LD=H/(L/2);
Fv=rho*(1/6)*ppval(Drag2D,(LD))*(L/2)*W*10^-6*CpXY*lambda;
Mv=Fv*(3/4)*((L/2)*10^-3)^3;
BQ(5,5)= (2*Mv+2*Mh);
```

Yaw

```
LD=L/(W/2);
Fh=rho*(1/6)*ppval(Drag2D,(LD))*(W/2)*H*10^-6*CpYZ*lambda;
Mh=Fh*(3/4)*((W/2)*10^-3)^3;
LD=W/(L/2);
Fv=rho*(1/6)*ppval(Drag2D,(LD))*(L/2)*H*10^-6*CpZX*lambda;
Mv=Fv*(3/4)*((L/2)*10^-3)^3;
BQ(6,6)= (2*Mv+2*Mh);
```

Linear Viscous Damping

```
%Roll and Pitch

BL(4,4)= 2*0.025*(I44+A44)*sqrt(C/(I44+A44));
BL(5,5)=2*0.025*(I55+A55)*sqrt(C/(I55+A55));

lambda0=0.16;
lambda1=BL(5,5)/BQ(5,5);
%Surge,Sway, heave and yaw
BL(1,1)=BQ(1,1)*lambda0;
BL(2,2)=BQ(2,2)*lambda0;
BL(3,3)=BQ(3,3)*lambda0;
BL(6,6)=BQ(6,6)*lambda1;
```

A.3 Experiment Result Reader

The digital version of this script is located in the folder:
"appendices/appendix A/ A.B - Experimental"

Contents

- Finding files in folder
- Setting constants
- Read input files
- Inserting velocity in the table
- Plotting forces
- Taking user input
- Setting correct baseline for recorders 1 and 2 (Force/Velocity)
- Finding Mean force from recorder 1 and 2
- Finding Torque for rotation tests
- Finding Acceleration results for Acceleration tests

- Removing inconsistencies in data sets
- Finding functions for forces and moments

```
%*****************************************************************
%*****************************************************************
%**   Force extractor from towing/rotation tests(ASCII)       **
%**                                                           **
%**                 Tests peformed in week 10-19              **
%**                                                           **
%**                                                           **
%**                        Made By :                          **
%**                  Ole Alexander Eidsvik                    **
%**                                                           **
%*****************************************************************
%*****************************************************************
clc
clear all
```

Finding files in folder

```
directory_name=uigetdir;
files = dir(directory_name);
fileIndex = find(~[files.isdir]);

% Running through all files in folder

for l=1:length(fileIndex)

 close all
 filename=files(fileIndex(l)).name;       % Name of Source File
```

Setting constants

```
F10=0;                          % Zero reference Force 1 [N]
F20=0;                          % Zero reference Force 2 [N]
V0=0;                           % Zero reference for  velocity
```

Read input files

```
VelZ=0;
file = fopen(filename,'r');
FileREAD = dlmread(fullfile(directory_name,filename));
Time=FileREAD(:,1);             % Time
Force1=FileREAD(:,2);           % Force recorder 1
Force2=FileREAD(:,3);           % Force recorder 2
PosX=FileREAD(:,4);             % Relative Horisontal Position
VelX=FileREAD(:,5);             % Relative Translational Velocity
PosZ=FileREAD(:,6);             % Relative Angular Position
Srate=1/(Time(2)-Time(1));      % sampling rate [Hz]
k=strfind(filename,'grad');
if k~=0
```

```
    R=1;              % if R=1 -> rotation test, else translation

    AP=[1;2;3;4;5;... % Velocities to evaluate acceleration Forces
        10;12.5;15;17.5;...
        20;25];
    if filename(2)=='g'
     N1=str2double(filename(1)); % Vel. inserted in result table
    elseif filename(3)=='g'
        N1=str2double(filename(1))*10+str2double(filename(2));
    else
        N1=str2double(filename(1))*10+str2double(filename(2))...
            +str2double(filename(4))*0.1;
    end
    N1=N1*pi/180
    figure(2)
    plot(Time,PosZ*0.5,'g')
    ylabel('Position[deg]');
    xlabel('Time [s]');
    title('Rotational motion ');
    legend('Angular position[deg]');
    for i=2:length(Time)
        VelZ(1)=0;
        VelZ(i)=(0.5*(PosZ(i)-PosZ(i-1)))*Srate;
    end
    figure(4)
    Vfunction = smooth(Time,VelZ,0.05,'loess');
    plot(Time,Vfunction)
    ylabel('Velocity[deg/s]');
    xlabel('Time [s]');
    legend('Angular Velocity')
    title(' Velocity over time ');
else
    R=0;

    AP=[0.05;0.08;0.10;... % Velocities to evaluate acc. forces
        0.12;0.15;0.2;0.25...
        ;0.50;0.60;0.70;0.80;...
        1.0;1.2;1.5;1.8];

    N1=str2double(filename(1))+str2double(filename(3))*0.1+...
        str2double(filename(4))*0.01;  % Velocity inserted in table
    % Plotting Velocities

    figure(2)
    plot(Time,VelX,'r');
    ylabel('Speed[m/s]');
    xlabel('Time [s]');
```

```
    title('Lateral motion ');
    legend('Translational Velocity[m/s]');
    hold off


    %Finding acceleration
 %  for i=2:length(Time)
 %       AccX(1)=0;
 %       AccX(i)=(0.5*(VelX(i)-VelX(i-1)))*Srate;
 %  end
 %  AccXX=zeros(length(Time));
 %         for i=Srate+1:length(Time)-Srate-1
  %          AccXX(1)=0;
   %         for j=-Srate:Srate
    %            AccXX(i)= AccXX(i)+AccX(i+j);
     %       end
      %    end
 %AccXX=AccXX/(2*Srate+1);

  %  figure(6)
  %  plot(Time,AccXX,'r');
   % ylabel('Acc[m/s^2]');
  %  xlabel('Time [s]');
  %  title('Lateral motion ');
  %  legend('Translational acce[m/s]');
  %  hold off
end

k=strfind(filename,'ss');
if k~=0
    A=1;                    % if A=1 -> Acceleration test
else
    A=0;                    % else A=0 -> Zero accelration
end
```

Inserting velocity in the table

```
ResultMatrix(1,1)=0;
ResultMatrix(1,2)=0;
ResultMatrix(l+1,1)= N1;
```

Plotting forces

```
figure(1)
plot(Time,Force1)
hold on
plot(Time,Force2,'r')
ylabel('Force [N]');
xlabel('Time [S]');
```

```
title('Force measurement');
legend('Recorder 1','Recorder 2');
hold off
```

Taking user input

```
if A==1
    disp('Acceleration test data selected ');
else
    disp('Constant velocity test data selected ');
end
disp(N1)
prompt = 'What is the min. value of the zero ref. int. ? \n ';
Rmin = input(prompt);         % Max value of ref. interval [s]
prompt = 'What is the max value of the zero ref. int. ? \n';
Rmax = input(prompt);           % Min value of ref. interval [s]
if Rmin>=Rmax
    disp('Error: Maximum value must be larger than minimum')
    break
end
prompt = 'What is the minimum value of the sample interval ? \n';
Smin=input(prompt);           % Min Value of sampling interval [s]
prompt = 'What is the maximum value of the sample interval ? \n';
Smax=input(prompt);           % Max Value of sampling interval [s]
if Smin>=Smax
    disp('Error: Maximum value must be larger than minimum')
    break
end
```

Setting correct baseline for recorders 1 and 2 (Force/Velocity)

```
for i=(Srate*Rmin+1):(Srate*Rmax)
F10 = F10+Force1(i);            % sum of zero value for recorder 1
F20 = F20+Force2(i);            % sum of zero value for recorder 2
V0=V0+VelX(i);
end
F10=F10/(Srate*(Rmax-Rmin));     % Zero value for recorder 1
F20=F20/(Srate*(Rmax-Rmin));     % Zero value for recorder 2
VelX=VelX-V0/(Srate*(Rmax-Rmin));% Zero value for  trans. velocity
```

Finding Mean force from recorder 1 and 2

```
MeanForce1=0;
MeanForce2=0;
for i=(Srate*Smin+1):(Srate*(Smax))
    MeanForce1=MeanForce1+Force1(i);% Sum of F 1 in sample domain
    MeanForce2=MeanForce2+Force2(i);% Sum of F 2 in sample domin
end

MeanForce1 =MeanForce1/(Srate*(Smax-Smin))-F10;% Mean force 1
```

```
MeanForce2 =MeanForce2/(Srate*(Smax-Smin))-F20;% Mean force 2

TotalForce = abs(MeanForce1)+abs(MeanForce2)
```

Finding Torque for rotation tests

```
if R==1
    TotalTorque = TotalForce*0.12*sqrt(2)
end
```

Finding Acceleration results for Acceleration tests

```
if A==1


disp(N1)

% Filtering values Averaging with a frequency of 2 hz
Facc(1,2)=0;
Facc(l,2)=0;
Facc(l+1,1)=N1;
NetForce1=zeros(length(Time),1) ;
NetForce2=zeros(length(Time),1) ;
          for i=Srate+1:length(Time)-Srate-1
            NetForce1(i)=0;
            NetForce2(i)=0;
            for j=-Srate*0.25:Srate*0.25
                NetForce1(i)= NetForce1(i)+(Force1(i+j,1)-F10);
                NetForce2(i)= NetForce2(i)+(Force2(i+j,1)-F20);
            end

          end


        if R==1
            NetForce1=NetForce1*0.12*sqrt(2)/(0.5*Srate+1);
            NetForce2=NetForce2*0.12*sqrt(2)/(0.5*Srate+1);
        else
            NetForce1=NetForce1/(0.5*Srate+1);
            NetForce2=NetForce2/(0.5*Srate+1);
        end


    plot(Time,abs(NetForce1)+abs(NetForce2))
    ylabel('Force');
    xlabel('Time [s]');
    title(' Net Force with constant Acceleration ');
```

```
    for i=1:length(AP)
        Facc(1,i+2)=AP(i);
        var=0;
        if R==1
            temp=abs(abs(VelZ)-AP(i));
        else
            temp=abs(abs(VelX)-AP(i));
        end
        temp(Srate*Smax:end)=[];
        [idx idx]=min(temp);
        closest=Time(idx);
        if closest>Smin
            if closest<Smax
                if min(temp)<0.01
                    for j=-2:2
                        var=var+(abs(NetForce1(idx+j)))...
                            +abs((NetForce2(idx+j)));
                    end
                    Facc(l+1,i+2)=var/5;
                end
            end

        end

    end
end
if R==1
    ResultMatrix(l+1,2)= TotalTorque;
else
    ResultMatrix(l+1,2)= TotalForce;
end
ResultMatrix=sortrows(ResultMatrix);

end
```

Removing inconsistencies in data sets

```
count=0;
%for i=3:length(ResultMatrix)
%    i=i-count;
%    if ResultMatrix(i,2)<=ResultMatrix(i-1,2)
%        if ResultMatrix(i-1,2)<=ResultMatrix(i-2,2)
%            ResultMatrix(i-2,:)=[];
%            count=count+1;
 %      else
 %          ResultMatrix(i,:)=[];
  %         count=count+1;
  %      end
  %  end
```

```
%end

if A==1;
sizeFacc=size(Facc);
for k=1:sizeFacc(1)
    for i=5:length(Facc)
        if Facc(k,i)<=Facc(k,i-1)
            if Facc(k,i)<=Facc(k,i-2)
                Facc(k,i)=0;
            else

            end
        end
    end
end
end
```

Finding functions for forces and moments

```
if A==1

for i=2:sizeFacc(1)
    count=0;
    InertiaForce(i-1,1)=Facc(i,1);
    var0=Facc;
    var0(:,1)=[];
    var1=var0(i,:);
    var2=Facc(1,:);
    var2(1)=[];
    var1=[var2;var1];

    for j=1:(length(var1))
        j=j-count;
    if var1(2,j)==0
        var1(:,j)=[];
        count=count+1;
    end
    end
    var=polyfit(var1(1,:),var1(2,:),2);

    InertiaForce(i-1,2)=var(1,1);
    InertiaForce(i-1,3)=var(1,2);
    InertiaForce(i-1,4)=var(1,3);
end



else
```

```
    disp(filename)
    % perform linear and quadratic regression
    %to find damping forces


    x=ResultMatrix(:,1);       % Reshape data into column vector
    y=ResultMatrix(:,2);

    for i=1:2
        n=i;                   % Degree of polynomial
        V(:,n+1) = ones(length(x),1,class(x));
        for j=n:-1:1
            V(:,j) = x.*V(:,j+1);
        end
        if i==1
            Dlin =lsqlin(V,y,[],[],0.^(n:-1:0),0)% Linear Damping
        else
            Dquad =lsqlin(V,y,[],[],0.^(n:-1:0),0)% Quad. Damp.
        end
    end

end
ResultMatrix=transpose(ResultMatrix);

%Plotting interpolation

if R==1
syms x
figure(6)

ezplot(Dquad(1).*x.*abs(x)+Dquad(2)*x)
hold on
scatter(ResultMatrix(1,:),ResultMatrix(2,:),'r')
axis([0 (ResultMatrix(1,end)+0.2) 0 (ResultMatrix(2,end)+0.2)])
ylabel('Moment [N]');
xlabel('Velocity[rad/s]');
title('Damping moment');
legend('Interpolation','Measured Values');
hold off
else
syms x
figure(6)

ezplot(Dquad(1).*x.*abs(x)+Dquad(2)*x)
hold on
scatter(ResultMatrix(1,:),ResultMatrix(2,:),'r')
axis([0 (ResultMatrix(1,end)+0.2) 0 (ResultMatrix(2,end)+0.2)])
```

```
ylabel('Force [N]');
xlabel('Velocity[m/s]');
title('Damping Force');
legend('Interpolation','Measured Values');
end
```

APPENDIX B

EMPIRICAL ESTIMATES

The excel Sheet containing the results from the empirical estimates can be found in the folder:
"appendices/appendix B"

APPENDIX C
NUMERICAL RESULTS

C.1 CFD

The Excel sheet containing the Results from the CFD calculations performed in SolidWorks Flow Simulation can be found in the folder:
"appendices/appendix C/C.1 - CFD"

C.2 WADAM

The Excel sheet containing the Results from the CFD calculations performed in SolidWorks Flow Simulation can be found in the folder:
"appendices/appendix C/C.2 - WADAM"

In addition can all WADAM run-files be found in the same folder

APPENDIX D

MODEL FILES

D.1 AC-ROV-100

The model files are located in the folder:
"appendices/appendix D/ D.1 - AC-ROV-100"

D.2 Neptunus

The model files are located in the folder:
"appendices/appendix D/ D.2 - Neptunus"

D.3 Seabotix LBV-600-6

The model files are located in the folder:
"appendices/appendix D/ D.3 - Seabotics LBV-600-6"

D.4 Sperre Sf-30k

The model files are located in the folder:
"appendices/appendix D/ D.4 - Sperre Sf-30k"

D.5 VideoRay PRO-4

The model files are located in the folder:
"appendices/appendix D/ D.5 - VideoRay PRO-4"

D.6 Reference Simulations

The model files for the sphere and rectangular rod are located in the folder:
"appendices/appendix D/ D.6 - Reference Simulations"

APPENDIX E

ROV SPECIFICATIONS

E.1 SF-30k

Specifications

Parameter	*Value*
LWH	$2500X1500X1600\ mm$
Frame	Aluminium, black anodized
Housings	2 or 3 pressure bottles
Weight in Air	approximately $1350kg$
Payload	$60\ kg$
Standard Working depth	$700m$
Power Input	230/400/440/690 VAC, 3 phase, $30kW$
Thrusters	6 thrusters with $3kW$, pressure compensated
Speed approx	Horizontal 2.1 knot, Vertical 1.8 knot, Lateral 0.9 knot, turn 90 deg/s
Pan/ Tilt	Pan angle 45 degrees, Tilt angle 90 degrees

Table E.1: Specification Standard Sf-30k [32] table 1 of 2

Parameter	*Value*
Camera	7 camera interfaces Color Camera 0.1 lux, Zoom camera Sony HD-SDI camera, option
Lights	6 x 250W Halogen Lights, 3 channel light dimmer Interface for, halogene, LED and HMI gas light 2 x 400W
Sensors	6 x 250W Halogen Lights, 4 channel light dimmer 2 x 400 W gas light HMI
Telemetry	Fiber optic CWDM system, Focal mux, model 907 4 video, synchronous, 16 RS 232 channels 5 RS 485 channels, 3port 20 base Ethernet
Auto Functions	AD, Auto depth, AH, Auto heading AT, Auto traction, option

Table E.2: Specification Standard Sf-30k [32] table 2:2

E.2 Seabotix LBV600-6

Parameter	*Value*
LWH	$540X484(300)X270\ mm$
Frame	Polyethylene
Speed at surface	$1.8\ m/s$
Weight in Air	$15.3kg$
Thruster configuration	6 brushless DC thrusters- 4 forward, 1 vertical and 1 lateral. Each thruster is isolated
Depth rating	$600m$
Bollard Thrust(forward)	$127N$
Bollard Thrust(vertical)	$29N$
Bollard thrust(lateral)	$29N$
Max operating Current	$1.02\ m/s$
Camera tilt	180 degrees
Range of View	270 degrees
Video Format	NTSC or PAL
Internal Lighting	700 Lumen LED array.

Table E.3: Specification Standard Seabotix LBV600-6 [37]

E.3 AC-ROV-100

Parameter	*Value*
LWH	$203X152X146\ mm$
Payload	200g
Weight in Air	$3kg$
Thruster configuration	6 thrusters- 4 horizontal vectored and 2 vertical and 1 lateral. Each thruster is isolated
Depth rating	$100m$
Output	Composite
Light	4 camera tracking LEDs.

Table E.4: Specification Standard AC-ROV-100 [38]

E.4 VideoRay PRO-4

Parameter	*Value*
LWH	$375X290X223\ mm$
Weight in Air	$6.1kg$
Thruster configuration	3 brushless thrusters- 2 horizontal and 1 vertical
Propellers	100mm horizontal and 65 mm vertical
	. Each thruster is isolated
Depth rating	$305m$
Output	Composite
Light	2 optimized LED Arrays 3600 Lumens.
Video format	NTSC or PAL
Vertical Camera Tilt	180°

Table E.5: Specification Standard VideoRay PRO-4 [39]

APPENDIX F

RESEARCH ARTICLE

A proposal for a research article were made during this thesis. The procedure for determining the hydrodynamic coefficients is tested on ROV Neptunus and the results from this exercise is presented in the article. The article is just a preliminary draft and will need further work, but the author feels it can in the current state still be relevant for the thesis.

Determination of hydrodynamic parameters for a ROV

Ole Alexander Eidsvik

Norwegian University of Science and Technology
olealeei@stud.ntnu.no

Abstract

In this paper the hydrodynamic parameters that characterize the behaviour of a general work class ROV are evaluated. A complete procedure for finding these coefficients are described. The procedure consists of an empirical method based on basic assumptions and available empirical coefficients in addition to a low cost experiment by the use of towing tank. The procedure is then used on the ROV Neptunus.The results are evaluated and the two methods are then compared with CFD results obtained by SolidWorks Flow Simulation.

ζ	Damping ratio(K_L/K_{Lcr})
ω_n	Natural frequency of oscillation
ν_1	linear velocities vector (u,v,w)
ν_2	angular velocities vector (p,q,r)
A	Added Mass matrix of ROV
A^D	Diagonal added mass given as a vector
B	Buoyancy
g	Restoring coefficient in single DOF
g(η)	Restoring matrix of ROV
C_P^{ij}	Projected area of ij-plane
COG	Center of Gravity
DOF	Degree of Freedom
K	Damping Matrix
K_L	Linear damping
K_Q	Quadratic damping
M	Mass matrix of ROV
m	Mass term in single DOF
(m,n,o)	local coordinate system used for C_p
m_a	Added mass term in single DOF
$\overline{X}$	Position or Euler angle of single DOF

Table 1: *Nomenclature*

I. Introduction

UNMANNED UNDERWATER VEHICLES(UUVs) are today common in deepwater industries such as oil and gas exploration, telecommunications, geotechnical investigations and mineral exploration[15].

The hydrodynamic properties describes the behaviour of the UUVs when operating in water. Required thrust, operational range, maximum speed and manoeuvrability are just some of the characteristics dictated by the hydrodynamic properties. It therefore follows that hydrodynamic properties plays a crucial role for the performance of UUVs. Hence knowledge of these properties are important not only for controller purposes but also in the design phase as good knowledge about the hydrodynamic properties can optimize the design and improve performance. In most cases theoretical derivation of these values is practically impossible, and experimental measurements are generally complicated and expensive[1]. In the design stage of a UUV empirical calculations can often estimate the hydrodynamic parameters with sufficient accuracy if only brief estimates are needed. However if accurate parameter estimation is required real experiments are often needed. Different experimental procedures exist, but the most conventional procedures involve towing tank trials of the vehicle itself or of a scaled model of the vehicle, expecting, in this case an error in the estimate of some parameters up to 50%[4] Literature suggests some experimental methods concerning particular procedures where onboard sensor data is used without requiring any towing tank tests[4]and [16]. Another experimental method using pendulum motion is described in Eng et. al 2009.[13].

One of the greatest problems encountered i designing model based controllers for the vehicles is the difficulty in knowing the values of the hydrodynamic coefficients. As the tasks performed by UUVs become increasingly more challenging the performance requirements for the automatic controllers become higher. Designing model based control systems can therefore be challenging since these controllers require accurate parameters.

In the following a complete procedure for determining the hydrodynamic coefficients of a small scale ROV is presented. The procedure consists of a conceptual empirical estimation and an experiment using a towing tank.

The empirical method can estimate the hydrodynamic coefficients in the design phase and no experimental data is needed. The inertia forces will not be evaluated experimentally, however they will be estimated empirically and numerically. The experiment is designed to be low cost and can be performed relatively fast, however a towing tank is needed.

The structure of this paper is as follows. In section 2 basic hydrodynamic theory is discussed and basic dynamic laws applicable to a UUV is reviewed. In section 3 a small class ROV on which the procedure will be tested is presented. In chapter 4 the parameter estimation is shown and performed on 2 DOFs(surge and roll). Chapter 5 reviews the experimental procedure, while the results are presented in chapter 6.

II. Method

A. Equation of Motion

The 6 DOF nonlinear dynamic equation can be expressed as:[17]

$$(M+A)\dot{\nu} + (C(\nu) + C_A(\nu))\nu + K(\nu)\nu + g(\eta) = \tau \quad (1)$$

where

$\mathbf{M}$	Inertia matrix
$\boldsymbol{A}$	Added mass matrix
$\boldsymbol{C}$	Rigid body Coriolis and centripetal matrix
$\boldsymbol{C_A}$	Added mass Coriolis and centripetal matrix
$\boldsymbol{K(\nu)}$	Damping matrix
$\mathbf{g}(\boldsymbol{\eta})$	Vector of gravitational forces and moments
$\boldsymbol{\tau}$	Vector of control inputs

It is now seen that dynamic equation of the ROV is described by 6 coefficient matrices and the control inputs. To determine the control inputs can be quite challenging because the thrust provided by the propellers are sensitive to e.g. propeller-hull effects[3] and relative velocity. The control inputs can be found by the use of open water tests and propulsion tests as shown in Egeskov et. al 1994.[5] However the control inputs will not be discussed in this paper as the focus is on the hydrodynamic parameters.

The acceleration vector $\dot{\nu}$ is multiplied with the rigid body mass(M) and the added mass (A) matrices. The coefficients in the rigid body mass matrix can for basic geometries (prism,sphere cylinder etc.)be found geometrically and using general formulas for moments and products of inertia[10]. No new theory will be introduced with regards to the mass matrix. Hence it will not be discussed further in this paper. Furthermore it can be shown that the rigid body Coriolis matrix(C) and added mass Coriolis matrix(C_A) are products of the mass terms/added mass terms, positions and velocities.[10] In other words Coriolis coefficients are products of mass coefficients. The Coriolis matrix will thus not be evaluated in this exercise.

The hydrodynamic damping for ocean vehicles are mainly caused by :

$\boldsymbol{K_P(\nu)}$	= Radiation-induced potential damping due to forced body oscillations.
$\boldsymbol{K_S(\nu)}$	= Linear skin friction due to laminar boundary layers and quadratic skin friction due to turbulent boundary layer.
$\boldsymbol{K_W(\nu)}$	= Wave drift damping.
$\boldsymbol{K_M(\nu)}$	= Damping due to vortex shedding. (Morison's Equation)

It is often convenient and practical to divide these damping terms into a linear term and a nonlinear term.[10] Where the linear term consists of the potential damping(K_P) and the linear skin friction(K_S). The nonlinear term hence consists of wave drift damping(K_W), damping due to vortex shedding(K_M) and quadratic skin friction due to turbulent boundary layer(K_S). In this study it will be assumed that a UUVs operational conditions is far below the free surface. I will therefore not generate any surface waves or be affected by incoming waves, hence both potential and wave drift damping are zero[10]. The linear damping of the ROV therefore consists of only linear skin friction. The nonlinear term which contains all higher order terms can very accurately be simplified to a quadratic damping function[2].(higher order terms are neglected[17]) Thus can the damping of the ROV be expressed with the two coefficients:K_L and K_Q.

The added mass is the extra inertia mass force/moment added to the system when the ROV accelerates. According to Fossen 1994[17] added mass should be understood as pressure-induced forces and moments due to the forced motion of the body which are proportional to the acceleration of the body. Added mass is

dependant of incoming wave frequency, but by assuming the ROV is far below the free surface the added mass coefficient simplifies to a matrix of constant terms.

The mass matrix and restoring matrices will not be discussed further as the coefficients in these matrices can be found fairly easy[10].

B. Added Mass

The added matrix consists of 36 coefficients. These coefficients can be found using potential flow theory. Programs like WAMIT(WADAM)[7] can integrate the velocity potential around the ROV and find the coefficient very accurately.
In this paper the coefficients will be found using empirical estimates instead. As coupling terms are very hard to find using empirical estimates the matrix needs to be simplified. Assuming that the UUV to evaluate has 3 planes of symmetry the off diagonal terms can be neglected[17]. The added mass matrix therefore simplifies to a diagonal matrix.

The diagonal terms are found using strip theory(2D) and 3D empirical data. To account for the difference in geometry between ROV Neptunus and the referenced prism the projected area coefficients are introduced. These coefficients are only meant to scale the added mass terms to correspond with the geometry. The calculations are further described in section IV.

C. Damping

As stated the damping matrix contains a linear term and quadratic term. According to Fossen [17] a rough approximation for the damping of underwater vehicles is to assume that the vehicle is performing a non-coupled motion, has three planes of symmetry and that the higher order terms are negligible.(the latter assumption has already been used) These assumptions will result in a damping matrix with no off-diagonal terms.

The quadratic translational terms are found using well known drag coefficients(Morisons equation). While for the translational quadratic damping a new method has to be applied as no other method is found. The quadratic damping terms are lastly multiplied with the projected area coefficients to account for the difference in geometry with the reference.
The linear damping is found by evaluating a viscously damped free vibration linear 1DOF system. As the free vibration equation is only valid for DOFs where a restoring force/moment exists the method can only be used in roll and pitch. Assuming a linear relationship between quadratic and linear damping exists the yaw linear damping is found. The translational terms are found using the scaling factor found in Eng et. al 2009 [13].

D. Experiment

As the experiment is performed on the full size ROV no scaling is necessary. The main assumption used in the experiment is that the damping forces from the mounting bracket can be subtracted from the combined damping of the ROV and the mounting bracket(superposition). In other words the mounting bracket and the ROV is assumed to be unaffected by each others presence.

III. ROV Neptunus

In this paper the procedure will be carried out on the ROV Neptunus which is a small foil shaped ROV developed by students at NTNU.[1]

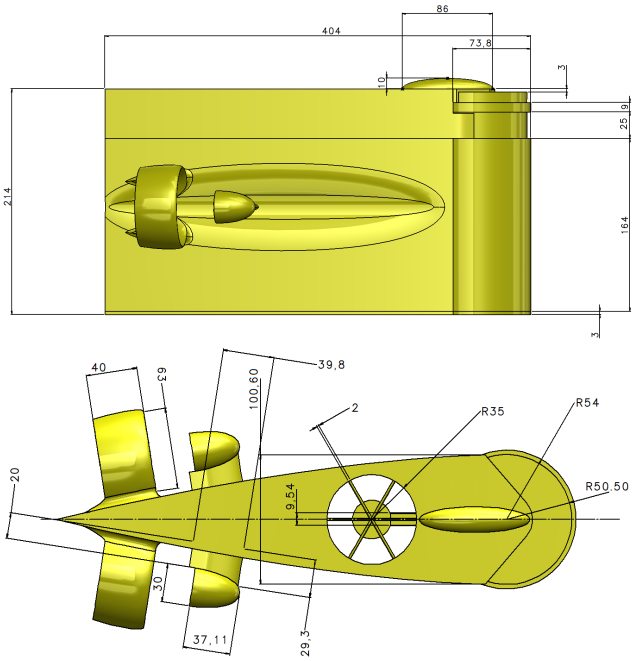

Figure 1: *Dimensions of ROV Neptunus*

[1]The ROV was designed by Jostein Follestad at NTNU during the autumn of 2014.

Figure 2: *Perspective view of ROV Neptunus*

Most underwater vehicles are either box shaped or slender and cylindrically shaped. For ROV's the operating velocities are usually fairly small they are therefore most often designed as a box. This design enables the ROV to carry different equipment and tools rather than having good hydrodynamic properties(i.e low drag). For AUV's high cruising velocities and range are important hence they are usually designed as slender cylinders to achieve low drag forces. As ROV Neptunus is designed as a large foil non of these usual shapes are applicable to describe the geometry.

A. Specifications

The length of the vehicle is 404mm, the breadth is 108mm and the height is 214 mm.(The propellers and propeller ducts are not included) The mass of the ROV is 3.46 kg hence the weight in air is 33.94 N. The ROV is neutrally buoyant hence a buoyancy force of 33.94 N. The top speed is 1 m/s and maximum forward thrust delivered by the two horizontal thrusters is 12 N. The center of gravity (COG) is located at $(145mm, 0, 100mm)$ from the front bottom center line. The center of Buoyancy (COB) is located 30 mm directly above the COG. The ROV is therefore passive stable in pitch and roll. The ROV has a total of 3 thrusters, 2 which produces thrust in surge and 1 that produces thrust in heave. The ROV is under actuated since sway cannot be controlled.

B. Hull

The body of the ROV is based on the NACA foil series with minimization of forward drag as the highest priority(surge). The hull consists of a multiple plastic sections glued together and a transparent plastic cylinder located in the front which contains the electric equipment such as camera and sensors. The battery package is located inside the foil to create a passive stable vehicle.

IV. Empirical Estimates

The Empirical estimates will be based on a method developed prior to this article by the author using empirical data contained in DNV-RP-H103[6]. The method is developed to find the added mass and drag forces for a prismatic shaped ROV. ROV Neptunus does not have a typical prismatic shape, but the method is still expected to give reasonable estimates.

A. Added Mass

DNV-RP-H103[6] uses a rectangular prism where two of three sides are equal as reference geometry. This is not correct for ROV Neptunus, the mean value of the height and width will therefore be used instead. Since the reference geometry is a solid prism the result also needs to be scaled to account for the difference between the ROV shape and a prism. This will be done by multiplying the results found with the projected area coefficient C_P^{ij} in each degree of freedom. Where $C_P^{ij} = A_P^{ij}/A^{ij}$, and A is the reference area and A_P is the projected area of ROV Neptunus.

As for the rotational degrees of freedom empirical 3D data were not found. A different approach therefore had to be used. Using knowledge about similar shapes one knows that the difference in added mass for a sphere (3D) and an infinitely long cylinder of same radius is 50% (Newman 1977[8] p. 144). By converting this relation to the problem at hand it is possible to create a procedure for the rotational degrees of freedom. The procedure is described below:

1. Find added mass for translational DOFs using empirical 3D data.
2. Find added mass for translational DOFs using 2D data and strip theory.
3. Calculate the difference in the two methods.(Scaling factor)
4. Find added mass for rotational DOFs using 2D data and strip theory.
5. Scale the results.

The procedure will be performed on the surge and roll DOFs respectively. The remaining DOFs will not be shown as they are performed similarly.

A.1 Surge

Starting with finding the empirical 3-D coefficient for A_{11} :

$$b/a = 404/161 \approx 2.51$$

Inserting this value into the reference added mass table gives the following added mass coefficient:

$$C_a(2.51) \approx 0.28$$

and the projected area coefficients become:

$$C_p^{XY} = \frac{A_p^{XY}}{A} = \frac{A_p^{XY}}{L*B} = \frac{31663mm^2}{(404mm)(108mm)} \approx 0.7257$$

$$C_p^{YZ} = \frac{A_p^{YZ}}{A} = \frac{A_p^{YZ}}{H*W} = \frac{23112mm^2}{(214mm)(108mm)} = 1$$

$$C_p^{XZ} = \frac{A_p^{XZ}}{A} = \frac{A_p^{XZ}}{L*H} = \frac{86456mm^2}{(404mm)(214mm)} = 1$$

The reference volume becomes:

$$V = ba^2 = 404mm(161mm)^2 = 10472084mm^3 \approx 0.01m^3$$

Inserting values into the formula for added mass:

$$A_{ij} = C_a V_r * \rho_{water}(C_p^{no})^2(C_p^{mo})(C_p^{mn}) \tag{2}$$

gives :

$$\begin{aligned} \boldsymbol{A_{11}} &= (0.28)(0.01m^3)(1000kg/m^3)(1)^2(1)(0.7257) \\ &\approx 2.1491kg \end{aligned}$$

Now strip theory will be used with 2-D coefficients given in Newman 1977[8] p. 145 and DNV rp-h103[6] p. 139. The breadth over height relation is:

$$a/b = 108/404 \approx 0.27$$

The added mass coefficient becomes:

$$C_a(0.27) \approx 1.87$$

The referenced area becomes:

$$\begin{aligned} A_R = \pi*(a)^2 &= \pi*(108mm*0.5)^2 \\ &= 9160.9mm^2 \approx 0.0092m^2 \end{aligned}$$

The 2-D added mass in Surge then becomes:

$$\begin{aligned} A_{11}^{2D} &= \rho*C_a A_r (C_p^{no})^2 (C_p^{mo})(C_p^{mn}) \\ &= 1000\frac{kg}{m^3}(1.87)(0.0092m^2)(1)^2(1)(0.7257) \\ &\approx 12.43\frac{kg}{m} \end{aligned}$$

Finally the 2D-added mass needs to be integrated over the entire length of the ROV(strip theory) in order to obtain the 3D-added mass:

$$A_{11} = \int_{-H/2}^{H/2} A_{11}^{2D} dz = \int_{-214mm/2}^{214mm/2} 12.43\frac{kg}{m} dz \approx 2.66kg$$

The difference between the two methods:

$$\lambda = \frac{A_{11}^{empirical3D}}{A_{11}^{strip-theory}} = \frac{2.15kg}{2.66kg} \approx 81\%$$

This relation will be used to calculate the added mass in the remaining translational DOFs as well as the rotational DOFs.

$$A_{ii} = A_{ii}^{strip-theory} * \lambda \tag{3}$$

A.2 Roll

For rotational DOFs the only empirical values available are for a 2D rectangle. Therefore strip theory will be used and scaled using the scaling factor (λ) found for the surge DOF.

The breadth over height relation is:

$$a/b = \frac{108mm*0.5}{214mm*0.5} \approx 0.50$$

Which gives the following added mass coefficient

$$C_a(0.50) \approx 0.15$$

The result is then inserted into the following equation for added mass in rotational degrees of freedom;

$$A_{ii}^{2D} = \rho*C_a*\pi*a^4*(C_p^{no}) \tag{4}$$

$$\begin{aligned} A_{44}^{2D} &= \rho*C_a*A_R*(C_p^{XZ}) \\ &= 1000\frac{kg}{m^3}*0.15*\pi*(214mm*0.5)^4(1) \\ &\approx 0.062kgm \end{aligned}$$

Integrating over the length of the body:

$$A'_{44} = \int_{-L/2}^{L/2} A_{44}^{2D} dx = \int_{-404mm/2}^{404mm/2} 0.062 kgm dx \approx 0.025 kgm^2$$

Finally adjust the result to correspond with the empirical 3D-data :

$$\boldsymbol{A_{44}} = A'_{44} * \lambda = 0.025 kgm^2 * 0.81 \approx 0.020 kgm^2$$

B. Damping

As discussed earlier damping forces can be divided into a quadratic and a linear term. As the quadratic term is described by a drag coefficient. The quadratic drag can be estimated using the same method as the added mass. The linear damping can be found using empirical formulas found in Fossen 2011 [10].

B.1 Quadratic Damping

The drag coefficients found in Blevins 2003[9] are shown in table 2

Degree of freedom	*L/D*	$C_D(2D)$	$C_D(3D)$
Surge	2.51	1.40	0.90
Sway	0.50	2.50	NA
Heave	1.98	1.58	NA

Table 2: *Drag Coefficients for ROV Neptunus*

The general equation for translational quadratic damping is:

$$(K_Q)_{jj} = \frac{\rho}{2} C_D A \lambda (C_p^{no}) \qquad j = 1,2,3 \qquad (5)$$

Now the difference between strip theory(2D) and 3D needs to be calculated:

$$\lambda = \frac{C_D(3D)}{C_D(2D)} = \frac{0.90}{1.17} \approx 0.77$$

Inserting values into equation (5) gives the following estimates for quadratic damping:

$$(\boldsymbol{K_Q})_{\boldsymbol{11}} = \frac{1000[\frac{kg}{m^3}]}{2} * 1.40 * 0.108[m] * 0.214[m](0.77)(1) \approx 12.46 \left[\frac{kg}{m}\right]$$

$$(\boldsymbol{K_Q})_{\boldsymbol{22}} = \frac{1000[\frac{kg}{m^3}]}{2} * 2.50 * 0.404[m] * 0.214[m](0.77)(1) \approx 83.21 \left[\frac{kg}{m}\right]$$

$$(\boldsymbol{K_Q})_{\boldsymbol{33}} = \frac{1000[\frac{kg}{m^3}]}{2} * 1.58 * 0.404[m] * 0.108[m](0.77)(0.73) \approx 19.38 \left[\frac{kg}{m}\right]$$

The rotations can not be estimated using the method above as rotational drag coefficients are not available. A new method will therefore be applied for these DOFs. The method builds on the fact that for small angles a rotational motion can be translated to a translational motion.
Firstly the ROV is divided into a total of 4 quadrants around each axis. Furthermore it will be assumed that each quadrant only moves in the horizontal or vertical direction. By looking at figure 3 this means that the solid quadrants will move horizontally and the stapled quadrants will move vertically. As stated earlier the most important assumption here is that the quadrants have small angular rotations.

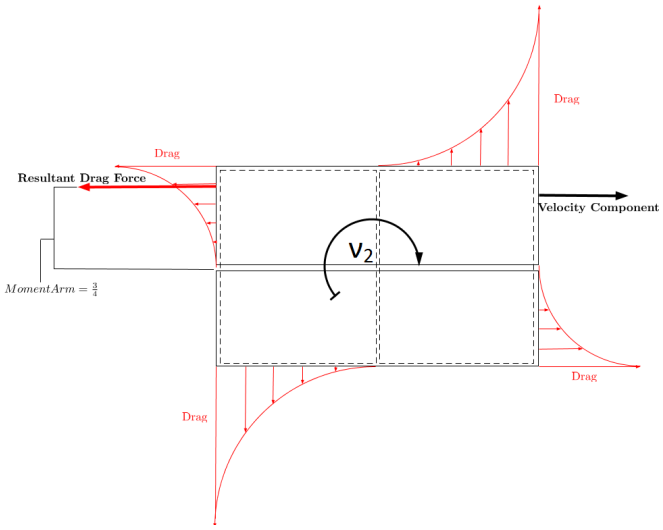

Figure 3: *Discretization of ROV for rotational DOFs*

Now an expression for the translational velocity for the different quadrant must be found. The points of interest are at the edges. The translational velocity for these points can be described using the relation below:(The choice of L,B or H depends on the degree of freedom)

$$\overline{v_2}[m/s] = v_2[rad/s] * \frac{(L/B/H)}{2}[m] \qquad (6)$$

Lastly the drag coefficients for each quadrant are needed. From Blevins 2003 table 10-20[9] these are found. The general equation for the drag force of each quadrant can be written:(Note that the correct C_P value is "om" for horizontal quadrants and "mn" for vertical quadrants)

$$F^j_{quadrant} = \frac{1}{2}\frac{1}{3}\rho C_D A C_P^{om/mn} \lambda \overline{v_2}\left|\overline{v_2}\right| \qquad j = 4,5,6 \quad (7)$$

Note that the term $\frac{1}{3}$ comes from the fact that the total force over a quadrant when a 2nd order load is applied becomes $\frac{1}{3}$ The calculations for the roll DOF will now be shown. For pitch and yaw only the results will be presented as the methods are identical. By assuming roll DOF the drag coefficients for the horizontal(solid-line) and vertical(dashed-line) quadrants become 2.10 and 1.14 respectively.
Inserting values into equation (7) gives the following damping force for each quadrant:

$$F^{hori}_{quad} = \frac{1000\left[\frac{kg}{m^3}\right]}{2*3}\left(2.10\right)\left(\frac{0.214[m]}{2}\right)\left(0.404\left[m\right]\right)\left(0.77\right)\left(1\right)\overline{p}\left|\overline{p}\right| \approx 11.67*\overline{p}\left|\overline{p}\right|\left[\frac{kg}{m}\right]$$

$$F^{vert}_{quad} = \frac{1000\left[\frac{kg}{m^3}\right]}{2*3}\left(1.14\right)\left(\frac{0.108[m]}{2}\right)\left(0.404\left[m\right]\right)\left(0.77\right)\left(0.73\right)\overline{p}\left|\overline{p}\right| \approx 2.33*\overline{p}\left|\overline{p}\right|\left[\frac{kg}{m}\right]$$

Now the forces are multiplied by the distance of 3/4 from the center of rotation(the resultant force of a 2nd order load function acts at a distance 3/4 from the center) and the expression for the translational velocity in equation (6) is inserted to obtain the damping moment for each quadrant:

$$M^{hori}_{quad} = 11.67\left[\frac{kg}{m}\right]*\frac{3}{4}*\frac{0.214\left[m\right]}{2}\left[kg\right]\left(\frac{0.214\left[m\right]}{2}*p\right)\left|\frac{0.214\left[m\right]}{2}*p\right| \approx 0.011*p*\left|p\right|\left[kgm^2\right]$$

$$M^{vert}_{quad} = 2.33*\left[\frac{kg}{m}\right]\frac{3}{4}*\frac{0.108\left[m\right]}{2}\left(\frac{0.108\left[m\right]}{2}*p\right)\left|\frac{0.108\left[m\right]}{2}*p\right| \approx 0$$

Now the damping for the horizontal and vertical quadrants are added together. For all 4 quadrants this gives a total drag moment of :

$$M_{tot} = 0.022\left[kgm^2\right]p\left|p\right|$$

The quadratic damping coefficient in roll therefore becomes:

$$(\boldsymbol{K_Q})_{\mathbf{44}} = 0.022\left[kgm^2\right]$$

Using the exact same approach on the pitch and yaw DOFs give:

$$(\boldsymbol{K_Q})_{\mathbf{55}} = 0.0552\left[kgm^2\right]$$

$$(\boldsymbol{K_Q})_{\mathbf{66}} = 0.1698\left[kgm^2\right]$$

B.2 Linear Damping

As stated earlier linear skin friction is a result of the boundary layer created when the ROV moves through the water. The linear damping can be very hard to estimate analytically. A number of general approximations exists, though most of them are for surface vessels. Fossen 2011[10] page 125 suggests one method for skin friction damping of a floating vessel. In this article a similar approach will be used, however with some modifications.
Starting with the equation of motion for a viscously damped(linear damped) free vibration linear 1DOF system :

$$(m + m_a)\ddot{\overline{X}} + K_L\dot{\overline{X}} + g\overline{X} = 0 \quad (8)$$

Dividing by the mass term gives:

$$\ddot{\overline{X}} + \frac{K_L}{m}\dot{\overline{X}} + \omega_n^2\overline{X} = 0 \quad (9)$$

According to Kreyzsig 2010[11] the equation has the roots:

$$\begin{Bmatrix}\lambda_1\\ \lambda_2\end{Bmatrix} = -\frac{K_L}{2m} \pm \sqrt{K_L^2 - 4mc} \quad (10)$$

It can now be seen that the critical damping occurs when K_L equals $2m\omega_n$. Introducing the critical damping to equation (9) it can be rewritten:

$$\ddot{\overline{X}} + 2\zeta\omega_n\dot{\overline{X}} + \omega_n^2\overline{X} = 0 \quad (11)$$

where

$$\zeta = \frac{K_L}{K_{Lcrit}} = \frac{K_L}{2m\omega_n} \quad (12)$$

It therefore follows that the linear damping can be estimated by three parameters. The mass and the natural frequency can be calculated whilst for the damping ratio a value must be assumed. For surface vessels the damping ratio in roll usually lies in the range of $2 - 10\%$

Fossen 2011[10] p.125 and SSC 1991[12] table 1. The damping ratio will be set to 2.5%.

As the natural frequency is given :

$$\omega_n = \sqrt{\frac{g}{m + m_a}}$$

(12) can be rewritten to :

$$K_L = 2\zeta m \sqrt{\frac{g}{m + m_a}} \tag{13}$$

The restoring matrix only have non-zero values in roll and pitch. The linear damping terms in these DOFs become:

$$(K_L)_{44} = 2 * 0.025 * (0.0166 + 0.020)[kgm^2] * \sqrt{\frac{1[Nm]}{(0.0166 + 0.020)[kgm^2]}} \approx 0.008\left[\frac{kgm^2}{s}\right] \tag{14}$$

$$(K_L)_{55} = 2 * 0.025 * (0.051 + 0.077)[kgm^2] * \sqrt{\frac{1[Nm]}{(0.051 + 0.077)[kgm^2]}} \approx 0.015\left[\frac{kgm^2}{s}\right] \tag{15}$$

The yaw damping is found by scaling the quadratic yaw damping with the ratio between linear and quadratic pitch/roll damping. For the translational DOFs the scaling factor is obtained from Eng 2009[13]. These estimations give the following values for the linear damping:

$$(K_L)_{11} = 1.99\left[\frac{kg}{s}\right]$$

$$(K_L)_{22} = 13.32\left[\frac{kg}{s}\right]$$

$$(K_L)_{33} = 3.08\left[\frac{kg}{s}\right]$$

$$(K_L)_{66} = 0.0368\left[\frac{kgm^2}{s}\right]$$

V. Experiment

The experimental setup is simple and the costs involved are small. The ROV is attached to the mounting bracket using screws and strips as shown in figure 4.

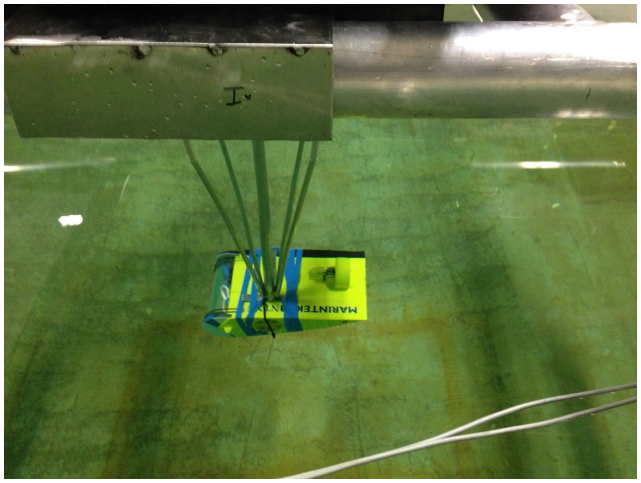

Figure 4: *ROV mounted to bracket with strips, tape and screws for tests in heave and pitch.*

On top of the mounting bracket the load cells are fastened. The two load cells are mounted diagonally with a distance of 0.12 m from the center of rotation. This setup enables both translational and rotational degrees of freedom to be measured without having to disassemble and reassemble the mounting bracket. The load cells are in turn mounted to the towing/rotation cart. The load cells are connected to a computer to record the horizontal force. At the bottom of the bracket the ROV is attached. For all DOFs the bracket is centered at the COG of the ROV. The ROV is fastened by screws and strips see figure 5. For the roll DOF waterproof tape also had to be applied in order to completely lock the ROV to the mounting bracket. For all test runs the following quantities are recorded:

- Time step
- Force from both load cells
- Angular position
- Horizontal position

The data is recorded with a sampling rate of 200 Hz.

Figure 5: *ROV Neptunus mounted for surge and yaw tests*

A. Experimental procedure

The towing cart is accelerated up to a given horizontal/rotational velocity and the corresponding forces are recorded. In this project, MATLAB^{TM} has been used to write a program script to extract the relevant values(force and position) and calculate the linear and quadratic damping terms(K_L and K_Q) using least squares algorithm. Due to large oscillations(especially for small velocities) the script takes the average values over the relevant domain.
An example of this can be seen in figure 6 where the relevant domain is between 30 and 50 seconds.

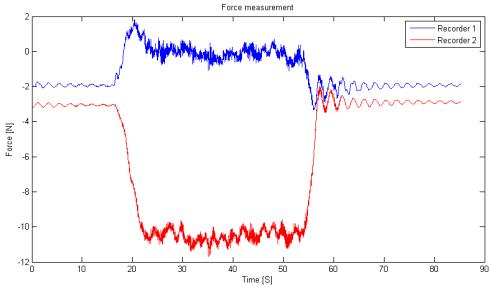

Figure 6: *Example of experiment force recordings. Note that the total force is the sum of the two recordings*

For the rotational DOFs the measured force is converted to angular moment by multiplying the measured force with the distance from center of rotation(0.12m) and $\sqrt{2}$ see figure 8

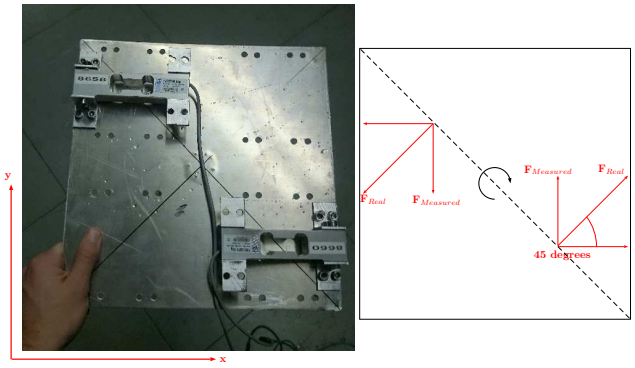

Figure 7: *Picture and sketch of load cells setup seen in the horizontal plane*

For each degree of freedom the tests are performed for 5-7 low velocities and 5-7 high velocities resulting in approximately 12 data points to generate damping functions. Lastly translation tests and rotation tests are performed for the bracket without the ROV and damping functions for the bracket in rotation and translation are computed.

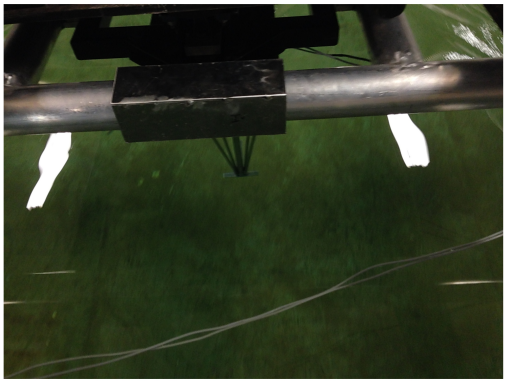

Figure 8: *Mounting Bracket Towing test*

VI. Results

A. Empirical Estimates

Using the empirical method described in the previous sections the following estimates were obtained.

Translation			
DOF	$K_Q[\frac{kg}{m}]$	$K_L[\frac{kg}{s}]$	A$[kg]$
Surge	12.4590	1.99	1.596
Sway	83.2442	13.32	15.033
Heave	19.2536	3.10	3.671

Rotation			
DOF	$K_Q[kgm^2]$	$K_L[\frac{kgm^2}{s}]$	A$[kgm^2]$
Roll	0.0220	0.0079	0.011
Pitch	0.0552	0.0150	0.041
Yaw	0.1698	0.0368	0.073

Table 3: *Estimated Damping and added mass*

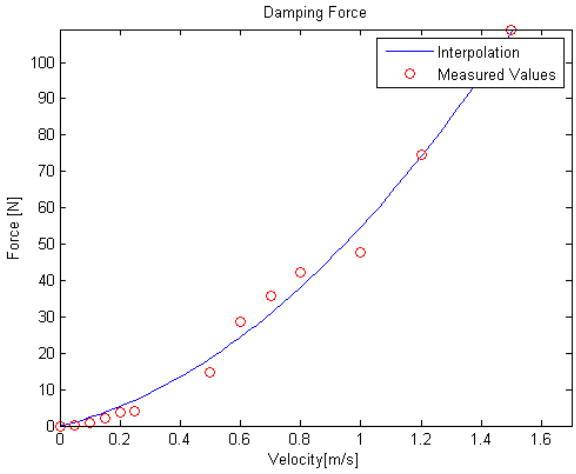

Figure 9: *Quadratic interpolation of heave results using LS-method*

B. Experiment

After the completion of the tests the data had to be analysed. Inconsistent measurements were removed and the damping functions were obtained using least squares algorithm.

Using linear superposition the damping contribution from the bracket itself was subtracted and thus the following damping coefficients were obtained:

Translation		
DOF	$K_Q[\frac{kg}{m}]$	$K_L[\frac{kg}{s}]$
Surge	4.0077	2.2907
Sway	35.2159	4.9804
Heave	10.3037	15.1897

Rotation		
DOF	$K_Q[kgm^2]$	$K_L[\frac{kgm^2}{s}]$
Roll	0	0.0025
Pitch	0	0.0093
Yaw	0	0.2605

Table 4: *Experimental damping coefficients*

Using least squares method on the results for the rotational DOFs gave linear damping functions.(The 2nd order terms were so small that they were neglected)

C. SolidWorks Flow simulation

The CFD analysis done in SolidWorks™ Flow simulation yielded the results given in table 5.

Translation		
DOF	$K_Q[\frac{kg}{m}]$	$K_L[\frac{kg}{s}]$
Surge	3.3800	-0.0526
Sway	42.032	2.4221
Heave	14.4123	0.0403

Rotation		
DOF	$K_Q[kgm^2]$	$K_L[\frac{kgm^2}{s}]$
Roll	0.0207	-0.0002
Pitch	0.0412	0.0011
Yaw	0.18	- 0.0013

Table 5: *Damping Coefficients found from CFD analysis*

D. WADAM

Performing the mentioned analysis in WADAM gave the following added mass matrix.

$$A=\begin{bmatrix} 2.005 & 0.541 & 0.010 & 0.032 & -0.241 & -0.05 \\ & 14.247 & -0.160 & 0.95 & -0.0649 & -0.871 \\ & & 2.273 & -0.011 & -0.001 & 0.009 \\ & \text{Sym} & & 0.635 & -0.004 & -0.058 \\ & & & & 0.0289 & 0.006 \\ & & & & & 0.146 \end{bmatrix}$$

VII. Comparrison of results

A. Added Mass

The added mass was in the previous sections calculated using two methods. One method based on empirical formulas combined with basic assumptions and one method using potential panel program.(WADAM) When performing the WADAM analysis a fine mesh with (2000 elements) were used and its therefore fair to assume the added mass values obtained to be close to the exact values. Comparing the estimated values with the WADAM values gives the following results:

DOF	$\left(\frac{Estimate}{WADAM}-1\right)$
Surge	-20.4%
Sway	5.5%
Heave	61.5%
Roll	-82.7%
Pitch	41.9%
Yaw	-50.0%

Table 6: *Estimated added mass values compared with WADAM result*

B. Damping

The Results for the translational degrees of freedom are shown in figures 10,11 and 12

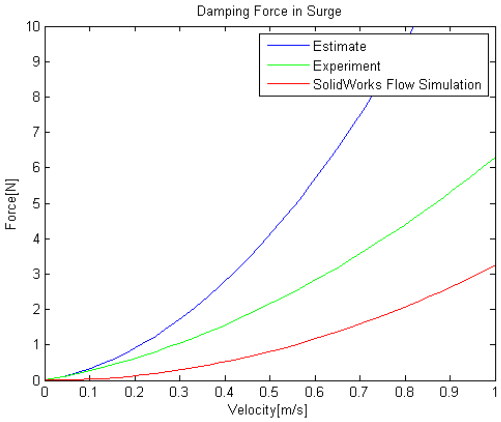

Figure 10: *Surge Damping*

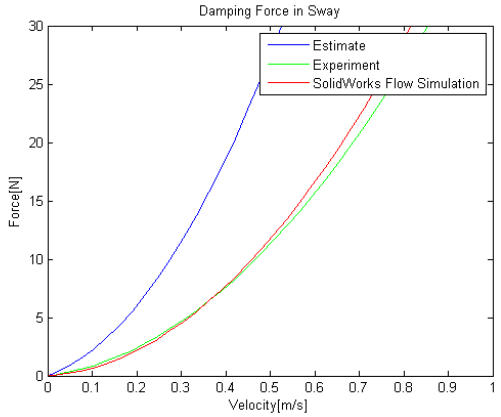

Figure 11: *Sway Damping*

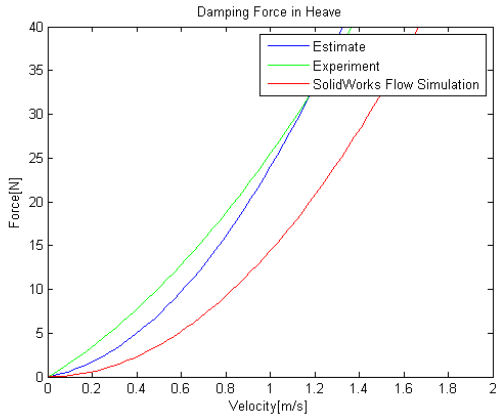

Figure 12: *Heave Damping*

For the rotational DOFs the results can be seen in figures 13,14 and 15

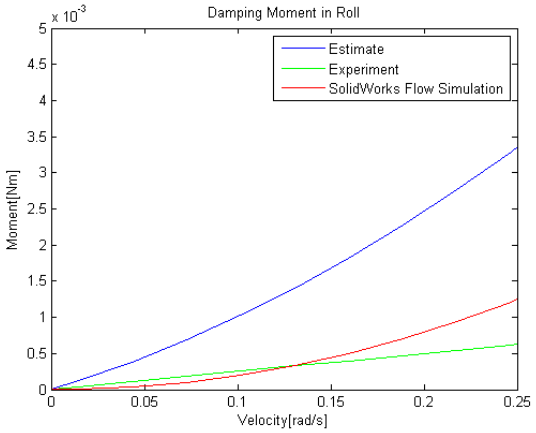

Figure 13: *Roll Damping*

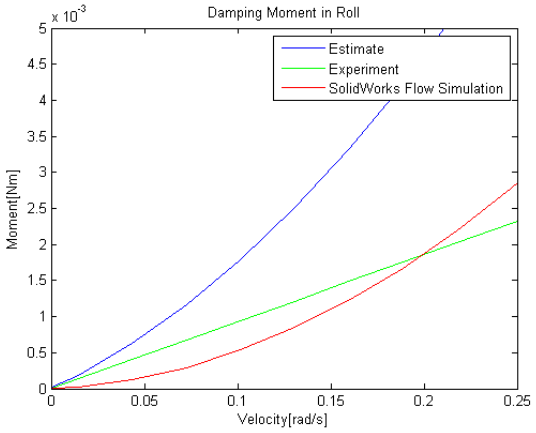

Figure 14: *Pitch Damping*

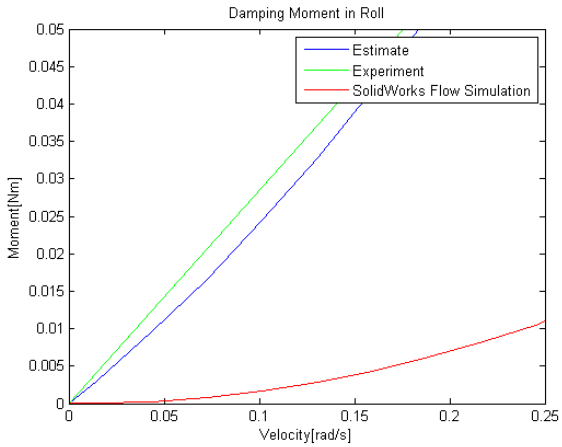

Figure 15: *Yaw Damping*

VIII. Discussion

A procedure for finding the diagonal hydrodynamic coefficients(added mass and damping) of a ROV has been proposed. The procedure is a combination of empirical, experimental and computational methods. The empirical method is based on basic assumptions and basic linear and nonlinear theory. For the estimate only a few parameters are needed and the results are obtained fairly quick. The experimental method presents a low cost and relative quick method for obtaining the damping coefficients. The computational method is mainly used for reference as no new theory is introduced on this part.

A. Empirical Estimates

A.1 Added Mass

The empirical added mass estimates show fairly good results for the translational DOFs.It is observed that the added mass estimate is very accurate for the Heave DOF. This is probably due to the fact that in heave ROV Neptunus has sharp edges(prismatic shape) which is assumed in the reference geometry. The rotational DOF are more inaccurate, especially the roll DOF. As the method is based on simple assumptions a 100% accuracy can not be expected.

A.2 Damping

The empirical data shows an overestimation for the translational DOFs. This does not come as a huge surprise as the calculation method assumes rectangular geometry and in surge and sway the foil geometry of ROV Neptunus differs substantially from the referenced geometry. It is again observed that the estimated value in heave corresponds well with the experimental value. The rotational DOFs estimates are much lower than the experimental values.(except for the Yaw DOF, but this will be discussed later) Since the procedure used is a new method only meant for basic estimate a large error is expected. It can however be noted that the estimated damping is of the same order as the experimental values. However more reference geometries should be tested to assure validity.

For conceptual design the empirical estimates can be useful as they are performed very quickly and provide results of the expected range. They can also be very useful for validation of other methods.As shown in [14] poor parameter estimation can for model based control system be accounted for by a parameter adaptation algorithm(APP).

B. Experiment

It is observed that the experiment gives a higher damping force for surge and heave than the CFD analysis. The Sway damping is very similar(in practice identical) for the CFD and experiment. The roll and pitch DOFs are also very similar to the referenced CFD values. Yaw however shows great variation between CFD and experimental values. This most likely comes from the fact that the yaw recordings were of poor quality. The loadcells did not realign to zero loading after each run and thus gave error in the results. In figure 16 it can be noted how load varied over time which should not be the case for a good test result.

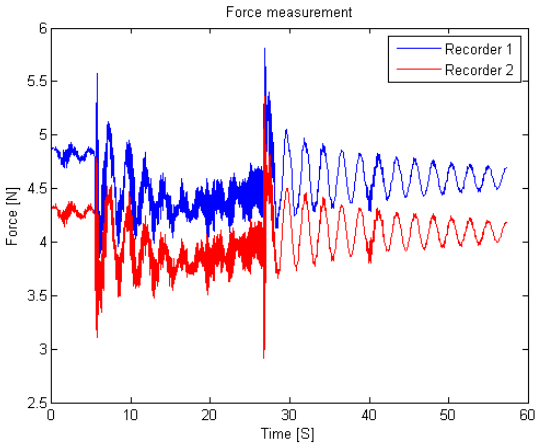

Figure 16: *Recorded yaw damping at 10[deg/s]. Note how the recorded forces vary over time*

Compared to the results of Eng 2009[13] the results obtained in this experiment show greater deviation between CFD and experimental values. As the experiment were performed with low cost load cells and with only one test run for each velocity per DOF some errors are bound to occur. The turbulence model used in the CFD analysis may also provide some error.

C. Improvements

Both methods described have great potential for improvements. As the empirical estimates are based on box shaped geometries improvements can be made to adjust for the foil-geometry of ROV Neptunus. For large velocities or unsymmetric geometry coupling terms become very important. An improvement would therefore be to incorporate coupling terms for the empirical estimates.

The experimental method can be improved by using loadcells between the ROV and the bracket instead of between the bracket and the towing cart. As waterproof loadcells were not available at the time of testing the loadcells had to be installed over the waterline. More test runs would also increase the confidence in the obtained results. For translational velocities over 1 m/s it was noticed that the bracket bended slightly due to the moment from the ROV. A more solid mounting bracket will remove this problem. The rotor disc were only able to move 270 degrees which meant the high speed rotation tests did not always reach a stable moment equilibrium see figure 16.

IX. Conclusion

The 2 methods for estimating the diagonal hydrodynamic coefficient shows promising results. The experimental results can easily be improved by using better equipment and performing more tests, and shows even for the low cost test performed in this paper accurate results. For the empirical estimates it is worth mentioning that the unconventional geometry of ROV Neptunus will give less accurate result than for a conventional prismatic ROV. The unconventional geometry shows that the procedure proposed is able to provide estimates for a variety of ROV geometries. The WADAM results obtained for the added mass matrix shows that for ROV Neptunus the off-diagonal terms cannot be neglected. The surge-yaw and sway-roll couplings are very large, hence they will greatly affect the behaviour of the ROV. It was noticed that for the rotational DOF's the damping moments were better described by linear interpolation functions. This coincides with the observations done in Caccia et. al 2000[4]. As the ROV is very small (3.46kg) the relative error in the measurements obtained in the experiment can become quite big. Simply because the forces and moments exerted on the vehicle are very small. Especially for the rotational DOFs.

References

[1] **G. Conte, S. M. Zanoli, D. Scaradozzi and A. Conti, 2004**
Evaluation of Hydrodynamics parameters of a UUV. A preliminary study.
Presented at International Symposium on Control, Communications and Signal Processing, ISCCSP, Hammamet, 2004.

[2] **A. T. Morrison, III and D. R. Yoerger, 1993**
Determination of the hydrodynamic parameters of an underwater vehicle during small scale, nonuniform, 1-dimensional translation.
Victoria, BC, Canada, 1993

[3] **A. Alessandri, R. Bono, M. Caccia, G. Indiveri, and G. Veruggio, 1998**
Experiences on the modelling and identification of the heave

motion of an open-frame UUV.
Presented at Oceans Conference Record (IEEE), Nice, Fr, 1998

[4] **M. Caccia, G. Indiveri, and G. Veruggio, 2000**
Modeling and identification of open-frame variable configuration unmanned underwater vehicles,
P IEEE Journal of Oceanic Engineering, Vol. 25, pp. 227-240, 2000.

[5] **P. Egeskov, A. Bjerrum, A. Pascoal, C. Silvestre, C. Aage, and L. W., 1994**
Design, construction and hydrodynamic testing of the AUV MARIUS,
Cambridge, MA, USA, 1994.

[6] **DNV, 2014**
DNV-RP-H103, Modelling and Analysis of Marine Operations,
https://exchange.dnv.com/publishing/Codes/download.asp?url=2010-04/rp-h103.pdf, 20.01.2015.

[7] **DNV, 2015**
Frequency domain hydrodynamic analysis of stationary vessels - Wadam,
https://www.dnvgl.com/services/frequency-domain-hydrodynamic-analysis-of-stationary-vessels-wadam-2412, 20.04.2015.

[8] **John N. Newman, 1977**
Marine Hydrodynamics,
Mitpress, Cambridge, Massachusetts, 1977.

[9] **Robert D. Blevins, 2003**
Applied Fluid Dynamics Handbook,
Krieger Publishing Company, Malabar, Florida, 2003.

[10] **Thor Inge Fossen, 2011**
HandBook of Marine Craft Hydrodynamics and Motion Control,
Wiley ,Sussex, United Kingdom, 1st Edition, 2011.

[11] **Erwin Kreyszig, 2011**
Advanced engineering mathematics,
10th Edition, Hoboken, N.J: Wiley,2011

[12] **SHIP STRUCTURE COMMITTEE, 1991**
SSC-359 Hydrodynamic Hull Damping (Phase I),
Ship Structure Committee, 1991.

[13] **Eng YH, Lau WS, Low E., Seet GGL and CS Chin, 2009**
Estimation of The Hydrodynamic Coefficients of an ROV using Free Decay Pendulum Motion,
Engineering Letters, 3rd Edition, 16.03.09.

[14] **J. YUH, 1990**
Modeling and Control of Underwater Robotic Vehicles,
TRANSACTIONS ON SYSTEMS, MAN, AND CYBERNETICS, Vol.20, No. 6, December 1990

[15] **Azis, F.A, Aras M.S.M, Rashid, M.Z.A, Othman M.N, Abdullah, S.S, 2012**
Problem Identification for Underwater Remotely Operated Vehicle(ROV): A Case Study ,
International Symposium on Robotics and Intelligent Sensors, 2012

[16] **P. Ridao, J. Batlle and M. Carreras, 2001**
Model identification of low-speed UUV,
Proceedings IFAC World Conference 2001, Barcelona, Spain

[17] **Thor I. Fossen, 1994**
Guidance and Control of Ocean Vehicles,
John Wiley & sons, West Sussex, England, 1994

Appendix A

DOF	Forces and Moments	Velocities	Positions & Euler angles
Surge	X	u	x
Sway	Y	v	y
Heave	Z	w	z
Roll	K	p	ϕ
Pitch	M	q	θ
Yaw	N	r	ψ

Table 7: *SNAME-notation*

DOF	m	n	o
Surge & roll	X	Y	Z
Sway & Pitch	Y	Z	X
Heave & Yaw	Z	X	Y

Table 8: *Projected area coefficient superscript (used in empirical calculations)*

The article can also be found in the folder :
"appendices/appendix F"

APPENDIX G

MC-LAB

This Appendix contains information about MC-lab which was the laboratory used for the experimental procedure. The information here is copied directly from : "http://www.ntnu.no/imt/lab/cybernetics"

The marine cybernetics laboratory is a small wave basin, located in what was originally a storage tank for ship models made of paraffin wax. The facility is especially suited for tests of motion control systems for marine vessels, due to the relatively small size and advanced instrumentation package. It is also suitable for more specialized hydrodynamic tests, mainly due to the advanced towing carriage, which has capability for precise movement of models in six degrees of freedom.

Capacities	*Experimental Set-ups*
• Tank Dimensions L X B X H = 400m X 6.45m X 1.5m • Wave maker(see below) • Towing carriage (see below): towing speed 2 m/s, 5(6) DOFs forced motions. • Computer system for control, data recording and analysis • Typical scaling ratios: I=50-150 • Typical ship model lengths: 1-3m • Positioning system (see below) measure 6DOF in real time	• DP and way-point tracking (wireless control) of ships and semi-submersibles • Crane operations • Propulsor and thruster control • Rapid control prototyping • Planar motion mechanism (PMM) and vertical motion mechanism (VMM) tests • Calibration of transducers • Hardware-in-the-loop (HIL) experiment laboratory.

The MC-lab is operated by the Department of Marine Technology. It is mainly used by Master students and PhD-candidates, but it is also available for external users. The software in use was developed using rapid prototyping techniques and automatic code generation under Matlab/Simulink and Opal. The target PC onboard the vessel runs the QNX real-time operating system while experimental results are presented in real-time on a host PC using Labview.

G.1 Towing Carriage

The carriage can be operated in manual or computer controlled mode. The manual operation is done from the consol on the carriage. There is made a special Labview and Opal application to setup regular or irregular movement of the different axes.

G.1.1 Axes

The axis limits given in the table refers to the absolute coordinates in the remote control system. The ranges are the safe and practical limits, as of May 2005. These may be subject to change. Normal Speed is the speed used when returning to reference position.

Axis		min	max	Max Speed	Max Acc
x	Main Carriage	-15.8[m]	8.5[m]	2.0[m/s]	0.5[m/s^2]
y	Transverse Car.	-2.4[m]	2.4[m]	1.0[m/s]	1.0[m/s^2]
U	Small Carriage	-0.4[m]	0.4[m]	1.0[m/s]	1.0[m/s^2]
C	Rotation Carriage	0 deg	270 deg	≈ 25 deg/s	–
Z	Vertical Axis Car.	-0.2 [m]	0.2[m]	0.5[m/s]	2.0[m/s^2]

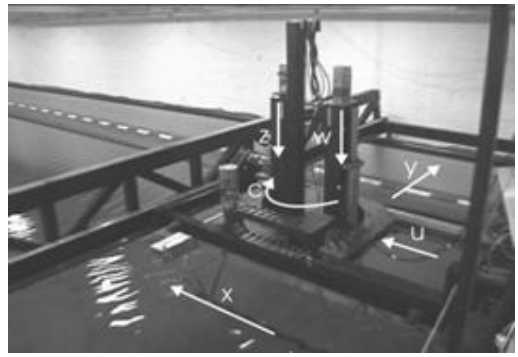

Figure G.1: Axis illustration of Towing/rotation rig
(taken from http://www.ntnu.no/imt/lab/cybernetics)